UNIVERSIDADE FEDERAL DO CEARÁ
CENTRO DE CIÊNCIAS
DEPARTAMENTO DE BIOQUÍMICA E BIOLOGIA MOLECULAR
PROGRAMA DE PÓS-GRADUAÇÃO EM BIOQUÍMICA

FRANCISCO LUCAS PACHECO CAVALCANTE

ABORDAGEM ÔMICA INTEGRADA NA INVESTIGAÇÃO DA ACLIMATAÇÃO AO ESTRESSE SALINO INDUZIDA PELA ATIVAÇÃO DO RETÍCULO ENDOPLASMÁTICO EM FEIJÃO-CAUPI (*VIGNA UNGUICULATA* [L.] Walp)

FORTALEZA
2026

FRANCISCO LUCAS PACHECO CAVALCANTE

ABORDAGEM ÔMICA INTEGRADA NA INVESTIGAÇÃO DA ACLIMATAÇÃO AO ESTRESSE SALINO INDUZIDA PELA ATIVAÇÃO DO RETÍCULO ENDOPLASMÁTICO EM FEIJÃO-CAUPI (*VIGNA UNGUICULATA* [L.] Walp)

Tese apresentada ao Programa de Pós-Graduação em Bioquímica da Universidade Federal do Ceará, como requisito parcial à obtenção do título de doutor em Bioquímica. Área de concentração: Bioquímica vegetal.

Orientador: Prof. Dr. Humberto Henrique de Carvalho.
Coorientador: Prof. Dr. Enéas Gomes Filho.

FORTALEZA
2026

FRANCISCO LUCAS PACHECO CAVALCANTE

ABORDAGEM ÔMICA INTEGRADA NA INVESTIGAÇÃO DA ACLIMATAÇÃO AO ESTRESSE SALINO INDUZIDA PELA ATIVAÇÃO DO RETÍCULO ENDOPLASMÁTICO EM FEIJÃO-CAUPI (*VIGNA UNGUICULATA* [L.] Walp)

Tese apresentada ao Programa de Pós-Graduação em Bioquímica da Universidade Federal do Ceará, como requisito parcial à obtenção do título de doutor em Bioquímica. Área de concentração: Bioquímica vegetal.

Aprovada em: 27/02/2026.

BANCA EXAMINADORA

_____
Prof. Dr. Humberto Henrique de Carvalho (Orientador)
Universidade Federal do Ceará (UFC)

_____
Prof. Dr. Murilo Siqueira Alves
Universidade Federal do Ceará (UFC)

_____
Dra. Stelamaris de Oliveira Paula Marinho
Universidade Federal do Ceará (UFC)

_____
Profa. Dra. Giselle Camargo Mendes
Instituto Federal de Educação, Ciência e Tecnologia de Santa Catarina (IFSC)

_____
Prof. Dr. Vanildo Silveira
Universidade Estadual do Norte Fluminense Darcy Ribeiro (UENF)

A minha amada avó, Francisca Cavalcante (*In memoriam*), mulher analfabeta que sempre me falava para estudar e ser “doutor”.

AGRADECIMENTOS

Ao Conselho Nacional de Desenvolvimento Científico e Tecnológico (CNPq), pelo apoio financeiro por meio da concessão de bolsa de doutorado (Processo nº 140905/2022-7).

O presente trabalho foi realizado com apoio da Coordenação de Aperfeiçoamento de Pessoal de Nível Superior – Brasil (CAPES) – Código de Financiamento 001.

Ao Instituto Nacional de Ciência e Tecnologia em Agricultura Sustentável no Semiárido Tropical – INCTAgriS (CNPq/FUNCAP/CAPES), processo CNPq nº 406570/2022-1.

A Deus, pela vida, pela saúde e pela força que me sustentou nos momentos de crise e incerteza ao longo desta jornada. Nas adversidades, aprendi a exercitar a resiliência, fortalecendo minha fé e minha determinação para concluir esta etapa.

À Universidade Federal do Ceará e ao Programa de Pós-Graduação em Bioquímica, instituição na qual construí minha trajetória acadêmica ao longo de seis anos, desde o mestrado até a conclusão do doutorado, pela sólida formação científica e pela oportunidade de desenvolver esta pesquisa.

Aos professores e demais profissionais do Programa de Pós-Graduação em Bioquímica, pelos ensinamentos e contribuições fundamentais para minha formação acadêmica.

Ao Prof. Dr. Humberto Henrique de Carvalho, pela orientação firme e criteriosa, pelo compromisso com a excelência científica e pela responsabilidade na formação de seus alunos. Sua paciência, compreensão, serenidade e postura equilibrada na condução da docência são exemplos que ultrapassam a dimensão acadêmica e representam, para mim, uma referência concreta do que significa ser professor.

Ao Laboratório de Fisiologia Vegetal e ao meu coorientador Prof. Dr. Enéas Gomes Filho, pelo ambiente científico estimulante e pelas discussões que contribuíram para o desenvolvimento deste trabalho. Agradeço também aos colegas que, em diferentes momentos, ofereceram auxílio pontual e colaboração, contribuindo para a realização desta pesquisa.

Aos membros da banca examinadora, Prof. Dr. Murilo Siqueira Alves, Profa. Dra. Stelamaris de Oliveira Paula Marinho, Prof. Dr. Vanildo Silveira e Profa. Dra. Giselle Camargo Mendes, pela honra de aceitarem participar da avaliação desta tese e pelas considerações técnicas e científicas que agregaram qualidade e rigor a este trabalho.

Aos laboratórios parceiros, representados pelo Prof. Dr. Danilo de Menezes

Daloso, pelo Prof. Dr. Murilo Siqueira Alves, pela Profa. Dra. Maria Raquel Alcântara de Miranda e pelo Prof. Dr. José Hélio Costa, pela colaboração científica, disponibilização de infraestrutura e contribuições técnicas que ampliaram a qualidade e a abrangência deste trabalho, com reconhecimento especial ao Prof. Dr. Danilo de Menezes Daloso pelo dedicado trabalho à frente da coordenação e pelo apoio oferecido em diferentes momentos desta trajetória.

À Escola Visconde do Rio Branco, instituição onde iniciei minha trajetória na docência, e às pessoas que, nesse ambiente, contribuíram para meu crescimento profissional e para a consolidação da minha identidade como professor. Sou grato pelo apoio e compreensão ao longo do período em que conciliei a prática docente com a formação acadêmica no doutorado.

Ao meu colega de laboratório e amigo Igor Rafael de Sousa Costa, pela parceria constante ao longo de toda essa trajetória, formando uma verdadeira dupla nos desafios acadêmicos e nas conquistas alcançadas. Pela cumplicidade, apoio mútuo e amizade construída nesses anos, que se tornaram parte fundamental desta caminhada. Sua empatia e seus valores sempre foram, para mim, fonte de inspiração pessoal e profissional.

Aos amigos verdadeiros e de longa data, que caminham comigo para além da vida acadêmica, pelo apoio, pelas conversas e por serem presença constante ao longo dos anos. Ainda que não mencionados individualmente, estão todos guardados no meu coração.

Aos amigos e colegas da vida científica, pela parceria intelectual, pelas discussões enriquecedoras, pelo apoio mútuo nos desafios da pesquisa e pela troca constante de experiências que fortaleceram minha formação acadêmica. De maneira especial, a Stelamaris, Camila Tomé, Profa. Rosilene Mesquita, Luana Minello, Gonzalo Burgos e Dalton Barreto, cuja convivência ultrapassou o ambiente científico e se consolidou também como amizade pessoal.

À minha família, meu alicerce e minha maior referência, por se orgulharem de mim e por caminharem ao meu lado em cada conquista, com destaque especial à minha prima, Luciliana Pacheco Silva, pela presença e incentivo constantes.

Em especial, aos meus pais, minha mãe, Lucineide Pacheco, e meu pai, Francisco Alberto, pelo amor, pelos valores ensinados e por sempre acreditarem em mim, celebrando cada passo dessa trajetória. Vindo de uma realidade simples, cada avanço foi construído com esforço, fé e com o apoio de vocês e de tantas pessoas que caminharam conosco. Ser o primeiro doutor da família torna esta conquista ainda mais significativa, mas ela é, acima de tudo, compartilhada.

RESUMO

A salinidade representa um dos principais fatores limitantes da produtividade agrícola, afetando a homeostase iônica, o equilíbrio redox, o metabolismo e o crescimento vegetal. Embora o retículo endoplasmático (RE) seja reconhecido como um importante centro de integração de sinais celulares sob estresse, os mecanismos pelos quais sua ativação pode modular a tolerância ao sal em feijão-caupi (*Vigna unguiculata* [L.] Walp.) ainda não estão completamente elucidados. Esta tese investigou se a estimulação controlada da sinalização adaptativa do retículo endoplasmático, via ativação transitória da UPR induzida por tunicamicina (TM), poderia funcionar como mecanismo de priming, aumentando a eficiência de aclimatação à salinidade. A aplicação foliar de TM foi selecionada para induzir sinalização sistêmica do retículo endoplasmático sem alterar diretamente a absorção de íons pelas raízes, permitindo a ativação controlada de vias adaptativas antes da exposição ao sal. Foi empregada uma abordagem integrativa e temporal, combinando análises fisiológicas, quantificação de Na^+ e K^+, determinação de peróxido de hidrogênio (H_2O_2), expressão gênica por qPCR de marcadores da resposta a proteínas mal dobradas (UPR) e de transportadores iônicos, além de análises metabolômica, lipidômica e proteômica quantitativa nas folhas. Os resultados demonstraram que o priming com TM atenuou significativamente os efeitos deletérios do NaCl, promovendo melhor desempenho fotossintético e maior crescimento. Observou-se redução do acúmulo de Na^+ na parte aérea, maior retenção de K^+ e aumento do sequestro iônico em raízes, indicando aprimoramento da homeostase iônica. A aplicação de TM induziu uma resposta rápida e transitória de estresse do RE, caracterizada por aumento inicial de H_2O_2 e expressão precoce de genes da via *UPR* com retorno aos níveis basais em 24 horas. Sob salinidade, plantas previamente tratadas com TM apresentaram menor acúmulo de H_2O_2, ativação antecipada e mais eficiente de vias associadas ao RE e ao transporte de sódio, além de redução na expressão de chaperonas e transportadores de Na^+. A análise proteômica evidenciou que o sal promoveu ampla repressão metabólica, com redução de enzimas do ciclo de Calvin e da glicólise (GAPDH, triosefosfato isomerase) e de proteínas ribossomais, enquanto o priming com TM atenuou essa supressão e favoreceu o reforço seletivo da maquinaria translacional e de proteínas associadas à adaptação ao estresse. Perfis metabolômicos e lipidômicos indicaram maior ajuste osmótico e remodelamento de membranas, reforçando a estabilidade celular sob estresse. Conclui-se que a ativação transitória do RE atua como mecanismo de pré-condicionamento fisiológico, coordenando regulação redox, proteostase, homeostase iônica e reprogramação metabólica. Os achados

ampliam a compreensão do papel do RE como hub regulatório na adaptação ao estresse salino e apontam alvos moleculares promissores para estratégias de melhoramento genético voltadas ao aumento da resiliência do feijão-caupi em ambientes salinizados.

Palavras-chave: Priming ao estresse abiótico; Biologia de sistemas; Aclimatação de plantas.

ABSTRACT

Salinity represents one of the main limiting factors for agricultural productivity, affecting ionic homeostasis, redox balance, metabolism, and plant growth. Although the endoplasmic reticulum (ER) is recognized as an important hub for integrating cellular signals under stress conditions, the mechanisms by which its activation can modulate salt tolerance in cowpea (*Vigna unguiculata* [L.] Walp.) remain incompletely understood. This thesis investigated whether the controlled stimulation of adaptive endoplasmic reticulum signaling, through transient activation of the unfolded protein response (UPR) induced by tunicamycin (TM), could function as a priming mechanism, increasing the efficiency of acclimation to salinity. Foliar application of TM was selected to induce systemic ER signaling without directly altering ion uptake by roots, allowing the controlled activation of adaptive pathways prior to salt exposure. An integrative and temporal approach was employed, combining physiological analyses, Na^+ and K^+ quantification, hydrogen peroxide (H_2O_2) determination, qPCR-based gene expression analysis of unfolded protein response (UPR) markers and ion transporters, as well as metabolomic, lipidomic, and quantitative proteomic analyses in leaves. The results demonstrated that TM priming significantly attenuated the deleterious effects of NaCl, promoting improved photosynthetic performance and enhanced plant growth. A reduction in Na^+ accumulation in the shoot, greater K^+ retention, and increased ionic sequestration in roots were observed, indicating improved ionic homeostasis. TM application induced a rapid and transient ER stress response, characterized by an initial increase in H_2O_2 and early expression of UPR-related genes, with a return to basal levels within 24 hours. Under salinity, plants previously treated with TM exhibited lower H_2O_2 accumulation, earlier and more efficient activation of pathways associated with ER signaling and sodium transport, as well as reduced expression of chaperones and Na^+ transporters. Proteomic analysis revealed that salinity promoted broad metabolic repression, including reductions in enzymes of the Calvin cycle and glycolysis (GAPDH, triose phosphate isomerase) and in ribosomal proteins, whereas TM priming attenuated this suppression and promoted selective reinforcement of the translational machinery and proteins associated with stress adaptation. Metabolomic and lipidomic profiles indicated enhanced osmotic adjustment and membrane remodeling, reinforcing cellular stability under stress conditions. It is concluded that transient ER activation acts as a physiological preconditioning mechanism, coordinating redox regulation, proteostasis, ionic homeostasis, and metabolic reprogramming. These findings expand the understanding of the ER as a regulatory hub in plant adaptation to salt stress and highlight promising molecular

targets for breeding strategies aimed at increasing cowpea resilience in salinized environments.

Keywords: Stress priming; Systems biology; Plant acclimation.

SUMÁRIO

1 INTRODUÇÃO

As mudanças climáticas e a maior frequência de eventos extremos vêm intensificando os desafios enfrentados pela agricultura em diferentes regiões do mundo, afetando a estabilidade dos sistemas produtivos e colocando em risco a segurança alimentar (ROSEGREANT et al., 2024; DENNING, 2025). Entre os fatores ambientais que mais comprometem a produtividade agrícola, a salinização dos solos ocupa posição de destaque, especialmente em regiões semiáridas e em áreas irrigadas onde o manejo inadequado da água favorece o acúmulo de sais (SANGA et al., 2024). O excesso de sal no solo desencadeia uma série de alterações nas plantas, como desequilíbrios iônicos, redução da razão K^+/Na^+, danos às membranas celulares e aumento da produção de espécies reativas de oxigênio (ROS), resultando em limitações ao crescimento e à produtividade das culturas (PRAXEDES et al., 2022; ATTA et al., 2023; ZHOU et al., 2024).

Nesse cenário, o feijão-caupi (*Vigna unguiculata* [L.] Walp.) assume grande relevância social e econômica, sobretudo em regiões tropicais e semiáridas, onde representa uma importante fonte de proteína vegetal e geração de renda para populações vulneráveis (SOUZA et al., 2022; EMBRAPA, 2025). Embora seja reconhecido por sua rusticidade e capacidade de adaptação a ambientes adversos, o desempenho produtivo do caupi ainda é sensível à salinidade, o que evidencia a necessidade de aprofundar o entendimento dos mecanismos que sustentam sua adaptação a essas condições.

A tolerância ao estresse salino não depende de um único processo, mas de uma resposta integrada que envolve ajustes fisiológicos, manutenção da homeostase iônica, reprogramação metabólica e reorganização estrutural das membranas (OBATA; FERNIE, 2012; BALASUBRAMANIAM et al., 2023). A regulação de transportadores de Na^+ e K^+, o acúmulo de osmólitos compatíveis e o equilíbrio do estado redox celular são determinantes para que a planta mantenha sua funcionalidade metabólica sob salinidade (EVELIN et al., 2019; FU; YANG, 2023; ZHOU et al., 2024). Nesse contexto, os transportadores iônicos desempenham papel central na manutenção da homeostase celular. Em condições de estresse salino, o excesso de Na^+ pode causar toxicidade e competir com o K^+ por sítios de ligação em enzimas e proteínas essenciais. Para evitar esses efeitos, as plantas utilizam diferentes sistemas de transporte que regulam a entrada, a extrusão e o compartimentalização desses íons. Entre os principais mecanismos está o sistema SOS (Salt Overly Sensitive), no qual o transportador SOS1, localizado na membrana plasmática, promove a extrusão de Na^+ para o meio externo. Essa atividade é regulada pelo complexo SOS2–SOS3, ativado por sinais de

cálcio gerados após a percepção do estresse salino. Paralelamente, transportadores do tipo NHX, presentes no tonoplasto, sequestram Na^+ para o interior do vacúolo, reduzindo sua concentração no citosol e contribuindo para o ajuste osmótico. Já os transportadores seletivos de K^+ ajudam a manter níveis adequados desse cátion essencial, preservando a atividade enzimática e o potencial osmótico celular (FU; YANG, 2023; ZHOU et al., 2024).

Além disso, a capacidade de perceber precocemente o estresse e integrar esses sinais em respostas sistêmicas mediadas por espécies reativas de oxigênio (EROs), cálcio e hormônios vegetais confere maior plasticidade e potencial de aclimatação (SUZUKI et al., 2012; MITTLER et al., 2022). Esses sinais atuam como mensageiros que coordenam a ativação de genes relacionados ao transporte iônico, à síntese de osmólitos e aos sistemas antioxidantes, permitindo que a planta restabeleça o equilíbrio iônico, osmótico e redox mesmo em ambientes salinizados.

Dentro dessa perspectiva, estratégias de pré-aclimatação, como o *priming* químico, têm despertado interesse crescente por sua capacidade de preparar a planta para enfrentar condições adversas subsequentes (ZULFIQAR et al., 2022). O *priming* estabelece um estado fisiológico prévio que favorece respostas mais rápidas e eficientes, envolvendo modulação redox, ajustes metabólicos e regulação pós-traducional (BRUCE et al., 2007; MAUCH-MANI et al., 2017). Como resultado, plantas previamente condicionadas tendem a apresentar melhor controle do acúmulo de peróxidos, maior estabilidade das membranas e manutenção mais eficiente da homeostase iônica quando expostas à salinidade.

Entre os compartimentos celulares envolvidos na integração desses sinais, o retículo endoplasmático (RE) destaca-se por seu papel central na manutenção da proteostase. Quando a homeostase proteica é perturbada, ativa-se a resposta a proteínas mal dobradas (do Inglês - *Unfolded Protein Response* – UPR), um mecanismo regulatório que amplia a capacidade de dobramento proteico e promove ajustes metabólicos para restabelecer o equilíbrio celular (HOWELL, 2013; LIU; HOWELL, 2016; ALIYA et al., 2024). Em níveis moderados, essa ativação pode contribuir para adaptações benéficas; contudo, sob estresse severo ou prolongado, pode resultar em efeitos prejudiciais ao crescimento (WILLIAMS et al., 2014; RUBERTI et al., 2015).

Nas plantas, a UPR é mediada principalmente por duas ramificações de sinalização: a via IRE1–bZIP60 (do inglês - (*Inositol-Requiring Enzyme* 1 e *Basic Leucine Zipper* 60, respectivamente) e a via dos fatores de transcrição bZIP17/bZIP28 ancorados à membrana do RE. O sensor IRE1, ao perceber o acúmulo de proteínas mal dobradas, ativa sua atividade endorribonuclease e promove o processamento não convencional do mRNA de

bZIP60, cuja forma processada migra para o núcleo e induz genes relacionados ao controle de qualidade proteica, como a chaperona BiP (do Inglês – *Binding protein*), a chaperona residente do RE GRP94 (do Inglês - *Glucose-Regulated Protein* 94) essencial para a maturação de proteínas secretórias, e enzimas redox como PDI (do Inglês – *protein disulfide isomerase*), among others (MARZEC et al., 2012; HOWELL, 2013; YU et al., 2022). Paralelamente, bZIP17 e bZIP28 são transportados ao complexo de Golgi, onde sofrem clivagem proteolítica, liberando domínios ativos que também atuam no núcleo, ampliando a expressão de genes associados à proteostase, ao controle de qualidade no RE e à adaptação ao estresse (LIU; HOWELL, 2016; YU et al., 2022).

Além dos componentes conservados em eucariotos, estudos recentes indicam que a UPR vegetal apresenta características específicas, incluindo a participação de reguladores exclusivos ou expandidos em plantas, como membros outras famílias gênicas, e a integração com vias de sinalização redox, hormonal e metabólica, reforçando o papel do RE como um centro integrador das respostas adaptativas (YU et al., 2022). Dessa forma, a UPR em plantas transcende a simples restauração do dobramento proteico, atuando como mecanismo coordenador entre crescimento, desenvolvimento e tolerância a estresses ambientais.

A tunicamicina, conhecida por inibir a N-glicosilação de proteínas, é amplamente empregada como indutora experimental de estresse no RE (ELBEIN, 1987; IWATA; KOIZUMI, 2005). Estudos recentes sugerem que sua aplicação controlada pode modular vias relacionadas à homeostase iônica e ao metabolismo redox, indicando que a ativação do RE pode participar da regulação da tolerância ao sal (CAVALCANTE et al., 2023; OLIVEIRA et al., 2025). Paralelamente, o aumento da atividade de dobramento proteico no retículo endoplasmático favorece a geração controlada de espécies reativas como o peróxido de hidrogênio (H_2O_2), que pode atuar como molécula sinalizadora, conectando a dinâmica redox do RE à reprogramação transcricional e ao ajuste de mecanismos antioxidantes (ČERNÝ et al., 2018).

Compreender essa rede de interações exige abordagens capazes de integrar diferentes níveis de organização biológica. Nesse sentido, ferramentas ômicas, como a proteômica quantitativa, a metabolômica, a lipidômica e a análise direcionada da expressão gênica, têm se consolidado como estratégias essenciais para mapear redes regulatórias complexas e identificar pontos-chave de controle sob condições de estresse (KOSOVÁ et al., 2018). A integração dessas camadas de informação permite relacionar eventos moleculares iniciais, em nível transcricional e proteico, a alterações no metabolismo primário e secundário, à dinâmica de lipídios de membrana e, consequentemente, a respostas fisiológicas

mais amplas.

Assim, este trabalho busca contribuir para o entendimento integrado de como a ativação do RE se conecta a mecanismos fisiológicos, metabólicos e moleculares associados à tolerância ao estresse salino em feijão-caupi, ampliando a base de conhecimento sobre estratégias de resiliência vegetal em ambientes salinizados.

2 HIPÓTESE

A ativação controlada do retículo endoplasmático funciona como mecanismo integrador capaz de antecipar e coordenar respostas moleculares, metabólicas e fisiológicas que aumentam a tolerância do feijão-caupi ao estresse salino.

3 OBJETIVOS

3.1 Objetivo geral

Investigar, por meio de uma abordagem ômica integrada, como a ativação transitória do retículo endoplasmático induzida por tunicamicina aplicada via foliar modula mecanismos moleculares, metabólicos e fisiológicos associados à tolerância ao estresse salino em feijão-caupi (*Vigna unguiculata* [L.] Walp.).

3.2 Objetivos específicos

- Caracterizar a dinâmica temporal da sinalização redox associada à ativação da UPR, avaliando a produção precoce e tardia de H_2O_2 como possível elo entre estresse do RE e reprogramação adaptativa sob priming e salinidade.
- Avaliar a expressão de genes relacionados à UPR e ao transporte iônico, a fim de identificar conexões entre a ativação do retículo endoplasmático e os mecanismos de homeostase Na^+/K^+.
- Mapear alterações proteômicas associadas à ativação do RE, com ênfase em proteínas envolvidas na proteostase, regulação redox e ajuste metabólico sob estresse salino.

- Investigar ajustes metabólicos e lipídicos associados ao estado “pré-condicionado”, relacionando-os à manutenção da integridade estrutural e funcional sob salinidade.
- Integrar dados fisiológicos, moleculares e proteômicos, estabelecendo um modelo explicativo que conecte a ativação do retículo endoplasmático aos mecanismos de tolerância ao estresse salino em feijão-caupi.

4 CAPÍTULO I: LEAF-APPLIED TUNICAMYCIN-INDUCED PRIMING ENHANCES SALINITY TOLERANCE IN *Vigna unguiculata* [L.] Walp.

4.1 Abstract

Salinity severely limits crop productivity by disrupting ionic homeostasis, redox balance, photosynthesis, and plant growth. Although endoplasmic reticulum (ER) stress signaling has been recognized as a regulator of plant stress acclimation, its role in cowpea (*Vigna Unguiculata* [L.] Walp.) salt tolerance remains unclear. In this study, we evaluated whether foliar tunicamycin (TM) priming, an ER stress inducer, enhances NaCl tolerance by promoting physiological, molecular, and metabolic responses in cowpea. Overall, foliar TM priming alleviated the negative effects of salinity. Under NaCl treatment, TM-treated plants exhibited improved photosynthetic performance and growth, associated with a favorable ionic balance, including reduced Na^+ accumulation in shoots, enhanced K^+ retention, and increased ion sequestration in roots. These responses were accompanied by tissue-specific modulation of ER stress and ion homeostasis-related genes. Under salinity, TM priming increased the expression of transcripts corresponding to the *V. unguiculata* orthologs of *VubZIP60* and *VuIRE1A* in both leaves and roots, whereas transcript levels of the orthologs *VuBiP1*, *VuPDI11, VuGRP94*, *VuNHX1*, and *VuSOS1* were downregulated relative to plants exposed to only salt stress. TM priming also mitigated salinity-induced oxidative stress, as indicated by reduced H_2O_2 accumulation in TM-primed plants under salinity. Metabolomic analysis revealed a higher relative abundance of carbohydrates associated with osmotic adjustment, while lipidomic profiling indicated modulation of membrane-related lipid classes. Taken together, these results indicate that prior ER induction by TM triggers coordinated transcriptional, ionic, and metabolic responses that enhance salt tolerance in cowpea.

Keywords: UPR. Metabolic reprogramming. Abiotic stress tolerance

4.2 Introduction

Climate change poses a significant threat to agricultural productivity, undermining global efforts to eradicate food scarcity (Rosegrant et al., 2024). Hence, actions focused on food security, coupled with investments in innovative technologies for sustainable agriculture, are essential to ensure the availability of accessible and nutritious food worldwide (UNICEF, 2025). A variety of mitigation strategies have been developed to enhance plant resilience, including improved irrigation techniques, foliar treatments, the application of exogenous compounds that activate plant defense mechanisms, the use of beneficial microorganisms, and the development of stress-tolerant genotypes to alleviate water deficit and heat stress (Terán & Pérez-Clemente, 2024). Future directions should prioritize the study of traditional crops and integrate efficient input use with agroecological practices to boost yields while reducing environmental impacts (Denning, 2025). Moreover, clarifying the metabolic pathways underlying stress signaling will be crucial for advancing genetic improvement and guiding the selection of stress-tolerant genotypes.

Cowpea (*Vigna unguiculata* [L.] Walp.) stands out as a promising crop for alleviating food scarcity in vulnerable regions (Kim et al., 2025). It is a legume of considerable social and economic importance. Cowpea is an eudicotyledonous species belonging to the Fabaceae family, originally from the African continent and widely cultivated throughout Brazil due to its remarkable ability to adapt to high temperatures and low rainfall conditions (Souza et al., 2022; Embrapa, 2025). Furthermore, it is a versatile crop frequently used in crop rotation systems and provides a valuable source of proteins, fibers, minerals, and B-complex vitamins, thereby contributing simultaneously to soil quality, human nutrition, and food security (Freitas et al., 2022; Souza et al., 2022). In Brazil, particularly in the semiarid Northeast, cowpea stands out as a traditional crop, which is a dietary staple and an important source of income for low-income households (EMBRAPA, 2025). Cowpea growth, development, and productivity can be affected by both biotic and abiotic factors, including nutrient deficiencies, drought, temperature fluctuations, light intensity, and salinity (Freitas et al., 2012). Among these stresses, soil salinization in irrigated systems, especially in semiarid tropical regions, emerges as one of the most significant abiotic constraints limiting crop productivity (Sanga et al., 2024).

Salt stress is a multifactorial condition that involves the interaction of osmotic, ionic, and oxidative components. Initially, reduced soil water potential imposes osmotic stress, limiting water uptake and impairing turgor and photosynthetic performance.

Subsequently, excessive accumulation of toxic ions, particularly Na^+, disrupts nutrient homeostasis by decreasing the K^+/Na^+ ratio, destabilizing cellular membranes, and interfering with metabolic processes. These disturbances enhance reactive oxygen species (ROS) production, intensify oxidative stress, and ultimately reduce growth, biomass accumulation, and productivity in salt-sensitive crops such as cowpea (Praxedes et al., 2022; Atta et al., 2023; Zhou et al., 2024; Souza et al., 2025).

To help plants better cope with abiotic stress, pre-acclimation strategies such as chemical priming have been increasingly investigated (Zulfiqar et al., 2022). These approaches induce faster and more efficient responses to adverse conditions by triggering physiological and biochemical adjustments that enhance plant tolerance to future stress events (Sahoo et al., 2025). Beyond establishing stress memory, chemical priming creates a physiological state characterized by adjustments in ion homeostasis and extensive metabolic and lipid remodeling, preparing plants to respond more efficiently to subsequent stress exposure (Zulfiqar et al., 2022). A primed state allows the modulation of ion transport and osmotic balance to maintain favorable K^+/Na^+ ratios, preventing ionic toxicity and preserving membrane integrity under saline conditions (Fu and Yang, 2023). At the metabolic level, primed plants often accumulate amino acids and organic acids that act as compatible solutes, contributing to osmotic adjustment and redox regulation (Evelin et al., 2019). In parallel, lipid remodeling supports membrane stability and signaling during salt stress by adjusting phospholipid and galactolipid composition (Guo et al., 2022). These combined adjustments improve cellular homeostasis and reduce oxidative damage, as reflected by decreased peroxide accumulation, ultimately enhancing tolerance to subsequent salinity exposure (Zulfiqar et al., 2022).

Salt tolerance in plants manifests across multiple biological levels, encompassing phenotypic and physiological changes, ionic adjustments, metabolic shifts, and activation of regulatory networks (Balasubramaniam et al., 2023; Zhou et al., 2024). The maintenance of structural and osmotic integrity relies on coordinated metabolic and lipid adjustments, including the accumulation of sugars, amino acids, and osmoprotectants, as well as membrane lipid remodeling. In parallel, the regulation of ion transporters contributes to the control of Na^+ exclusion and compartmentalization, helping to maintain cellular ionic balance under saline conditions (Obata and Fernie, 2012). Moreover, the preservation of photosynthetic efficiency and redox balance plays a central role in translating these cellular adjustments into improved physiological performance under salinity stress (Chaves et al., 2009; Miller et al., 2010; Zhao et al., 2020).

Recent studies indicate that some of these adaptive responses are linked to signaling pathways associated with endoplasmic reticulum (ER) stress. Modulation of ER stress sensors such as *SbbZIP60*, membrane transporter genes (*SbNHX1* and *SbSOS1*), and ER chaperones such as *SbPDI* suggests that controlled activation of ER stress responses can reprogram cellular homeostasis under salinity. Collectively, these findings indicate that chemical priming with ER stress inducers, such as tunicamycin (TM) and dithiothreitol (DTT), may enhance salt acclimation by improving ion regulation, activating stress-related metabolic pathways, and modulating unfolded protein response (UPR)-related gene expression, thereby strengthening plant tolerance to salinity.

Recently, tunicamycin (TM) has been described as a potential chemical seed priming agent, it acts as an endoplasmic reticulum (ER) stress inducer that promotes salt acclimation in rice seedlings (Oliveira et al., 2025). This treatment enhances biomass production, maintains stable potassium (K^+) levels, reduces sodium (Na^+) accumulation and reactive oxygen species (ROS), and activates osmoprotectant metabolites and ER-related genes such as *OsIRE1*, *OsbZIP50*, and *OsbZIP60*. Indeed, tunicamycin is a nucleoside antibiotic that inhibits N-linked glycosylation by preventing the transfer of N-acetylglucosamine to nascent polypeptides, leading to the accumulation of misfolded proteins in the endoplasmic reticulum (ER) and consequent activation of the unfolded protein response (UPR) to deal with this stress (Takatsuki et al., 1971; Elbein, 1987; Iwata and Koizumi, 2005).

In plants, the UPR is primarily mediated by two major signaling branches: the IRE1–bZIP60 pathway and the membrane-associated transcription factors bZIP17 and bZIP28. Under non-stress conditions, ER-resident chaperones such as BiP bind to luminal domains of these sensors, maintaining them in an inactive state. Upon accumulation of unfolded proteins, BiP dissociates to assist in protein folding, allowing sensor activation. Activated IRE1 undergoes oligomerization and autophosphorylation, triggering its endoribonuclease activity, which catalyzes the unconventional splicing of bZIP60 mRNA. The spliced form encodes an active transcription factor lacking the transmembrane domain, enabling its translocation to the nucleus, where it induces genes associated with protein folding (BiP, GRP94), disulfide bond formation (PDI), ER-associated degradation (ERAD), and redox balance. In parallel, bZIP17 and bZIP28 are transported from the ER to the Golgi apparatus, where they undergo regulated intramembrane proteolysis. The released cytosolic domains then migrate to the nucleus and activate overlapping but partially distinct sets of stress-responsive genes, expanding ER folding capacity and reinforcing adaptive responses.

Beyond restoring proteostasis, UPR activation also influences redox homeostasis, metabolic reprogramming, and ion transporter regulation, linking ER stress signaling to broader stress acclimation mechanisms. The UPR has proven effective in reprogramming cellular homeostasis and stress signaling, as demonstrated by recent studies (Ko and Brandizzi, 2024; Liu et al., 2022). In contrast, prolonged TM exposure can intensify stress, reduce the expression of ER-related genes, and impair primary metabolism (Lima et al., 2022). Conversely, low to moderate ER stress can activate the UPR and induce differential stress tolerance among Sorghum bicolor varieties (Cavalcante et al., 2023). Moreover, the combined application of NaCl and ER stress inducers mitigates the harmful effects of salt stress by maintaining growth parameters and reducing Na^+ accumulation (Queiroz et al., 2020).

Despite these advances, the role of ER-mediated priming induced by TM in Fabaceae species, such as cowpea, remains largely unexplored in an integrated framework linking molecular, metabolic, and physiological responses. Therefore, we hypothesized that TM foliar spraying activates the ER as a priming signal, leading to enhanced salt tolerance in cowpea. To test this hypothesis, we analyzed ionic homeostasis, photosynthetic efficiency, antioxidant control, primary metabolism, and lipid reprogramming associated with salt stress responses. Thus, this study aimed to elucidate, in an integrated manner, the physiological, biochemical, metabolic, and molecular mechanisms underlying salt stress tolerance, highlighting the central role of ER activation and metabolic reprogramming in TM-induced acclimation.

4.3 Material and methods

4.3.1 Plant material and experimental design

Cowpea (*Vigna unguiculata* [L.] Walp.) seeds were obtained from the Germplasm Bank of the Department of Crop Science at the Federal University of Ceará (UFC; accession CE088) and germinated in vermiculite until the V2 stage. Seedlings were then transferred to a hydroponic system containing one-quarter-strength Hoagland's nutrient solution and grown until the V4 stage (third fully expanded trifoliate leaf). At this stage, plants were subjected to foliar priming by uniformly spraying 1 mL of solution per plant onto all fully expanded leaves from a distance of approximately 15 cm, ensuring homogeneous surface coverage. The tunicamycin (TM) stock solution was prepared by dissolving TM in dimethyl sulfoxide

(DMSO). For foliar priming, the stock was diluted in distilled water containing 0.05% (v/v) Tween 20 to obtain a final TM concentration of 0.25 μg mL^{-1}. Control plants received distilled water supplemented with 0.05% (v/v) Tween 20 (Oliveira et al., 2025).

Two complementary experiments were conducted under greenhouse conditions at different periods. The first experiment (April–May 2024) focused on morphological, physiological, biochemical, and molecular analyses, whereas the second experiment (July–August 2025) evaluated gas exchange and leaf thermography using the same experimental design and priming strategy. Plants were grown under comparable greenhouse conditions in both experiments, with average daytime temperatures ranging from 31.8 to 33.5 °C and nighttime temperatures from 26.0 to 26.5 °C.

Throughout the experimental period, plants were grown under controlled greenhouse conditions, with comparable average daytime and nighttime temperatures across experiments (approximately 33.5-31.8 °C during the day and 26.5-26.0 °C at night). At the end of the experimental period, leaf, stem, and root tissues were harvested for subsequent physiological, biochemical, and molecular analyses.

After 24 h of priming, plants were transferred to nutrient solutions either without salt (0 mM NaCl) or gradually supplemented with NaCl in daily aliquots of 37.5 mM until reaching a final concentration of 75 mM NaCl, following an adaptation of the method described by Praxedes et al. (2014). Nutrient solutions were continuously aerated, renewed every three days, and maintained at pH 5.5. The experimental design consisted of four treatments:

- Control: foliar spray with desalinated water + 0.05% Tween 20; plants maintained under non-saline conditions (0 mM NaCl).
- TM: foliar spray with TM solution (0.25 μg mL^{-1} + 0.05% Tween 20); plants maintained under non-saline conditions (0 mM NaCl).
- 75 mM NaCl: foliar spray with desalinated water + 0.05% Tween 20; plants exposed to gradual salinization up to 75 mM NaCl.
- TM + 75 mM NaCl: foliar spray with TM solution (0.25 μg mL^{-1} + 0.05% Tween 20); plants exposed to gradual salinization up to 75 mM NaCl.

At the designated sampling time, all fully expanded leaves were harvested, immediately processed or stored as appropriate, and used for the respective physiological, biochemical, and molecular analyses.

4.3.2 Morphological and growth assessments

After harvest, plants were photographed to document and compare morphological changes. Subsequently, plant tissues were dried in a forced-air oven at 60 °C for 72 h, and dry mass was determined using an analytical balance.

4.3.3 Ion analyses

To quantify Na^+ and K^+ contents, 50 mg of dried leaf, stem, and root material were individually homogenized in 5 mL of deionized water. The homogenates were incubated in a water bath at 75 °C for 1 h, mixing every 20 min, and centrifuged at 3,000 × g for 10 min at room temperature. Ion concentration readings were obtained using a flame photometer (Micronal®, model B462), with 1.0 M NaCl and 1.0 M KCl standard solutions, according to Malavolta et al. (1997). For chloride (Cl^-) determination, the method was based on the reaction of Cl^- with $Hg(SCN)_2$, resulting in the formation of $HgCl_2$ and the release of SCN^-. Briefly, 2 mL of the homogenate (leaf, stem, or root) was mixed with 5 mL of 0.06% $Hg(SCN)_2$ and $Fe_2(SO_4)_3$ solution. Absorbance was measured at 450 nm using a SynergyMx Biotek spectrophotometer, and Cl^- concentrations were quantified using a standard calibration curve (Schales and Schales, 1941; Silva, 1999).

4.3.4 Gas exchange measurements

Gas exchange measurements were performed 14 days after salt exposure, prior to harvest, at 09:00 h. Net photosynthetic rate (*A*), transpiration rate (*E*), stomatal conductance (*gs*), and internal CO_2 concentration (*Ci*) were measured using an infrared gas analyzer (IRGA; LI-6400XT, LI-COR, USA), with a reference CO_2 concentration of 400 μmol mol^{-1} and an artificial light intensity of 1.200 μmol m^{-2} s^{-1} applied to the middle third of the third fully expanded leaf.

4.3.5 Leaf thermography

Thermal images of leaves were captured at 24 h, 7 days, and 14 days after salt exposure using a FLIR (Forward Looking Infrared) CX-series C5 thermal camera. Images were acquired in manual mode at an approximate distance of 30 cm from the leaves, around

12:00 h on cloudless days (Gómez-Bellot et al., 2015), using a rainbow color palette to enhance thermal contrast. Average leaf temperatures were obtained from the same central leaflet using the Ellipse tool. Differential temperature (ΔT) was calculated as the difference between leaf temperature and ambient temperature at each time point.

4.3.6 Hydrogen peroxide content

Extracts were prepared by macerating 200 mg of fresh plant tissue in 1 mL of 5% (w/v) trichloroacetic acid (TCA) for 2 min. The homogenate was centrifuged at 12,000 × g for 15 min at 4 °C. For H_2O_2 determination, the reaction mixture consisted of 100 µL of the TCA extract, 100 µL of 10 mM potassium phosphate buffer (pH 7.0), and 200 µL of 1 M potassium iodide (Velikova et al., 2000). Hydrogen peroxide content was quantified using a standard curve and measured at 390 nm.

4.3.7 Metabolic and lipid profiling

Metabolite and lipid profiles were obtained using gas chromatography coupled to mass spectrometry (GC–MS; QP-PLUS 2010, Shimadzu, Japan). For metabolite extraction, approximately 50 mg of tissue was sequentially mixed with methanol, chloroform, and ultrapure water. The upper polar aqueous-methanol phase (200 µL) was collected (Lisec et al., 2006). Lipid extraction was performed using 300 mg of frozen tissue, and 200 µL of the lower chloroform phase (non-polar fraction) was collected (Bligh and Dyer, 1959). All aliquots were dried in a vacuum concentrator at room temperature.

For derivatization, dried extracts were treated with N-methyl-N-(trimethylsilyl)-trifluoroacetamide (MSTFA) and incubated with shaking at 37 °C for 30 min (Lisec et al., 2006). Metabolic profiling was performed by injecting 1 µL of the derivatized sample in split mode (1:5). Helium was used as the carrier gas at a flow rate of 1.2 mL min^{-1}, and separation was achieved on an RTX-5MS capillary column (30 m × 0.25 mm × 0.25 µm). The oven temperature was initially set at 80 °C for 2 min, increased at 10 °C min^{-1} to 315 °C, and held for 8 min. The injection port and ion source temperatures were set at 250 °C, and the MS interface at 230 °C. Mass spectra were acquired at 70 eV over a scan range of 40–700 m/z, with a solvent delay of 3 min.

Lipid profiling was performed by injecting 1 µL of each sample in split mode (1:15), with an injection temperature of 300 °C. Helium was used as the carrier gas at a

pressure of 1.8 kPa, a flow rate of 1.6 mL min^{-1}, and a linear velocity of 46.6 cm s^{-1}. The oven temperature was initially set at 80 °C for 5 min, then increased at 4 °C min^{-1} to 300 °C and held for 45 min.

Chromatograms and mass spectra were analyzed using Xcalibur™ 2.1 software and compared with the Golm Mass Spectral Library, NIST 14, or analytical-grade standards. Relative metabolite abundance was calculated by normalizing peak areas to ribitol (metabolomics) or cholesterol (lipidomics) internal standards and fresh tissue weight. Metabolites were identified and classified using the Kyoto Encyclopedia of Genes and Genomes (KEGG) and PubChem databases.

4.3.8 Expression profile by RT-qPCR

For gene expression analysis, plants were sampled 14 days after transfer to the saline solution. Total RNA was isolated from leaves using the TRIzol™ Total RNA Isolation System (Promega Corporation), according to the manufacturer's protocol. Extracted RNA was quantified using an Epoch spectrophotometer, and its integrity was verified by electrophoresis on a 1.5% (w/v) agarose gel using a Pharmacia Biotec electrophoresis system operated at 100 V and 50 mA. Complementary DNA (cDNA) was synthesized using Moloney Murine Leukemia Virus (M-MLV) Reverse Transcriptase (Promega Corporation), following the manufacturer's instructions.

Quantitative real-time PCR (RT-qPCR) was performed using the CFX Opus 96 Dx system (Bio-Rad), based on fluorescence detection, following the manufacturer's instructions. *VuUBQ3* (*Ubiquitin 3*) and *VuF-box3* (*F-box Protein 3*) were used as reference genes to normalize cDNA levels in each reaction. Primers for target genes related to endoplasmic reticulum (ER) response and salt transport were designed using Primer3 software (Untergasser et al., 2012), based on sequences retrieved from public databases. All primer pairs were subsequently evaluated for specificity using BLASTn against the cowpea genome (Phytozome) to avoid off-target amplification (Supplementary Table S1). Primer efficiency was determined by standard curve analysis and ranged from 90% to 110%. Relative gene expression levels were calculated using mean Ct values according to the $2^{-\Delta\Delta Ct}$ method (Livak and Schmittgen, 2001).

4.3.9 Statistical analysis

The results were analyzed using a 2 × 2 factorial design, comprising two levels of TM spraying (0 and 0.25 μg mL^{-1}) and two NaCl concentrations (0 and 75 mM) in hydroponic solution. Data were subjected to analysis of variance (ANOVA), and mean comparisons were performed using Tukey's test ($p \leq 0.05$) with the SISVAR statistical software (Ferreira, 2014).

For metabolomic and lipidomic analyses, the MetaboAnalyst 6.0 web platform was used (Pang et al., 2024). Data was log-transformed and Pareto-scale prior to multivariate analysis. Partial least squares–discriminant analysis (PLS-DA) was performed separately for leaves and roots, and variable importance in projection (VIP) scores greater than 1.0 were used to identify the main discriminating metabolites. Model performance was evaluated based on goodness of fit (R^2 close to 1.0) and predictive ability ($Q^2 > 0.4$), indicating good reliability and absence of overfitting, which was further confirmed by permutation tests (Supplementary Table S2).

Mean metabolite values were compared using Tukey's test ($p \leq 0.05$) with the SISVAR statistical software. For enrichment analyses (over-representation analysis, ORA), metabolites showing significant differences in the Tukey test were used in the following pairwise comparisons: TM + 75 mM NaCl vs. 75 mM NaCl; control vs. 75 mM NaCl; and control vs. TM.

4.4 Results

4.4.1 TM priming alleviates salinity-induced growth inhibition in cowpea

Plant growth parameters were evaluated to determine whether TM priming could mitigate the inhibitory effects of salinity on cowpea development. Salinity markedly impaired plant growth, as shown in Figure 1A and Supplementary Table S3. Significant reductions in leaf, stem, and root biomass were observed, resulting in smaller plant size compared with the control treatment. TM pre-treatment alone did not differ from the control, indicating that TM application under non-saline conditions did not affect growth. In contrast, plants subjected to TM + 75 mM NaCl exhibited greater size and vigor than those exposed to salt stress alone. Increases of 61%, 86%, and 70% in leaf, stem, and root biomass, respectively, were observed in the TM + 75 mM NaCl treatment relative to the 75 mM NaCl treatment (Figures 1B–D).

Figure 1 - Growth parameters of cowpea plants measured 14 days after salt stress. (A) Plant phenotype, (B) Leaf dry mass (LDM), (C) Stem dry mass (SDM), (D) Root dry mass (RDM). V4 stage cowpea plants were sprayed with tunicamycin or water (TM and Control, respectively) as priming for 24 h, and grown in 0 mM NaCl (control), or 75 mM NaCl. Values are the average of 5 replications, and bars represent standard error. The four treatments were compared by presence or absence of foliar priming and salt levels using the Tukey test (p<0.05). Lowercase letters compare treatments (Control and TM). Uppercase letters compare salinity (with and without NaCl).

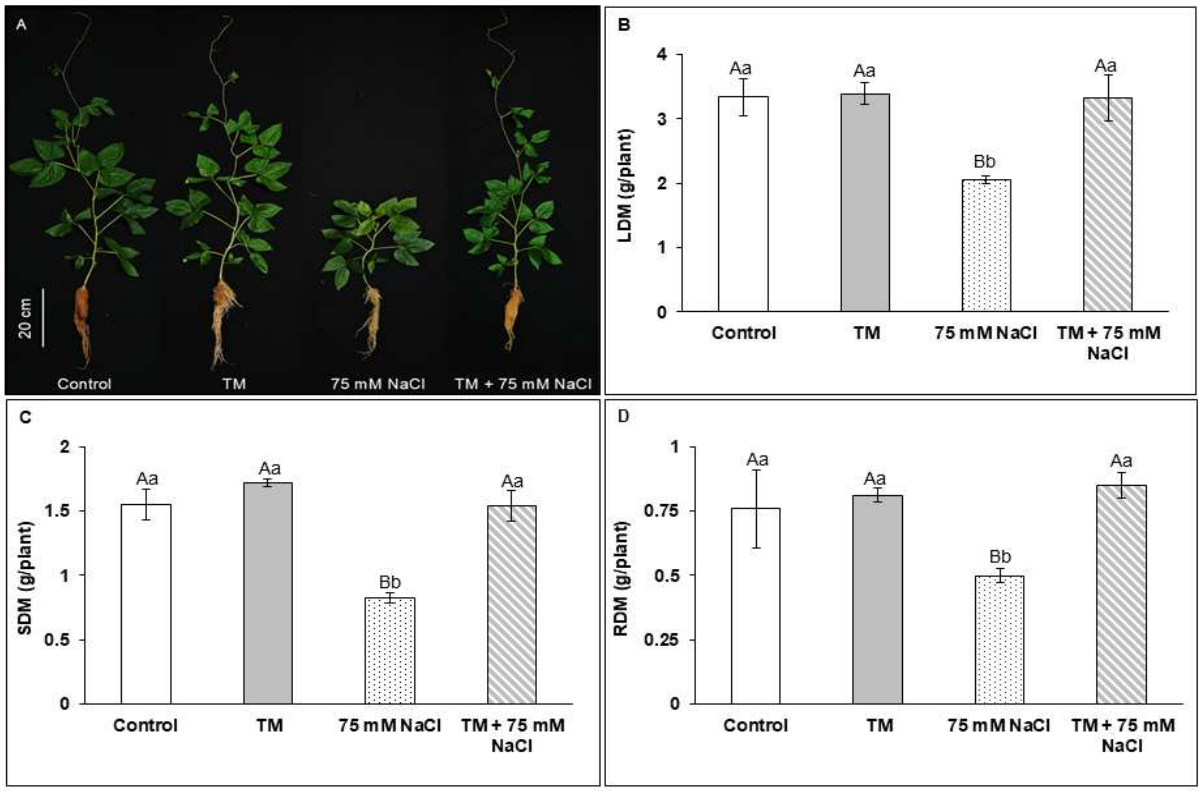

Source: Prepared by the author.

4.4.2 TM priming modulates ion distribution and improves ionic homeostasis under salinity

The concentrations of Na^+, K^+, and Cl^- were quantified in different cowpea organs to assess whether TM priming affects ionic homeostasis under saline conditions (Figure 2, Supplementary Table S4). Overall, TM priming markedly altered the distribution of ions within the plants. In TM-primed plants exposed to salinity, Na^+ and Cl^- concentrations were reduced in leaves and stems, whereas higher amounts of these ions accumulated in the roots compared with non-primed plants. In contrast, K^+ exhibited an opposite distribution pattern, with reduced levels in roots and increased accumulation in leaves and stems.

Figure 2 - Radar graph of inorganic ion content in different parts of cowpea plants measured 14 days after salt stress. Leaf, stem, and root of V4 plants after 14 days of the treatments: control, 75 mM NaCl, TM, and TM + 75 mM NaCl. Sodium (Na^+), potassium (K^+), and chloride (Cl^-) values are the average of 5 replications and bars represent standard error. The four treatments were compared by presence or absence of foliar priming and salt levels using the Tukey test (p<0.05). Lowercase letters compare treatments (Control and TM). Uppercase letters compare salinity (with and without NaCl). Detailed Statistical analysis is provided in supplementary Table S3.

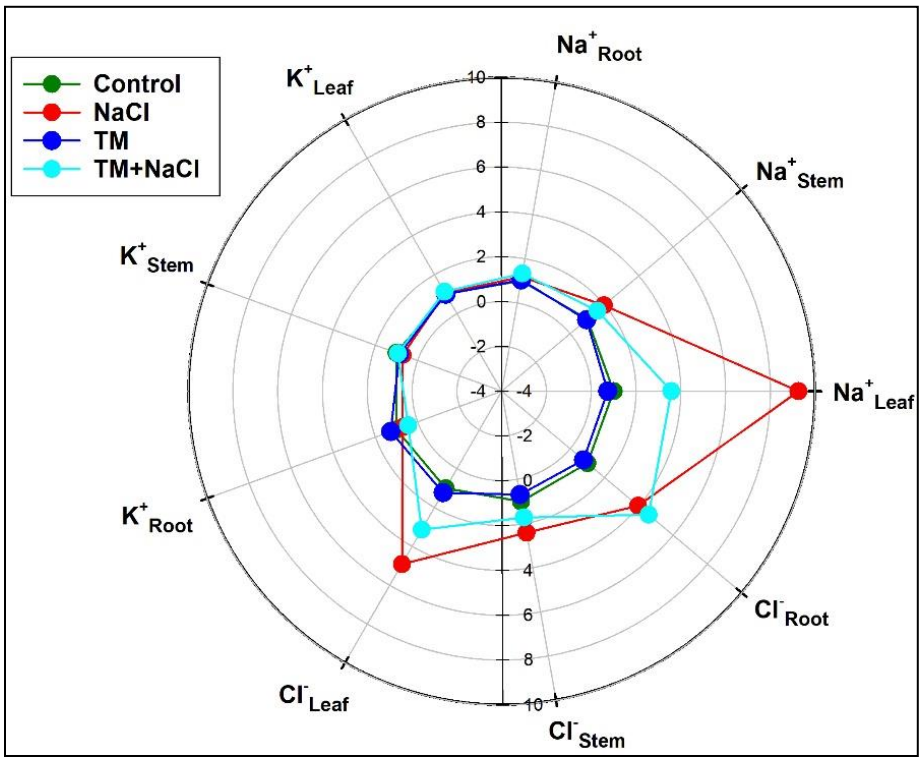

Source: Prepared by the author.

4.4.3 TM priming sustains gas exchange and improves thermal regulation under salinity

Gas exchange parameters were evaluated to determine whether TM priming could mitigate the effects of salinity on photosynthetic performance and stomatal regulation in cowpea. Both salinity and TM priming significantly affected photosynthetic activity and gas exchange. For the net carbon assimilation rate (A), a significant interaction between salinity and TM was observed (Figure 3A; supplementary Table S3). Under non-saline conditions, no differences were detected between control and TM treatments, whereas TM + 75 mM NaCl plants exhibited higher A than plants exposed to 75 mM NaCl alone and showed the highest values overall.

Stomatal conductance (*gs*) followed a similar pattern. Salinity markedly reduced *gs*; however, TM + 75 mM NaCl plants maintained significantly higher *gs* compared with the 75 mM NaCl treatment, with no differences observed between control and TM under non-saline conditions (Figure 3B). The intercellular-to-ambient CO_2 ratio (*Ci/Ca*; Figure 3C) and transpiration rate (*E*; Figure 3D) were also influenced by salinity and TM priming. Under saline conditions, TM + 75 mM NaCl plants exhibited lower Ci/Ca ratios and higher E values than plants subjected to salt stress alone, while no significant differences were observed between control and TM treatments. Considering the treatment effects, significant differences were detected between control and 75 mM NaCl, as well as between TM and TM + 75 mM NaCl, for *gs, Ci/Ca*, and *E*. These results indicate that TM priming consistently mitigated salinity-induced limitations on gas exchange, contributing to improved photosynthetic performance under saline conditions.

Figure 3 - Gas exchange parameters of cowpea plants after 14 days of salt stress. (A) Assimilation rate, (B) stomatal conductance (*gs*), (C) Internal and ambiental carbon, and (D) Transpiration. Values are the average of 3 replications, and bars represent standard error. The four treatments were compared based on presence or absence of foliar priming and salt levels using the Tukey test (p<0.05). Lowercase letters compare treatments (Control and TM). Uppercase letters compare salinity (with and without salt).

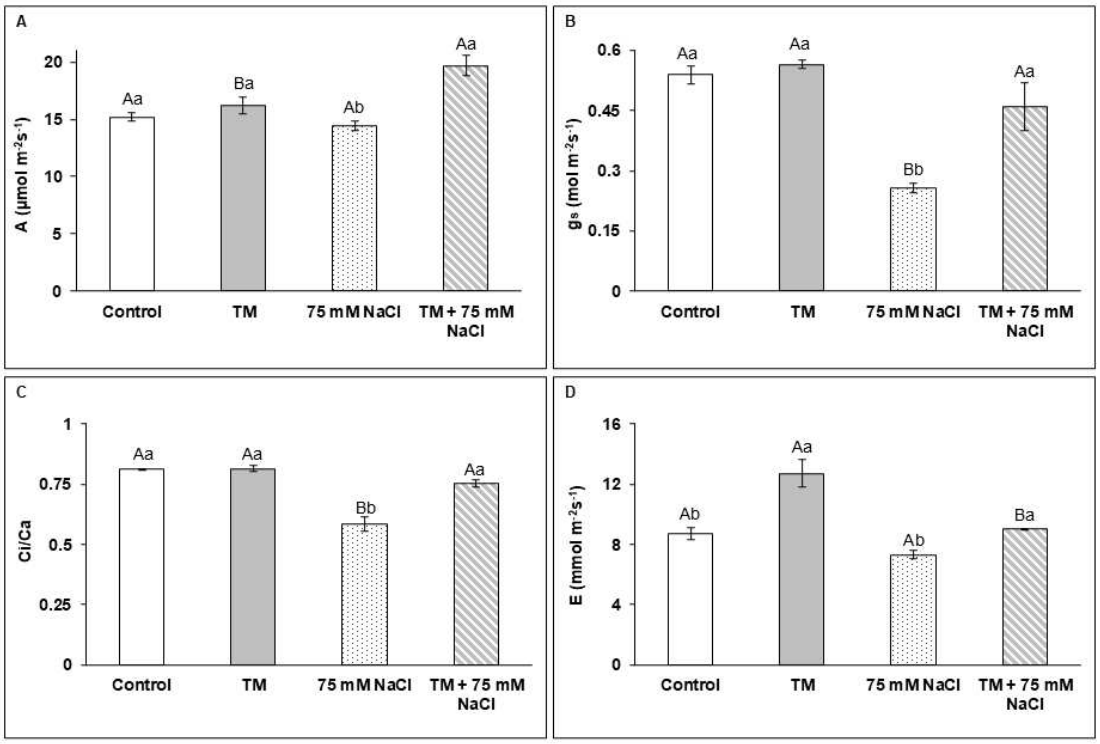

Source: Prepared by the author.

Leaf temperature variation (ΔT) was evaluated to determine whether TM priming modulates thermal regulation in cowpea under saline conditions (Figure 4). Salinity significantly increased ΔT, whereas TM priming attenuated this effect. At 14 days after salt exposure, ΔT values remained higher in salt-treated plants compared with TM + 75 mM NaCl plants, while control and TM treatments showed similar values, as evidenced by the thermal images (Figures 4B–E). Significant differences were detected between control and 75 mM NaCl treatments, as well as between TM and TM + 75 mM NaCl. Temporal analysis further supported these findings (Supplementary Figure S1) in which shows ΔT values measured at 24 h and 7 days after the onset of salinity. Over this period, plants exposed to salt stress exhibited a progressive increase in ΔT, whereas TM + 75 mM NaCl plants maintained consistently lower ΔT values.

Figure 4 - Thermal analysis of cowpea plants after 14 days of salt stress. (A) Leaf temperature variance and (B, C, D, and E) thermal images. Values are the average of 4 replications, and bars represent standard error. The four treatments were compared based on presence or absence of foliar priming and salt levels using the Tukey test ($p<0.05$). Lowercase letters compare treatments (Control and TM). Uppercase letters compare salinity (with and without NaCl). ANOVA is provided in supplementary Table S3.

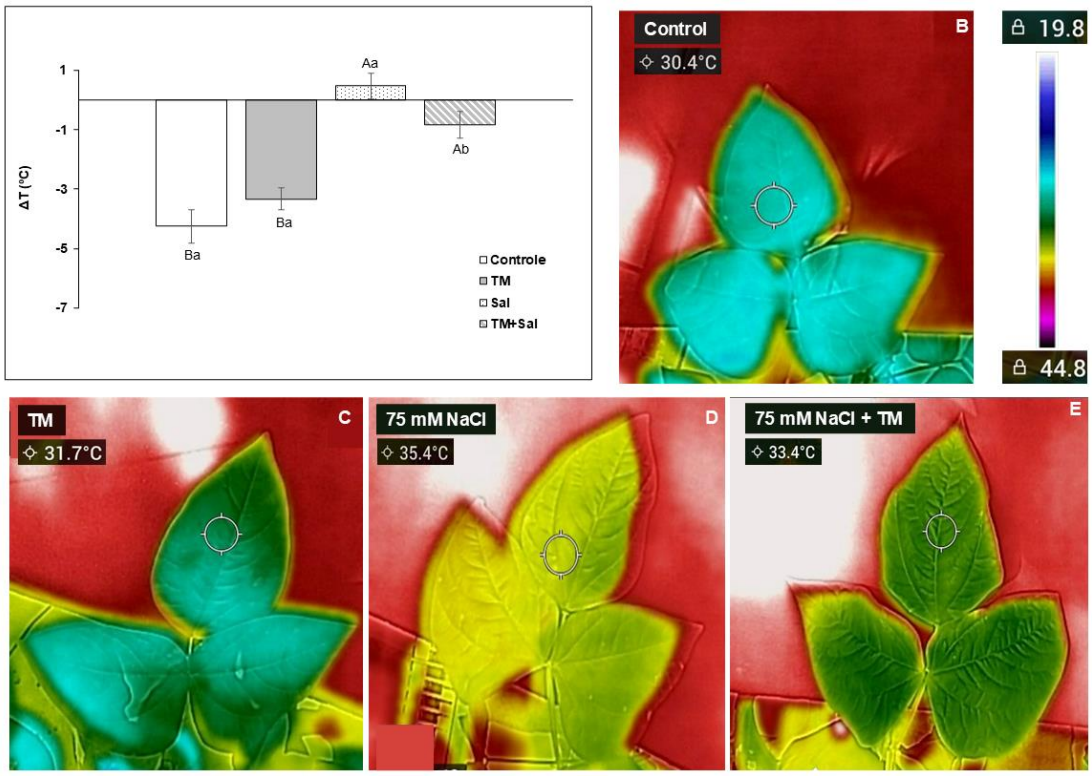

Source: Prepared by the author.

4.4.4 TM priming modulates salinity-induced oxidative stress in leaves and roots

Hydrogen peroxide (H_2O_2) levels were quantified in leaves and roots to assess whether TM priming influences oxidative responses under salinity (Supplementary Table S3). Both salinity and TM priming significantly affected H_2O_2 accumulation. In leaves, salt-treated plants (75 mM NaCl) exhibited higher H_2O_2 levels compared with control and TM treatments, whereas TM + 75 mM NaCl markedly reduced this accumulation (Figure 5A). In roots, H_2O_2 levels were also elevated under salinity but decreased significantly in TM-primed plants, with clear differences between the 75 mM NaCl and TM + 75 mM NaCl treatments (Figure 5B). Notably, TM treatment alone did not differ from the control, indicating that TM effects were specific to stress conditions. Overall, these results show that salinity enhanced oxidative stress through increased H_2O_2 accumulation, while TM priming effectively moderated this response, reducing oxidative stress without altering basal H_2O_2 levels under non-saline conditions.

Figure 5 - Hydrogen peroxide (H_2O_2) concentration in cowpea plants measured 14 days after salt stress. (A) leaves, and (B) roots. V4 stage cowpea plants were grown in control, 75 mM NaCl, TM, and TM + 75 mM NaCl treatments. Values are the average of 5 replications, and bars represent standard error. The four treatments were compared using the Tukey test (p<0.05). Lowercase letters compare treatments (Control and TM). Uppercase letters compare salinity (with and without NaCl).

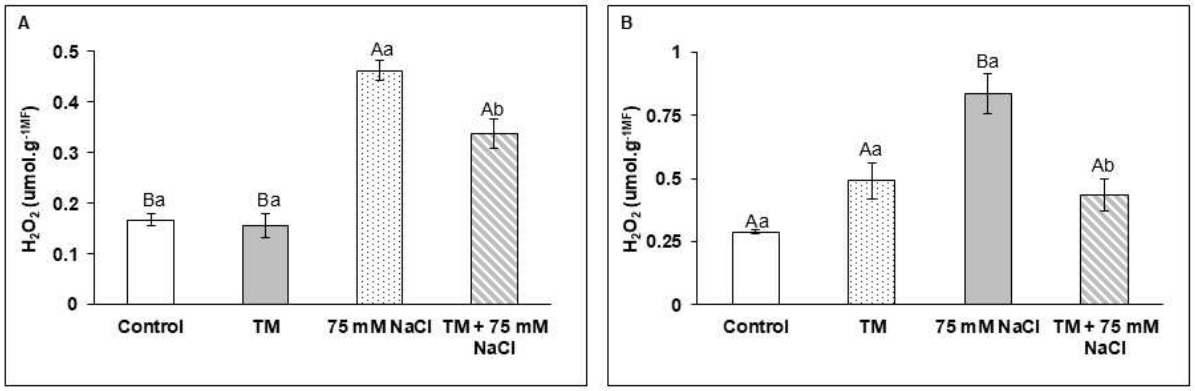

Source: Prepared by the author.

4.4.5 TM priming reshapes metabolic and lipid profiles in leaves and roots under salinity

Metabolic and lipid profiling by GC–MS was performed to determine whether TM priming induces coordinated metabolic reprogramming in cowpea leaves and roots under

salinity. A total of 50 metabolites were detected in the metabolomic analysis, including carbohydrates, organic acids, and amino acids (Supplementary Table S5). In addition, 27 lipid-related compounds associated with lipid biosynthesis and membrane composition were identified across treatments (Supplementary Table S6).

In leaves, score plots revealed a clear separation of the 75 mM NaCl treatment from the other groups, with PC1 and PC2 accounting for 17.0% and 20.7% of the total variance, respectively, although a slight overlap with the control treatment was observed (Figure 6A). In roots, partial overlaps occurred between control and salt, as well as between control and TM treatments; however, overall discrimination among the four treatments was evident, particularly for TM + 75 mM NaCl, with PC1 and PC2 explaining 44.2% and 28.9% of the total variance, respectively (Figure 6B). For lipidomic profiles, PLS-DA of leaf samples showed a similar pattern to that observed in leaf metabolomics, with clear separation among all treatments (Figure 6C). In roots, the NaCl treatment was distinctly separated from the other groups (Figure 6D). In leaves, PC1 and PC2 explained 18.1% and 31.9% of the total variance, respectively, whereas in roots these components accounted for 52.2% and 29.3% of the variance.

Figure 6 - Partial least squares-discriminant analysis (PLS-DA) of metabolic and lipid profiling in leaves and roots measured 14 days after salt stress. (A,B) PLS-DA of metabolic profiles in leaves and roots, respectively; (C,D) PLS-DA of lipid profiles in leaves and roots, respectively. V4 stage cowpea plants were grown under four treatments: control, 75 mM NaCl, TM, and TM + 75 mM NaCl. Ellipses represent the 95% confidence interval of each group.

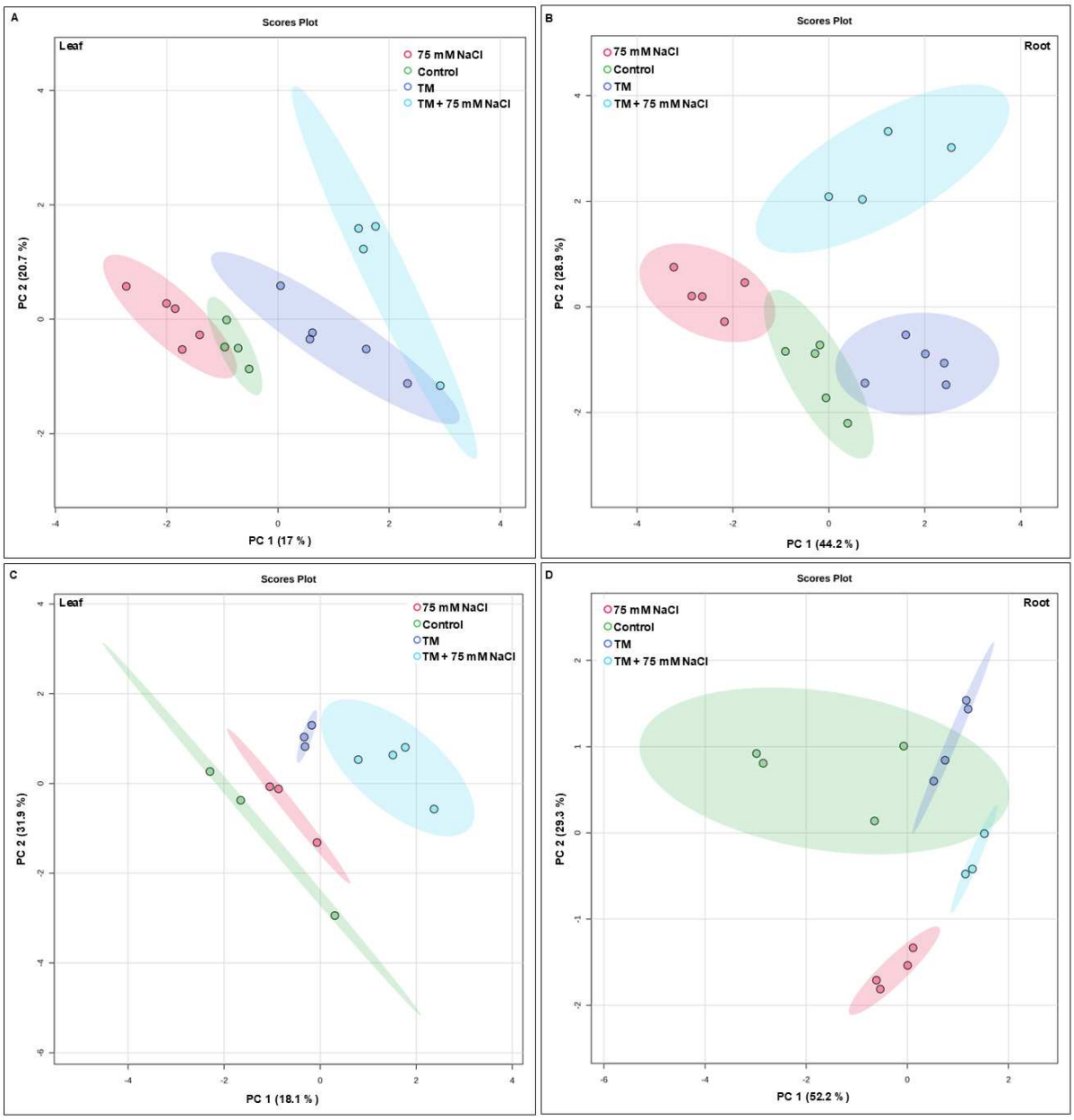

Source: Prepared by the author.

PLS-DA models identified metabolites and lipids with the highest contribution to group discrimination, based on variable importance in projection (VIP) scores greater than 1.0 (Supplementary Figure S2). In leaf metabolomics, 17 metabolites showed VIP > 1, of which 16 were also significant according to Tukey's HSD test ($p < 0.05$), including sugars, amino acids, organic acids, and polyamines such as glucose, galactose, sorbitol, ribose-5-phosphate, proline, branched-chain amino acids, and malonic acid. Only cadaverine did not show statistical significance. In root metabolomics, six metabolites simultaneously showed VIP > 1 and significant differences between treatments: β-alanine, glutamic acid, pyroglutamic acid, succinic acid, glycine, and lactic acid. In leaf lipidomics, eight compounds presented VIP > 1, five of which were significant by Tukey's HSD, including heptadecanoic acid, mevalonic acid, α-tocopherol acetate, all-trans-squalene, and farnesol. In contrast, glycerol-3-phosphate, linoleic acid (9,12-octadecadienoic acid), and myo-inositol 2-phosphate did not differ significantly. In roots, three lipid-related compounds showed both VIP > 1 and significant differences between treatments: glycerol, β-sitosterol, and linoleic acid.

All metabolites and lipids were subsequently organized according to their biochemical relationships within major metabolic pathways, generating an integrated metabolic map (Figure 7). It summarizes how TM priming modulates interconnected carbohydrate, amino acid, and lipid pathways under salinity, highlighting the main metabolic adjustments identified by both multivariate and univariate analyses.

Figure 7 - Integrative pathway of the metabolomic and lipid profile of cowpea leaves and roots measured 14 days after salt stress. The diagram displays all compounds identified in the metabolic and lipid profile analyses, organized according to their biochemical relationships in the main affected pathways. The metabolites in gray were included solely to interconnect the pathways. Metabolites with VIP > 1 in the PLS-DA model were highlighted for their greatest importance to the differentiation between treatments. Furthermore, metabolites with significant differences in ANOVA and Tukey HSD test ($p < 0.05$) were presented.

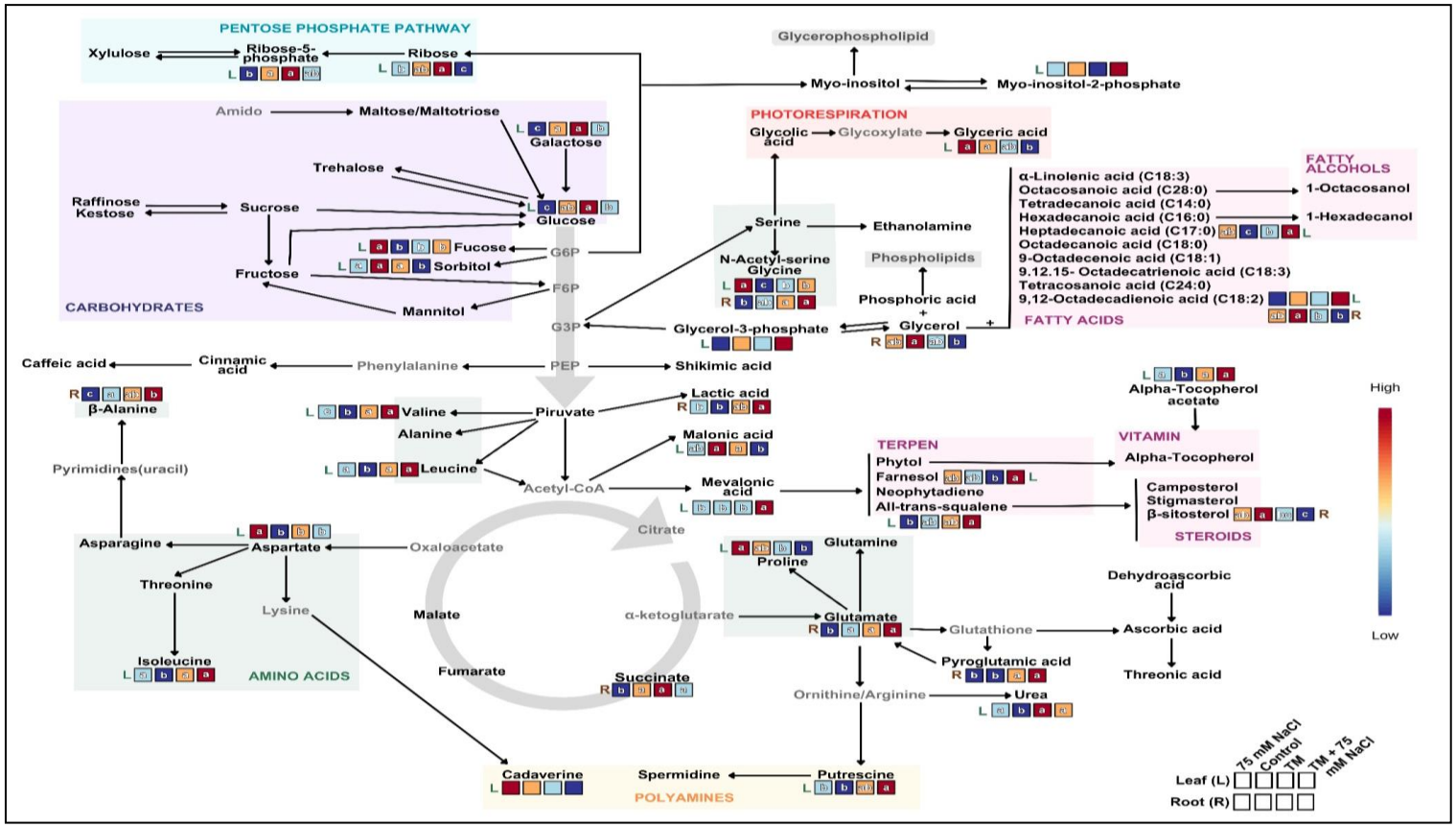

Source: Prepared by the author.

Enrichment analysis was performed using the metabolites that were significantly altered according to Tukey's HSD test ($p < 0.05$) in the TM + 75 mM NaCl treatment, with the aim of identifying metabolic pathways associated with the priming response under salt stress. Statistical details, including p-values and false discovery rate (FDR) values, are provided in Supplementary Table S7. This approach allowed us to focus specifically on metabolic pathways directly involved in the TM-induced priming effect.

In leaf metabolomics (Figure 8A), galactose metabolism was the only pathway significantly enriched. In addition, several pathways exhibited enrichment trends, including fructose and mannose metabolism, the pentose phosphate pathway, and glutathione metabolism. Nominal enrichment was also detected for glyoxylate and dicarboxylate metabolism, glycine, serine and threonine metabolism, and arginine and proline metabolism. In root metabolomics (Figure 8B), glutathione metabolism was significantly enriched. Other pathways that also reached significance after FDR correction included butanoate metabolism and propanoate metabolism. Furthermore, alanine, aspartate and glutamate metabolism, glyoxylate and dicarboxylate metabolism, porphyrin metabolism, nitrogen metabolism, and arginine biosynthesis showed nominal enrichment. In both leaves and roots, the remaining detected pathways did not exhibit significant or nominal enrichment. For leaf lipidomics (Figure 8C), enrichment analysis identified two pathways: terpenoid backbone biosynthesis and steroid biosynthesis. Terpenoid backbone biosynthesis showed nominal enrichment, whereas steroid biosynthesis did not reach statistical significance. In contrast, enrichment analysis for root lipidomics could not be performed because only one differential compound (β-sitosterol) was detected between treatments, which was insufficient to support statistically robust pathway enrichment.

Figure 8 - Enrichment analysis of TM priming-responsive metabolites measured 14 days after salt stress. The figure displays the metabolomic (A–B) and lipidomic (C) pathways significantly enriched and responsive to tunicamycin priming under salt stress. Panels A and B correspond to leaves and roots from the metabolomic dataset, while C represents the lipidomic profiles. Analyses were performed in MetaboAnalyst, using the KEGG database as a reference. The Y-axis lists the metabolic pathways, and the X-axis represents the significance level ($^{-\log_{10}}$ *p*-value). Pathways with p<0.05 and FDR<0.05 were considered significantly enriched.

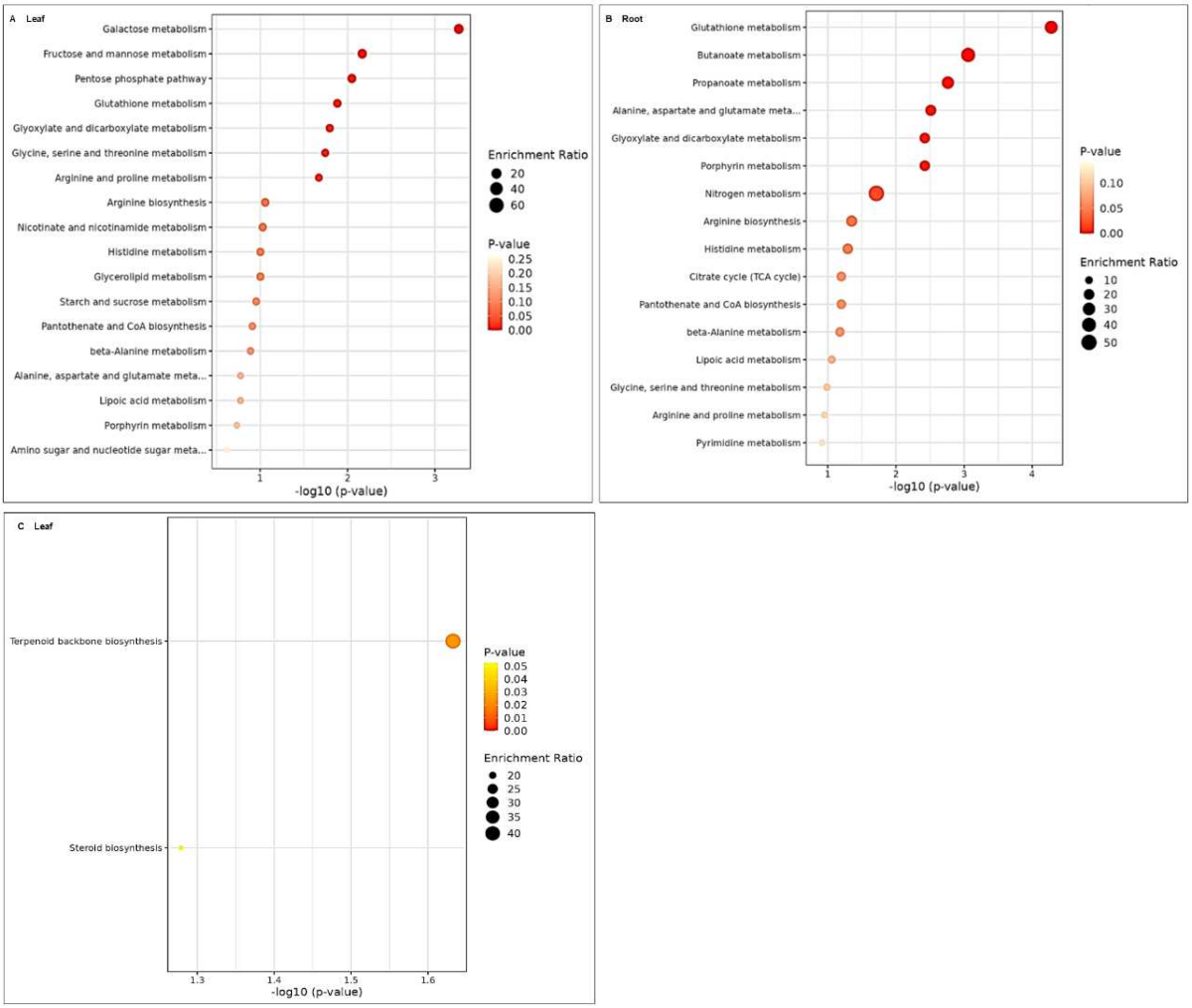

Source: Prepared by the author.

Additional enrichment analyses for metabolic and lipid profiles corresponding to the comparisons (1) Control vs. 75 mM NaCl and (2) Control vs. TM are presented in the Supplementary Material (Supplementary Table S8 and Figure S3). In some cases, pathway enrichment was not detected due to the limited number of significant metabolites available for

statistical analysis.

4.4.6 TM priming modulates ER- and ion homeostasis–related gene expression under salinity

Gene expression analysis was performed to determine whether TM priming alters the transcriptional regulation of genes associated with endoplasmic reticulum (ER) stress signaling and ionic homeostasis under salinity. Relative transcript levels ($2^{-\Delta\Delta Ct}$) varied according to treatment and salinity conditions. In leaves, *VuIRE1A* expression (Figure 9A) was higher in TM + 75 mM NaCl plants than in plants exposed to 75 mM NaCl alone. For *VubZIP60* (Figure 9B), significant differences were observed between TM and TM + 75 mM NaCl, as well as between control and 75 mM NaCl. The ER chaperone genes *VuBiP1, VuPDI11*, and *VuGRP94* (Figures 9C–E) showed a similar pattern, with increased expression under 75 mM NaCl followed by reduced expression in TM + 75 mM NaCl plants.

Figure 9 - Relative gene expression of *VuIRE1A* (A), *VubZIP60* (B), *VuBiP1* (C), *VuPDI11* (D), and *VuGRP94* (E) in cowpea leaves measured 14 days after salt stress. V4-stage plants were subjected to four treatments: control, 75 mM NaCl, TM, and TM + 75 mM NaCl. After 14 days of exposure to saline or non-saline conditions following TM foliar priming, transcript levels were quantified in leaf tissues by qRT-PCR. Gene expression was normalized using *VuUBQ3* and *VuF-box3* as reference genes. Values represent the mean of three biological replicates, and bars indicate standard error. Different lowercase letters indicate significant differences between priming treatments (Control vs. TM), whereas different uppercase letters indicate significant differences between salinity conditions (with and without NaCl), according to Tukey's test ($p < 0.05$).

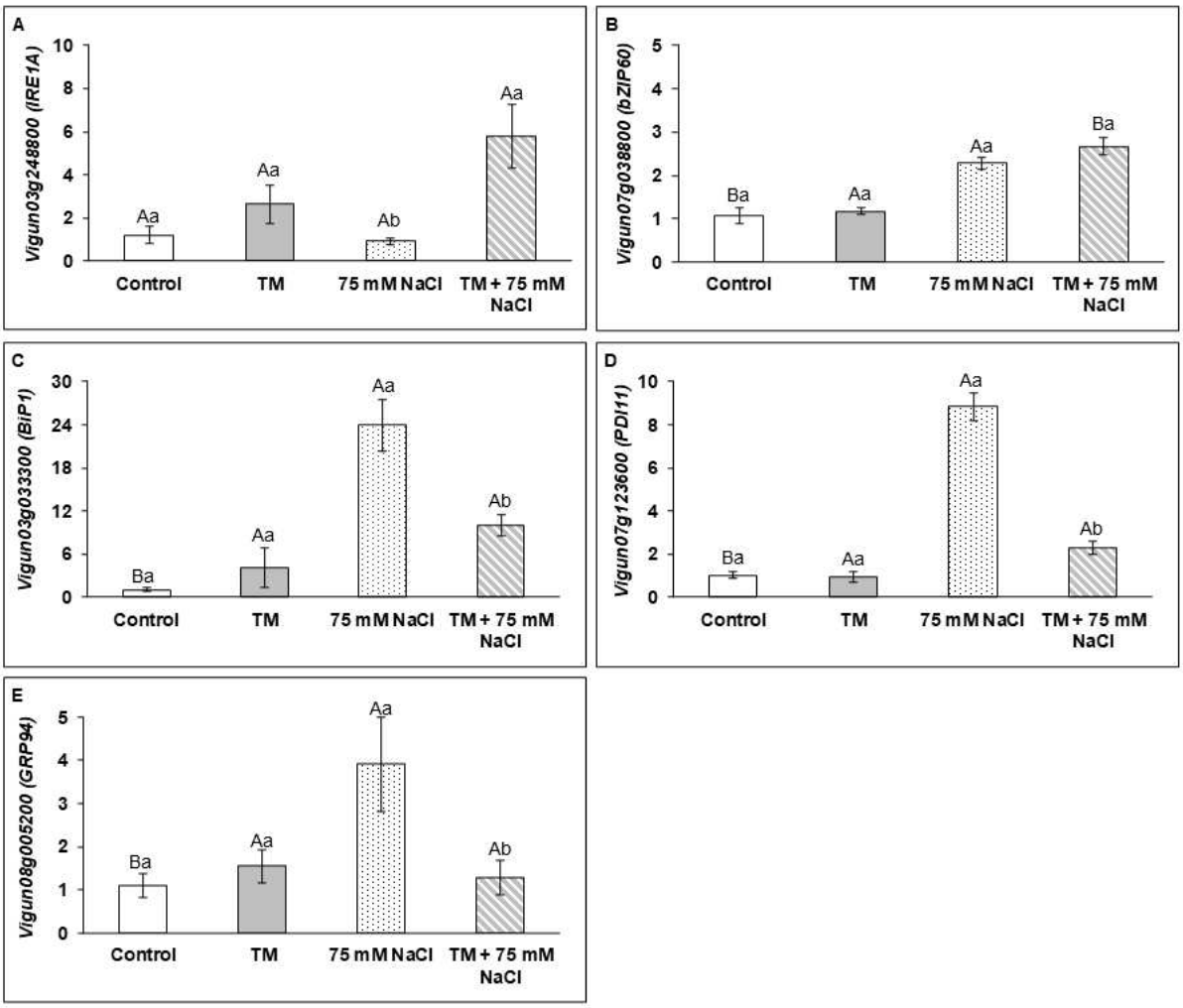

Source: Prepared by the author.

In roots, the expression of *VuIRE1A* (Figure 10A), *VubZIP17* (Figure 10C), *VuBiP1* (Figure 10D), *VuPDI11* (Figure 10E), and *VuGRP94* (Figure 10F) was higher under 75 mM NaCl than under TM + 75 mM NaCl. In contrast, under saline conditions, *bZIP60* expression (Figure 10B) was higher in TM + 75 mM NaCl plants compared with those exposed to salt stress alone.

Figure 10 - Relative gene expression of *VuIRE1A* (A), *VubZIP60* (B), *VubZIP17* (C), *VuBiP1* (D), *VuPDI11* (E), and *VuGRP94* (F) in cowpea roots measured 14 days after salt stress. V4-stage plants were subjected to four treatments: control, 75 mM NaCl, TM, and TM + 75 mM NaCl. After 14 days of exposure to saline or non-saline conditions following TM foliar priming, transcript levels were quantified in root tissues by qRT-PCR. Gene expression was normalized using *VuUBQ3* and *VuF-box3* as reference genes. Values represent the mean of three biological replicates, and bars indicate standard error. Different lowercase letters indicate significant differences between priming treatments (Control vs. TM), whereas different uppercase letters indicate significant differences between salinity conditions (with and without NaCl), according to Tukey's test ($p < 0.05$).

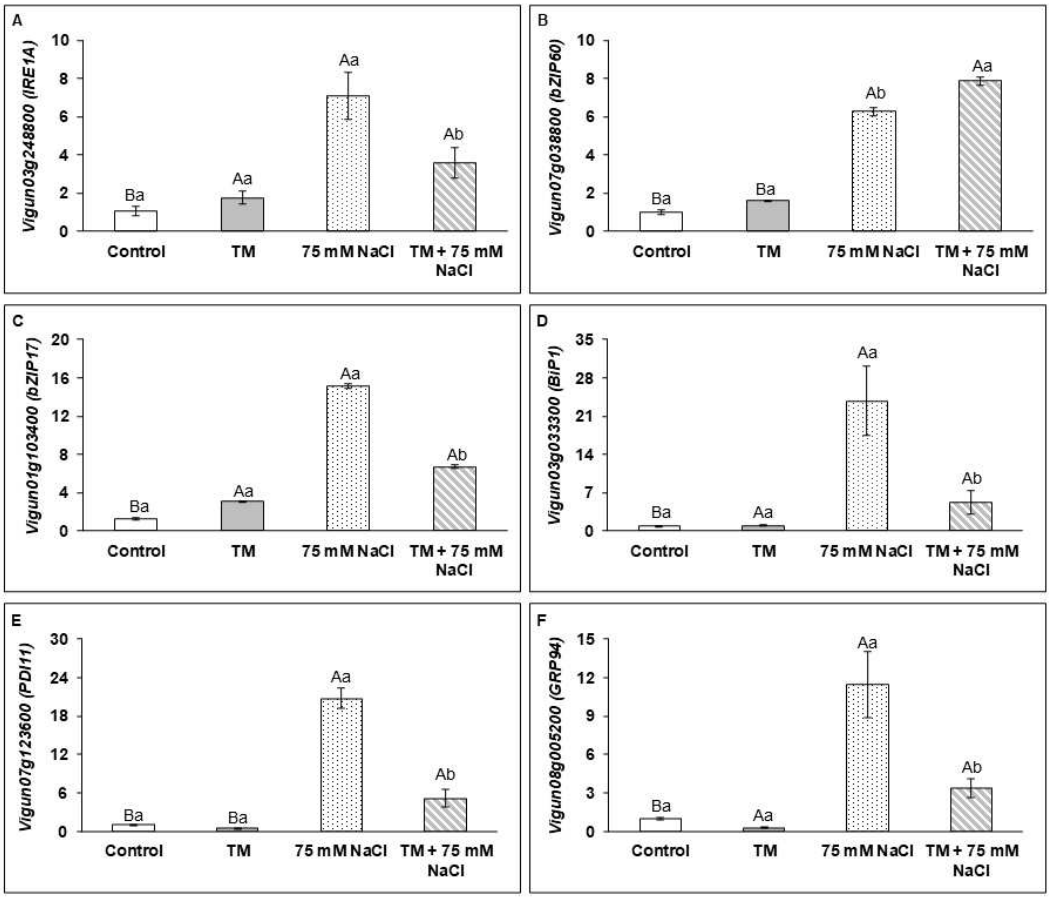

Source: Prepared by the author.

Regarding genes associated with ionic homeostasis in leaves, *VuSOS3* (Figure 11A), *VuSOS1* (Figure 11C), and *VuNHX1* (Figure 11D) exhibited higher expression under 75 mM NaCl, with reduced expression in TM + 75 mM NaCl plants. For *VuSOS2* (Figure 11B), no significant differences were detected among treatments, although a trend toward increased expression under salinity was observed.

Figure 11 - Relative gene expression of *VuSOS3* (A), *VuSOS2* (B), *VuSOS1* (C), and *VuNHX1* (D) in cowpea leaves measured 14 days after salt stress. V4-stage plants were subjected to four treatments: control, 75 mM NaCl, TM, and TM + 75 mM NaCl. After 14 days of exposure to saline or non-saline conditions following TM foliar priming, transcript levels were quantified in leaf tissues by qRT-PCR. Gene expression was normalized using *VuUBQ3* and *VuF-box3* as reference genes. Values represent the mean of three biological replicates, and bars indicate standard error. Different lowercase letters indicate significant differences between priming treatments (Control vs. TM), whereas different uppercase letters indicate significant differences between salinity conditions (with and without NaCl), according to Tukey's test ($p < 0.05$).

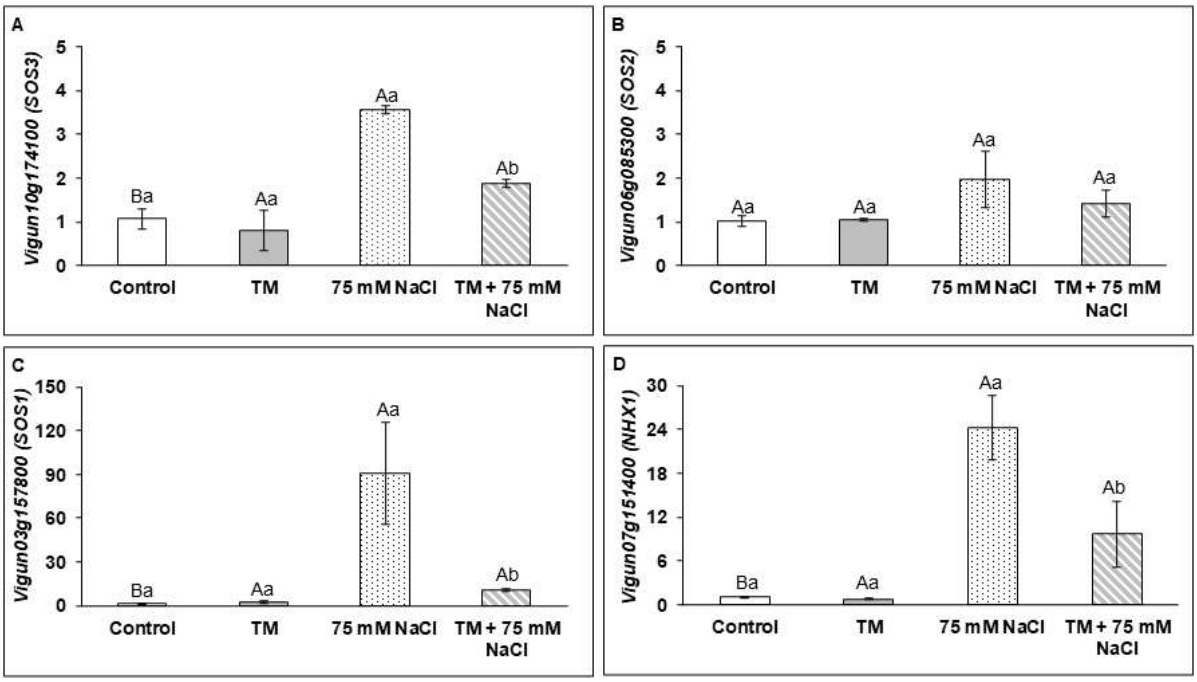

Source: Prepared by the author.

In roots, no significant differences were observed for *VuSOS3* (Figure 12A) or *VuSOS2* (Figure 12B) between the 75 mM NaCl and TM + 75 mM NaCl treatments. In contrast, *VuSOS1* (Figure 12C) and *VuNHX1* (Figure 12D) showed higher relative expressions under 75 mM NaCl than under TM + 75 mM NaCl.

Figure 12 - Relative gene expressions of *VuSOS3* (A), *VuSOS2* (B), *VuSOS1* (C), and *VuNHX1* (D) in cowpea roots measured 14 days after salt stress. V4-stage plants were subjected to four treatments: control, 75 mM NaCl, TM, and TM + 75 mM NaCl. After 14 days of exposure to saline or non-saline conditions following TM foliar priming, transcript levels were quantified in root tissues by qRT-PCR. Gene expression was normalized using *VuUBQ3* and *VuF-box3* as reference genes. Values represent the mean of three biological replicates, and bars indicate standard error. Different lowercase letters indicate significant differences between priming treatments (Control vs. TM), whereas different uppercase letters indicate significant differences between salinity conditions (with and without NaCl), according to Tukey's test ($p < 0.05$).

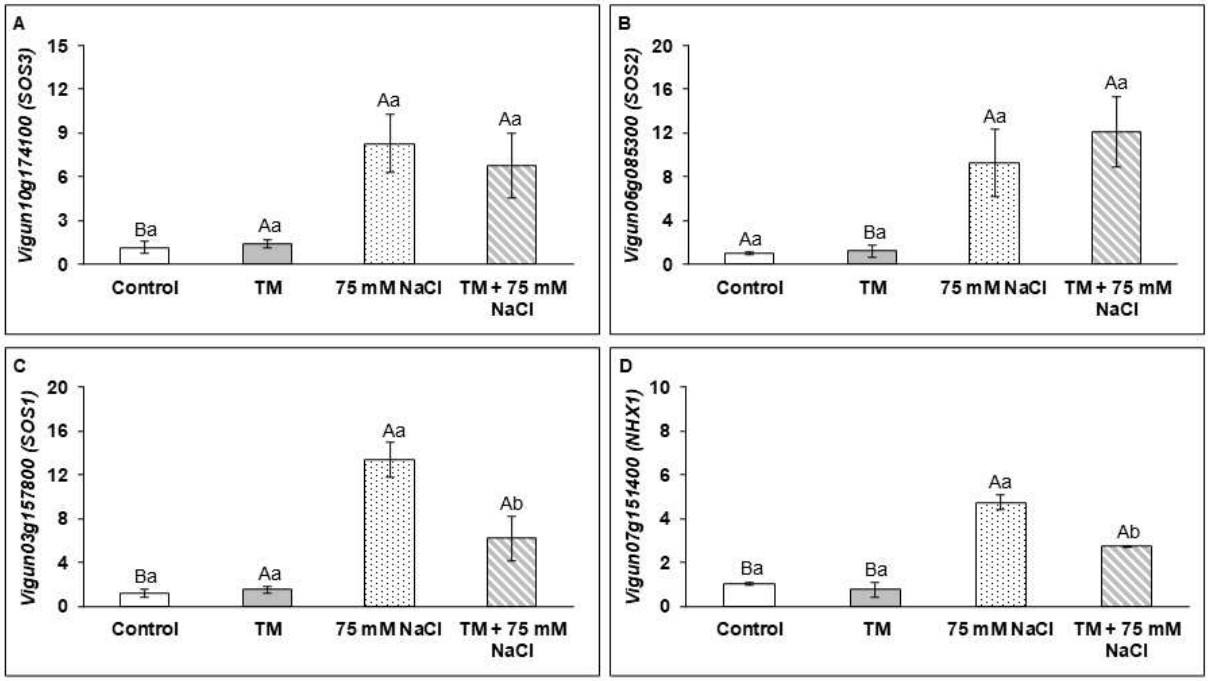

Source: Prepared by the author.

4.5 Discussion

4.5.1 TM spray reduces the harmful effects of salinity in cowpea through integrated physiological, ionic, and transcriptional regulation

Salinity severely limits plant growth and photosynthetic performance by disrupting ionic homeostasis, as also observed in cowpea plants subjected to salt stress in this study (Freitas et al., 2012; Oliveira et al., 2025). Although chemical priming strategies such as proline, hydrogen peroxide, and melatonin have been reported to mitigate salinity effects (Savvides et al., 2016), most studies focus primarily on physiological outcomes, with limited integration of molecular and metabolic responses. In contrast, our results demonstrated that ER-mediated priming with tunicamycin modulates salinity responses at multiple levels, including transcriptional regulation of ER stress signaling components and ion transporters, redox balance, and metabolic and lipidomic adjustments. These findings support the emerging view that the endoplasmic reticulum acts as a central hub coordinating protein folding, redox homeostasis, and ion regulation during salt stress acclimation (Çakır Aydemir et al., 2020; Zhang et al., 2022).

The improved growth and photosynthetic performance observed in TM-primed cowpea plants under salinity suggest that ER-mediated priming contributed to enhanced stress acclimation. In line with these physiological responses, gene expression analyses indicate that TM priming influenced the transcriptional regulation of ER-related and stress signaling genes in both leaves and roots. Specifically, although salinity alone can induce ER stress signaling to some extent, the increased expression of *VuIRE1A* under TM + 75 mM NaCl compared with salt alone suggests a potentiation or priming effect on ER stress signaling pathways. This observation is consistent with recent evidence showing that ER stress-responsive transcriptional networks are dynamically modulated under abiotic stress conditions, including salinity (Liu et al., 2022; Ko and Brandizzi, 2024). The differential expression of *VubZIP60* across treatments further reflects the sensitivity of UPR-associated transcription factors to both salt and ER-derived signals, a response previously reported in crop species exposed to combined stresses (Liu et al., 2022; Guan et al., 2025). Moreover, the induction of the chaperone genes *VuBiP1, VuPDI11*, and *VuGRP94* under salinity, followed by their reduced expression under TM + 75 mM NaCl, highlights the fine regulation of protein folding and quality control mechanisms associated with ER homeostasis. Such modulation has been linked to improved stress resilience in several plant systems (Liu et al., 2022; Ko and

Brandizzi, 2024). Taken together, these results support the role of the ER as a central hub integrating transcriptional, ionic, redox, and metabolic responses, thereby coordinating cowpea acclimation to salinity under TM priming.

In *Sorghum bicolor*, the concomitant treatment of NaCl and ER inducers modulates ER stress sensors and the expression of ion transporter genes, linking the unfolded protein response (UPR) to mechanisms of ionic adjustment under saline conditions (Queiroz et al., 2020). Subsequently, Lima et al. (2022) demonstrated that ER stress influences the metabolic profile of *Sorghum* seedlings over time, revealing that prolonged activation of ER signaling alters amino acid and organic acid pathways associated with growth regulation and redox balance. Recently, a previous work demonstrated that rice seed priming with TM treatment activates ER and improves seed germination and seedling acclimation to salinity (Oliveira et al., 2025). Building on this conceptual framework, the present study tested if foliar priming with tunicamycin (TM) mitigates the detrimental effects of NaCl in cowpea plants by enhancing growth, photosynthetic performance, and ion homeostasis. Our findings showed that foliar spraying is protective against salinity in cowpea at later developmental stages.

The greater dry biomass observed in leaves, stems, and roots of TM + 75 mM NaCl plants, compared with those exposed only to salt, suggests that TM spray may activate ER-mediated cellular reprogramming to promote redox regulation and metabolic adjustment. This kind of physiological preconditioning likely enhances the cellular capacity to maintain homeostasis and sustain growth under saline environments, consistent with the effects of other priming agents reported to induce salt tolerance in cowpea (Zulfiqar et al., 2022; Praxedes et al., 2022). ER stress and the UPR are functionally interconnected with cellular homeostasis and stress signaling pathways, including the regulation of ion transport and balance, through coordinated transcriptional responses (Ko and Brandizzi, 2024). Under concomitant salt and ER stresses, there was a favorable ion balance due to the activation of transporters such as the NHX and SOS family members in *Sorghum bicolor* (Queiroz et al., 2020). These transporters play complementary roles in maintaining ionic homeostasis under salinity. The plasma membrane Na^+/H^+ antiporter SOS1 mediates the extrusion of excess Na^+ from the cytosol, while vacuolar Na^+/H^+ exchangers such as NHX1 compartmentalize Na^+ into vacuoles, contributing to cytosolic detoxification and osmotic adjustment. Together, these systems help preserve the K^+/Na^+ balance required for enzymatic stability and metabolic functionality.

In this context, it is plausible that UPR activation contributes indirectly to the modulation of NHX and SOS systems under saline conditions. By restoring proteostasis and

stabilizing membrane-associated proteins, UPR may help maintain the structural integrity and functional efficiency of ion transporters. Furthermore, ER stress-responsive transcriptional reprogramming has been shown to interact with broader stress adaptation networks, including those involved in ion regulation and redox balance (Liu et al., 2022; Ko and Brandizzi, 2024). The redistribution of inorganic ions observed in TM-primed plants further supports the hypothesis of a functional interplay between ER stress signaling and ion homeostasis under salinity. Maintaining a favorable K^+/Na^+ ratio is a well- established hallmark of salt tolerance, as K^+ is crucial for enzyme activation, photosynthesis, and protein synthesis, whereas Na^+ disrupts these processes (Sackey et al., 2025). In the present study, foliar TM application reduced Na^+ and Cl^- accumulation in leaves and stems by promoting their preferential retention and sequestration in roots, while simultaneously maintaining higher K^+ levels in aerial tissues, thereby contributing to a more favorable ionic balance. This redistribution may involve enhanced vacuolar compartmentalization mechanisms and modulation of ion transport activity rather than a simple upregulation of the canonical SOS pathway at the transcriptional level. This ionic pattern may reflect improved selectivity and compartmentalization, processes essential for osmotic adjustment and detoxification, and which is consistent with evidence that UPR interacts with ion homeostasis pathways (Ruberti and Brandizzi, 2018; Queiroz et al., 2020).

Gas-exchange modulation also highlighted the protective effects of TM priming. Under salinity, TM-treated plants sustained higher photosynthetic rates (*A*) and stomatal conductance (*gs*), along with lower *Ci/Ca* ratios and higher transpiration (*E*), compared with salt-stressed plants without priming. These responses may indicate more efficient CO_2 assimilation and stomatal regulation, likely linked to the preservation of chloroplast integrity and to an enhanced antioxidant defense system, patterns consistent with other priming studies that preserved photosynthetic efficiency under stress (Iqbal et al., 2024; Matkowski and Daszkowska-Golec, 2025). The lower leaf temperature (ΔT) observed in TM + 75 mM NaCl plants relative to salt-only treatment suggests better evaporative cooling and heat dissipation, which aligns with improved gas exchange and water-use efficiency (Chaves et al., 2009) following the role of ER in heat stress tolerance. Altogether, these results indicate that TM priming mitigates the negative impacts of salinity on photosynthetic performance and temperature regulation, possibly by stabilizing chloroplast membranes and inducing ER-associated protective proteins, as also reported in rice seedlings primed with TM (Oliveira et al., 2025).

The content of hydrogen peroxide (H_2O_2) added another layer to hypothesize an

antioxidant mechanism linked to tolerance induced by ER that still to be tested. Salt exposure markedly increased H_2O_2 levels in both leaves and roots. Certainly, salt stress induces oxidative imbalance in cowpea, leading to the accumulation of reactive oxygen species (ROS) and activation of antioxidant defenses (Rahali-Osmane et al., 2020). Under salinity, ROS are mainly produced in chloroplasts and mitochondria due to electron leakage from photosynthetic and respiratory electron transport chains, as well as in peroxisomes during photorespiration and at the plasma membrane via NADPH oxidases. However, TM + 75 mM NaCl plants decreased the H_2O_2 levels, suggesting a controlled accumulation of reactive oxygen species (ROS). It implies that TM does not suppress ROS generation entirely but rather fine-tunes redox signaling, allowing the activation of defense pathways without triggering oxidative damage. Such regulation has been documented in more tolerant plant species, where ER stress and the UPR modulate ROS levels to maintain cellular homeostasis (Araújo et al., 2021; Zulfiqar et al., 2022). In *Arabidopsis thaliana*, ER stress plays a role in ROS signaling and modulates the antioxidant defense system to restore redox balance, coordinating UPR activation with oxidative metabolism (Ozgur et al., 2014; Ozgur et al., 2018). These findings suggest that the redox fine-tuning observed in ER-associated responses may represent a general mechanism that contributes to enhanced stress tolerance, consistent with the moderated oxidative response elicited by TM priming in our study. Moderate ROS levels play essential signaling roles, activating antioxidant enzymes, secondary metabolism, and stress-response pathways such as UPR regulation (Özgür et al., 2018; Cao et al., 2022). Indeed, the TM-induced redox homeostasis likely arises from the coordinated activity of ER chaperones and antioxidant systems, such as catalase and peroxidases, which maintain cellular balance under stress (Ruberti and Brandizzi, 2018; Cao et al., 2022).

These results reinforce the concept that ER-mediated signaling and stress memory are central components of chemical priming, while highlighting TM as a biotechnological tool for advancing the understanding of cowpea performance in saline conditions.

4.5.2 Salt stress alters metabolomic and lipidomic dynamics within an integrated transcriptional response, and TM priming mitigates these effects

Beyond ionic regulation, transcriptional changes in ER stress–related genes provided a molecular framework to interpret the metabolic and lipidomic adjustments observed under salinity and TM priming. In both leaves and roots, the modulation of key UPR components, including *VuIRE1A, VubZIP17, VuBiP1, VuPDI11,* and *VuGRP94*, suggests that

ER signaling influences cellular metabolism by coordinating protein folding demand, redox balance, and energy allocation (Howell, 2013; Ko and Brandizzi, 2024). Such regulation is consistent with the metabolomic profiles showing alterations in carbohydrate and amino acid metabolism under salt stress (Lima et al., 2022), and with lipidomic changes indicative of membrane remodeling (Garcia et al., 2023). ER-driven control of protein quality and redox homeostasis has been shown to affect primary metabolism and lipid composition in plants, linking prolonged ER signaling to shifts in carbon allocation and membrane stability (Ruberti and Brandizzi 2014; Srivastava et al., 2018). In this context, the attenuation of ER chaperone gene expression under TM priming may reflect a preconditioned ER state, reducing metabolic costs associated with sustained stress responses and enabling the reestablishment of metabolic and lipid homeostasis (Lima et al., 2022; Ko and Brandizzi, 2024).

Consistent with the ER-associated transcriptional adjustments, TM priming attenuated salt-induced proline accumulation and membrane lipid remodeling, contributing to the restoration of metabolic homeostasis under stress. Here, our results indicate that TM reorganizes primary metabolism, alleviating the detrimental effects of salinity by enhancing the integration of carbohydrate, amino acid, and lipid metabolism. This reprogramming effect reflects TM's ability to act as a chemical preconditioning agent, enabling plants to preserve redox stability and energy efficiency under saline conditions (Zulfiqar et al., 2022; Iqbal et al., 2024; Oliveira et al., 2025).

The clear discrimination among treatments observed in the PLS-DA models reinforces this, particularly in roots, where PC1 and PC2 together explained over 70% of the variance. This strong separation indicates that priming acted as a physiological modulator capable of preconditioning plants for more efficient metabolic adjustments when exposed to salinity, which is consistent with the improved biomass accumulation and photosynthetic performance observed in TM-primed plants under salt stress. These integrative responses reinforce the idea that TM not only reprograms metabolism at the biochemical level but also translates this adjustment into enhanced physiological efficiency and growth stability. Similar behavior was described in *Arabidopsis thaliana* and *Oryza sativa*, where mild ER stress induced by TM activated the UPR, leading to enhanced metabolic coordination and adaptive resilience under adverse conditions (Ruberti and Brandizzi, 2018; Iqbal et al., 2024; Oliveira et al., 2025). In these studies, mild ER stress triggered signaling networks that synchronized carbon metabolism, protein folding, and antioxidant defenses, allowing plants to maintain cellular homeostasis and sustain growth under prolonged stress.

The metabolomic adjustments observed here suggest that TM contributes to

redox-related metabolic reprogramming under salinity. Previous studies have demonstrated that ER stress functions as a regulatory signal in plants, triggering the unfolded protein response (UPR) and promoting metabolic reprogramming under stress. Mild chemically induced ER stress activates UPR sensors and leads to adjustments in carbohydrate and amino acid metabolism, supporting osmoprotection through the accumulation of soluble sugars and compatible amino acids (Lima et al., 2022; Cavalcante et al., 2023). Concurrently, ER stress–UPR signaling increases the expression of molecular chaperones (such as *VuBiP* and *VuPDI1*), improving protein folding efficiency and maintaining ER functionality (Ozgur et al., 2018). This coordinated response is intimately linked to redox regulation, as the UPR intersects with ROS-scavenging pathways and enhances antioxidant capacity to sustain cellular homeostasis during prolonged stress exposure (Cao et al., 2022).

In leaves, most metabolites with higher VIP scores, such as glucose, galactose, sorbitol, and ribose-5-phosphate are central to carbohydrate metabolism and osmoprotection (Zulfiqar et al., 2022). These compounds not only stabilize cellular structures but also sustain NADPH production, supporting antioxidant activity and maintaining redox homeostasis (Zulfiqar et al., 2022; Tripathi et al., 2024). The enrichment analysis confirmed that galactose metabolism was significantly affected in leaves, while fructose and mannose metabolism, the pentose phosphate pathway, and glutathione metabolism showed enrichment trends. Additional nominal enrichments were detected for glyoxylate and dicarboxylate metabolism, glycine, serine, and threonine metabolism, and arginine and proline metabolism, suggesting that TM modulated carbohydrate and redox-related metabolism even though most changes were modest under the applied conditions (Cao et al. 2022; Zulfiqar et al., 2022).

Amino acid accumulation, particularly proline, glycine, and branched-chain amino acids (valine, leucine, and isoleucine), further supports the hypothesis that TM also induced osmotic adjustment under salinity. These molecules act as osmoprotectants, signaling intermediates, and alternative carbon and energy sources under stress (Araújo et al., 2021; Ghosh et al., 2021). In roots, significant enrichment of glutathione metabolism, together with butanoate and propanoate metabolism corroborated the activation of antioxidants and short-chain organic acid pathways in TM-primed plants. Nominal enrichment of alanine, aspartate and glutamate metabolism, glyoxylate and dicarboxylate metabolism, porphyrin metabolism, nitrogen metabolism, and arginine biosynthesis further indicates a broad adjustment of nitrogen- and carbon-related pathways. These results are consistent with the observed increases in glutamic and pyroglutamic acids in roots, pointing to enhanced nitrogen recycling through the γ-glutamyl cycle and reinforcing glutathione metabolism. This connection

between ER signaling and antioxidant metabolism aligns with recent studies linking UPR activation to glutathione biosynthesis and redox balance reinforcing cellular protection against ROS accumulation against abiotic stress conditions (Ozgur et al., 2018; Czékus et al., 2023).

The elevated levels of organic acids such as malonic, glyceric, succinic, and lactic acids indicate active tricarboxylic acid (TCA) cycle functioning and metabolic flexibility. These changes imply that TM-primed plants preserve mitochondrial efficiency under salinity, maintaining ATP supply and redox coupling even under stress. Similar metabolic resilience has been reported in salt-tolerant legumes, where the maintenance of TCA intermediates supports sustained energy metabolism and growth (Cavalcante et al., 2023; Sackey et al., 2025). Collectively, these metabolomic shifts support the hypotheses that TM priming helps maintain carbon and nitrogen equilibrium, energy flow, and antioxidative capacity, three essential elements of effective salt acclimation and higher carbon assimilation.

Lipidomic profiling corroborated these metabolic findings, showing that TM priming mitigates the lipid remodeling induced by salinity. Salt stress caused major changes in fatty acid and terpenoid metabolism, but these effects were partially inhibited by foliar TM application. In leaves, the accumulation of heptadecanoic acid, mevalonic acid, α-tocopherol acetate, and squalene under TM + NaCl suggests enhanced ER-linked lipid synthesis and antioxidant lipid production. Tocopherols and squalene contribute to membrane stabilization and oxidative protection under stress. Tocopherols reinforce chloroplast and endomembrane integrity while enhancing ROS-scavenging systems and antioxidant enzymes during salt stress, improving cellular resilience (Naqve et al., 2021; Taie and Rady, 2024). Likewise, squalene acts as a highly efficient membrane-associated antioxidant, preventing lipid peroxidation and protecting cellular structures under oxidative pressure (Micera, 2020). The enrichment analysis showed nominal enrichment of terpenoid backbone biosynthesis, while steroid biosynthesis was not significantly affected. These results indicate that, although TM modulated ER-associated lipid metabolism, the changes were moderate at the pathway level. In roots, the enrichment analysis could not be performed due to the detection of only one significant compound (β-sitosterol), which limits statistical inference. However, the increased abundance of β-sitosterol, glycerol, and linoleic acid in TM-primed roots suggests membrane restructuring and adjustments in signaling lipids. Phytosterols such as β-sitosterol are known to improve membrane fluidity and ion transport, enhancing tolerance to salinity (Valitova et al., 2024). Linoleic acid, a precursor of oxylipins and jasmonate-like molecules, contributes to systemic stress signaling (He and Ding, 2020).

The integrated metabolic map highlighted that TM priming redirects central

carbon metabolism, with increased coordination of glycolytic and tricarboxylic acid (TCA) cycle–related pathways, coupled with adjustments in amino acid and lipid metabolism. This reorganization supports redox balance and antioxidant capacity, forming an adaptive metabolic network under salinity, as further corroborated by pathway enrichment analysis. The selective enrichment of glutathione metabolism, galactose metabolism, and terpenoid backbone biosynthesis reveals a convergence between energy production, detoxification, and lipid-based signaling. This metabolic signature resembles the metabolic memory observed in *Oryza sativa* and *Arabidopsis thaliana* after TM exposure, where mild ER stress triggers a long-lasting acclimation effect and enhanced tolerance to subsequent salt exposure (Iqbal et al., 2024; Oliveira et al., 2025). Thus, a schematic summary of the integrated physiological, molecular, and metabolic mechanisms underlying TM-mediated salt tolerance (Figure 13).

Figure 13. Foliar TM priming initiates a coordinated adjustment of metabolic, redox, and cellular homeostasis that supports plant performance under salinity. In leaves, TM sustains photosynthetic activity and gas exchange, maintaining carbon flux from atmospheric CO_2 fixation to cytosolic carbon pools. This metabolic reprogramming enhances osmoprotection and redox homeostasis, reducing H_2O_2 accumulation and supporting lipid remodeling associated with membrane stabilization. Attenuated oxidative pressure contributes to fine-tuned unfolded protein response (UPR) signaling, characterized by modulation of ER stress regulators (*VuIRE1/VubZIPs*) and reduced induction of UPR effector genes (*VuBiP, VuPDI11* and *VuGRP94*). In roots, TM priming promotes energy- and redox-related metabolic adjustments and structural lipid remodeling, supporting membrane integrity and active ionic containment. This is reflected by enhanced Na^+ and Cl^- retention and vacuolar sequestration, preferential K^+ translocation to the shoot, and a modulated expression of ion transporters (*VuSOS1, VuNHX1*), while *VuSOS2* and *VuSOS3* remain unchanged. Together, these leaf- and root-specific responses indicate a systemically coordinated strategy by which TM priming integrates metabolic support, redox balance, membrane stability, ER stress modulation, and ionic homeostasis to confer salt tolerance.

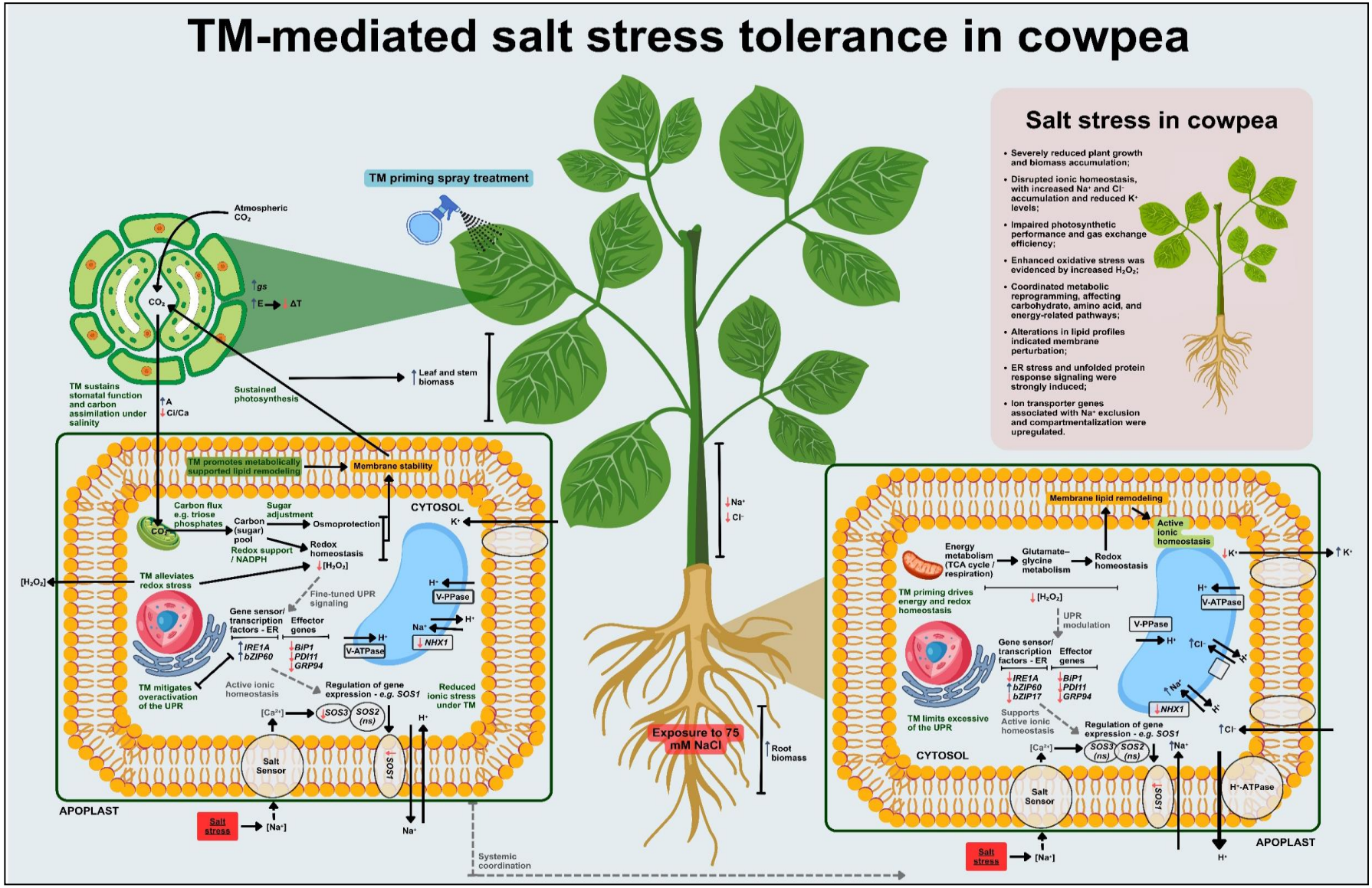

Source: Prepared by the author.

4.6 Conclusion

Foliar priming with tunicamycin enhanced cowpea tolerance to salinity, reinforcing the concept that controlled activation of endoplasmic reticulum (ER) stress can function as a preparatory signal rather than a damaging response. The coordinated physiological, transcriptional, and metabolic adjustments observed indicate that ER acts as an integrative regulatory mechanism, enabling plants to better cope with ionic and osmotic constraints imposed by salinity.

Notably, the metabolic and lipidomic reprogramming associated with TM priming highlights the ER as a central hub linking membrane dynamics, redox balance, and stress signaling, thereby supporting cellular stability under saline conditions. These findings point to ER-mediated priming as a promising approach for improving salt tolerance in cowpea and potentially other leguminous crops. Future studies should investigate the persistence of this primed state, its interaction with multiple stresses, and its feasibility within sustainable crop management strategies in salt-affected environments.

4.7 References

Araújo, G.D.S., Lopes, L.S., Paula-Marinho, S.O., Mesquita, R.O., Nagano, C.S., Vasconcelos, F.R., Carvalho, H.H., Moura, A.A.A.N., Marques, E.C., and Gomes-Filho, E. (2021). H_2O_2 priming induces proteomic responses to defense against salt stress in maize. Plant Mol. Biol. **106**: 33–48.

Atta, K., Mondal, S., Gorai, S., Singh, A.P., Kumari, A., Ghosh, T., Roy, A., Hembram, S., Gaikwad, D.J., Mondal, S., Bhattacharya, S., Jha, U.C., and Jespersen, D. (2023). Impacts of salinity stress on crop plants: Improving salt tolerance through genetic and molecular dissection. Front. Plant Sci. **14**: 1241736.

Balasubramaniam, T., Shen, G., Esmaeili, N., and Zhang, H. (2023). Plants' response mechanisms to salinity stress. Plants **12**: 2253.

Bligh, E.G., and Dyer, W.J. (1959). A rapid method of total lipid extraction and purification. Can. J. Biochem. Physiol. **37**: 911–917.

Cavalcante, F.L.P., Silva, S.J., Sousa Lopes, L., Oliveira Paula-Marinho, S., Guedes, M.I.F., Gomes-Filho, E., and Carvalho, H.H. (2023). Unveiling a differential metabolite modulation of sorghum varieties under increasing tunicamycin-induced endoplasmic reticulum stress. Cell Stress Chaperones. **28**: 889–907.

Cao, J., Wang, C., Hao, N., Fujiwara, T., and Wu, T. (2022). Endoplasmic Reticulum Stress and Reactive Oxygen Species in Plants. Antioxidants. **11**: 1240.

Chaves, M.M., Flexas, J., and Pinheiro, C. (2009). Photosynthesis under drought and salt stress: Regulation mechanisms from whole plant to cell. Ann. Bot. **103**: 551–560.

Czékus, Z., Milodanovic, D., Koprivanacz, P., Bela, K., López-Climent, M.F., Gómez-Cadenas, A., and Poór, P. (2023). The role of salicylic acid on glutathione metabolism under endoplasmic reticulum stress in tomato. Plant Physiol. Biochem. **205**: 108192.

Çakır Aydemir, B., Yüksel Özmen, C., Kibar, U., Mutaf, F., Büyük, P.B., Bakır, M., and Ergül, A. (2020). Salt stress induces endoplasmic reticulum stress-responsive genes in a grapevine rootstock. *PLoS One* **15**: e0236424.

Denning, G. (2025). Sustainable intensification of agriculture: The foundation for universal food security. NPJ Sustain. Agric. **3:** 7**.**

Elbein, A.D. (1987). Inhibitors of the biosynthesis and processing of N-linked oligosaccharides. Annu. Rev. Biochem. **56**: 497–534.

Embrapa (2025). Agrobalsas 2025: Cultivares de feijão-caupi marcam presença em debate e vitrine tecnológica. Embrapa, Brasília, DF, Brazil.

Evelin, H., Devi, T.S., Gupta, S., and Kapoor, R. (2019). Mitigation of salinity stress in plants by arbuscular mycorrhizal symbiosis: Current understanding and new challenges. Front. Plant Sci. **10**: 470.

Ferreira, D.F. (2014). Sisvar: A guide for its bootstrap procedures in multiple comparisons. Cienc. Agrotec. **38**: 109–112.

Freitas, A.D.S., Silva, A.F., and Sampaio, E.V.S.B. (2012). Yield and biological nitrogen fixation of cowpea varieties in the semi-arid region of Brazil. Biomass Bioenergy **45**: 109–114.

Freitas, T.K.T., Gomes, F.O., Araújo, M.S., Silva, I.C.V., Silva, D.J.S., Damasceno Silva, K.J., and Rocha, M.M. (2022). Potential of cowpea genotypes for nutrient biofortification and cooking quality. Rev. Cienc. Agron. **53:** e20218048.

Fu, H., and Yang, Y. (2023). How plants tolerate salt stress. Curr. Issues Mol. Biol. **45**: 5914–5934.

Garcia, G., Zhang, H., Moreno, S., Tsui, C.K., Webster, B.M., Higuchi-Sanabria, R., and Dillin, A. (2023). Lipid homeostasis is essential for a maximal ER stress response. Elife **12**: e83884.

Ghosh, U.K., Islam, M.N., Siddiqui, M.N., and Khan, M.A.R. (2021). Understanding the roles of osmolytes for acclimatizing plants to changing environment: A review of potential

mechanism. Plant Signal. Behav. **16**: 1913306.

Gómez-Bellot, M.J., Nortes, P.A., Sánchez-Blanco, M.J., and Ortuño, M.F. (2015). Sensitivity of thermal imaging and infrared thermometry to detect water status changes in *Euonymus japonica* plants irrigated with saline reclaimed water. Biosyst. Eng. **133**: 21–32.

Guan, P., Zhao, D., Zhang, C., Qiu, Z., Chen, Q., Solyanikova, I.P., Sun, P., Cui, P., Yu, R., Zhang, X., Li, Y., and Hu, L. (2025). Identification and analysis of endoplasmic-reticulum-stress- and salt-stress-related genes in *Solanum tuberosum* genome: StbZIP60 undergoes splicing in response to salt stress and ER stress. Agronomy **15**: 1224.

Guo, Q., Liu, L., Rupasinghe, T.W.T., Roessner, U., and Barkla, B.J. (2022). Salt stress alters membrane lipid content and lipid biosynthesis pathways in the plasma membrane and tonoplast. Plant Physiol. **189:** 805–826.

He, M., and Ding, N.Z. (2020). Plant unsaturated fatty acids: Multiple roles in stress response. Front. Plant Sci. **11**: 562785.

Howell, S.H. (2013). Endoplasmic reticulum stress responses in plants. Annu. Rev. Plant Biol. **64**: 477–499.

Iqbal, N., Ördög, A., Koprivanacz, P., Kukri, A., Czékus, Z., and Poór, P. (2024). Salicylic acid- and ethylene-dependent effects of the ER stress-inducer tunicamycin on the photosynthetic light reactions in tomato plants. J. Plant Physiol. **295**: 154222.

Iwata, Y., and Koizumi, N. (2005). Unfolded protein response followed by induction of cell death in cultured tobacco cells treated with tunicamycin. Planta **220**: 804–807.

Kim, D.-K., Ochar, K., Iwar, K., Ha, B.-K., and Kim, S.-H. (2025). Cowpea (*Vigna unguiculata* L.) production, genetic resources and strategic breeding priorities for sustainable food security: a review. Front. Plant Sci. **16:** 1562142.

Ko, D.K., and Brandizzi, F. (2024). Dynamics of ER stress-induced gene regulation in plants. Nat. Rev. Genet. **25**: 513–525.

Lima, K.R.P., Cavalcante, F.L.P., Paula-Marinho, S.O., Pereira, I.M.C., Lopes, L.S., Nunes, J.V.S., Coutinho, Í.A.C., Gomes-Filho, E., and Carvalho, H.H. (2022). Metabolomic profiles exhibit the influence of endoplasmic reticulum stress on sorghum seedling growth over time. Plant Physiol. Biochem. **170**: 192–205.

Lisec, J., Schauer, N., Kopka, J., Willmitzer, L., and Fernie, A.R. (2006). Gas chromatography mass spectrometry-based metabolite profiling in plants. Nat. Protoc. **1**: 387–396.

Liu, Y., Lv, Y., Wei, A., Guo, M., Li, Y., Wang, J., Wang, X., and Bao, Y. (2022). Unfolded protein response in balancing plant growth and stress tolerance. Front. Plant Sci. **13**: 1019414.

Livak, K.J., and Schmittgen, T.D. (2001). Analysis of relative gene expression data using real-time quantitative PCR and the 2(-Delta Delta C(T)) method. Methods **25**: 402 408.

Malavolta, E., Vitti, G.C., and Oliveira, S.A. (1997). Avaliação do estado nutricional das plantas: Princípios e aplicações. 2nd ed., revised and updated. Potafos, Piracicaba, SP, Brazil. 319 p.

Matkowski, H., and Daszkowska-Golec, A. (2025). Wisdom comes after facts – An update on plants priming using phytohormones. J. Plant Physiol. **305**: 154414.

Micera, M., Botto, A., Geddo, F., Antoniotti, S., Bertea, C.M., Levi, R., Gallo, M.P., and Querio, G. (2020). Squalene: More than a step toward sterols. Antioxidants **9**: 688.

Miller, G., Suzuki, N., Ciftci-Yilmaz, S., and Mittler, R. (2010). Reactive oxygen species homeostasis and signalling during drought and salinity stresses. Plant Cell Environ. **33:** 453–467.

Naqve, M., Wang, X., Shahbaz, M., Mahmood, A., Bibi, S., and Fiaz, S. (2021). Alpha tocopherol-induced modulations in the morphophysiological attributes of okra under saline conditions. Front. Plant Sci. **12**: 800251.

Obata, T., and Fernie, A.R. (2012). The use of metabolomics to dissect plant responses to abiotic stresses. Cell Mol. Life Sci. **69**: 3225–3243.

Oliveira, F.D.B., Pereira, I.M.C., Costa, I.R.S., Cavalcante, F.L.P., Coutinho, I.A.C., Alves, M.S., Paula-Marinho, S.O., Gomes-Filho, E., and Carvalho, H.H. (2025). Endoplasmic reticulum activation via tunicamycin seed priming enhances salt acclimation in rice seedlings. Plant Sci. **358**: 112567.

Ozgur, R., Turkan, I., Uzilday, B., and Sekmen, A.H. (2014). Endoplasmic reticulum stress triggers ROS signalling, changes the redox state, and regulates the antioxidant defence of *Arabidopsis thaliana*. J. Exp. Bot. **65**: 1377–1390.

Ozgur, R., Uzilday, B., Iwata, Y., Koizumi, N., and Turkan, I. (2018). Interplay between the unfolded protein response and reactive oxygen species: A dynamic duo. J. Exp. Bot. **69**: 3333–3345.

Pang, Z., Lu, Y., Zhou, G., Hui, F., Xu, L., Viau, C., Spigelman, A.F., MacDonald, P.E., Wishart, D.S., Li, S., and Xia, J. (2024). MetaboAnalyst 6.0: Towards a unified platform for metabolomics data processing, analysis and interpretation. Nucleic Acids Res. **52**: W398–W406.

Praxedes, S.C., DaMatta, F.M., Lacerda, C.F., Prisco, J.T., and Gomes-Filho, E. (2014). Salt stress tolerance in cowpea is poorly related to the ability to cope with oxidative stress. Acta Bot. Croat. **73**: 51–62.

Praxedes, S.S.C., Neto, M.F., Loiola, A.T., Santos, F.J.Q., Umbelino, B.F., Silva, L.A., Moreira, R.C.L., Melo, A.S., Lacerda, C.F., Fernandes, P.D., Dias, N.S., and Sá, F.V.S. (2022). Photosynthetic responses, growth, production, and tolerance of traditional varieties of cowpea under salt stress. Plants. **11**: 1863**.**

Queiroz, C.S., Pereira, I.M.C., Lima, K.R.P., Bret, R.S.C., Alves, M.S., Gomes-Filho, E., and Carvalho, H.H. (2020). Combined NaCl and DTT diminish harmful ER-stress effects in the sorghum seedlings CSF 20 variety. Plant Physiol. Biochem. **147:** 223–234.

Rahali-Osman, S., Boulahia, K., Djebbar, R., and Abrous-Belbachir, O. (2020). Assessment of oxidative stress and proline metabolism genes expression of cowpea plants (*Vigna unguiculata* L.) under saline conditions. Analele Univ. Oradea Fascic. Biol. **27**: 7 16**.**

Rosegrant, M.W., Sulser, T.B., Dunston, S., Mishra, A., Cenacchi, N., Gebretsadik, Y., Robertson, R., Thomas, T., and Wiebe, K. (2024). Food and nutrition security under changing climate and socioeconomic conditions. Glob. Food Secur. **41**: 100755.

Ruberti, C., and Brandizzi, F. (2014). Conserved and plant-unique strategies for overcoming endoplasmic reticulum stress. Front. Plant Sci. **5**: 69.

Ruberti, C., Lai, Y., and Brandizzi, F. (2018). Recovery from temporary endoplasmic reticulum stress in plants relies on the tissue-specific and largely independent roles of bZIP28 and bZIP60, as well as an antagonizing function of BAX-Inhibitor 1 upon the pro-adaptive signaling mediated by bZIP28. Plant J. **93**: 155–165.

Sackey, O.K., Feng, N., Mohammed, Y.Z., Dzou, C.F., Zheng, D., Zhao, L., and Shen, X. (2025). A comprehensive review on rice responses and tolerance to salt stress. Front. Plant Sci. **16**: 1561280.

Sahoo, L., Swain, B., and Yadav, D. (2025). A review on different priming strategies to mitigate abiotic stress in plants. Discov. Appl. Sci. **7**: 618.

Sanga, D.L., Mwamahonje, A.S., Mahinda, A.J., and Kipanga, E.A. (2024). Soil salinization under irrigated farming: A threat to sustainable food security and environment in semi-arid tropics. J. Agric. Sci. Pract. **9**: 32–47.

Savvides, A., Ali, S., Tester, M., and Fotopoulos, V. (2016). Chemical priming of plants against multiple abiotic stresses: Mission possible? Trends Plant Sci. **21**: 329–340.

Schales, O., and Schales, S.S. (1941). A simple and accurate method for the determination of chloride in biological fluids. J. Biol. Chem. **140**: 879–884.

Silva, D.J. (1999). Análise de nutrientes em plantas: Métodos químicos e instrumentais. Universidade Federal de Viçosa, Viçosa, MG, Brazil. 165 p.

Souza, C.L.C., Rocha, M.M., Silva, K.J.D., Coelho, A.P., Lemos, L.B., and Mingotte,

F.L.C. (2022). Adaptability and yield stability of cowpea genotypes in the Mid-North region of Brazil. Rev. Bras. Cienc. Agrar. **17:** e1614.

Souza, J.R.M., Leal, L.Y.C., Paulino, M.K.S.S., Nunes, J.A., Medeiros, R.L.S., Santos, M.A., Lins, C.M.T., Souza Júnior, V.S., Schaffer, B., and Souza, E.R. (2025). Cowpea (*Vigna unguiculata*) water relations, growth, and productivity as affected by salinity in two soils with contrasting mineralogies. Soil Syst. **9**: 36.

Srivastava, R., Li, Z., Russo, G., Tang, J., Bi, R., Muppirala, U., Chudalayandi, S., Severin, A., He, M., Vaitkevicius, S.I., Lawrence-Dill, C.J., Liu, P., Stapleton, A.E., Bassham, D.C., Brandizzi, F., and Howell, S.H. (2018). Response to persistent ER stress in plants: A multiphasic process that transitions cells from prosurvival activities to cell death. Plant Cell **30**: 1220–1242.

Taie, H.A.A., and Rady, M.M. (2024). α-Tocopherol mediates alleviation of salt stress effects in *Glycine max* through up-regulation of the antioxidant defense system and secondary metabolites. Acta Physiol Plant. **46**: 39.

Takatsuki, K., Arima, K., and Tamura, G. (1971). Tunicamycin, a new antibiotic. I. Isolation and characterization of tunicamycin A. J. Antibiot (Tokyo). **24**: 215–223.

Terán, F., Vives-Peris, V., Gómez-Cadenas, A., and Pérez-Clemente, R.M. (2024). Facing climate change: plant stress mitigation strategies in agriculture. Physiol. Plant. **176**: e14484.

Tripathi, D.K., Bhat, J.A., Antoniou, C., Kandhol, N., Singh, V.P., Fernie, A.R., and Fotopoulos, V. (2024). Redox regulation by priming agents toward a sustainable agriculture. Plant Cell Physiol. **65**: 1087–1102.

UNICEF (2025). *Nutrition*. Available at: https://www.unicef.org/nutrition.

Untergasser, A., Cutcutache, I., Koressaar, T., Ye, J., Faircloth, B.C., Remm, M., and Rozen, S.G. (2012). Primer3—new capabilities and interfaces. Nucleic Acids Res. **40**: e115.

Valitova, J., Renkova, A., Beckett, R., and Minibayeva, F. (2024). Stigmasterol: An enigmatic plant stress sterol with versatile functions. Int. J. Mol. Sci. **25**: 8122.

Velikova, V., Yordanov, I., and Edreva, A. (2000). Oxidative stress and some antioxidant systems in acid rain-treated bean plants: Protective role of exogenous polyamines. Plant Sci. **151**: 59–66.

Zhang, H., Zhu, J., Gong, Z., and Zhu, J.-K. (2022). Abiotic stress responses in plants. Nat. Rev. Genet. **23**: 104–119.

Zhao, C., Zhang, H., Song, C., Zhu, J.-K., and Shabala, S. (2020). Mechanisms of plant responses and adaptation to soil salinity. The Innovation **1**: 100017.

Zhou, H., Shi, H., Yang, Y., Feng, X., Chen, X., Xiao, F., Lin, H., and Guo, Y. (2024).

Insights into plant salt stress signaling and tolerance. J. Genet. Genomics. **51**: 16–34.

Zulfiqar, F., Nafees, M., Chen, J., Darras, A., Ferrante, A., Hancock, J.T., Ashraf, M., Zaid, A., Latif, N., Corpas, F.J., Altaf, M.A., and Siddique, K.H.M. (2022). Chemical priming enhances plant tolerance to salt stress. Front. Plant Sci. **13**: 946922.

4.8 Supplementary data

Supplementary Table S1 - Reference and target gene primer sequences.

Gene symbol	Gene Identifier	Functional Annotation	Primer sequence (5'-3')	Annealing temperature
UBQ3	Vigun 03g105700	Protein ubiquitination; constitutive expression	F- TCTTGTCTTGCGACTCCGTG	55 ºC
			R- TCGTGTCTGAACTCTCGACC	
F-box3	Vigun 11g167000	Protein ubiquitination (SCF E3 ligase component)	F- AAATGAATATGGCCGAAGCATT	57 ºC
			R- AATGCAGACGAGCGAACCTT	
IRE1A	Vigun 03g248800	Inositol-requiring enzyme 1A; ER stress response	F- TTTTGCGTGACACCAGTGAC	55 ºC
			R- TTTTCCACCCAAGGCATCTG	
bZIP60	Vigun 07g038800	Basic leucine zipper 60; UPR-related transcription factor	F - TTGAGGAATAGGGATGCTGCTG	62 ºC
			R - AGCAGCACTGAAGCAAATGC	
bZIP17	Vigun 01g103400	Basic leucine zipper 17; ER stress–responsive transcription factor	F - AATTCCGATTCTCCGCGTTC	52 ºC
			R - AACATCAACCGCGTCATGTG	
BiP1	Vigun 03g033300	Binding immunoglobulin protein 1; ER protein folding chaperone	F- AACGACAAGGACAAGCTTGC	57 ºC
			R- TCATCGAGCCATTCCAATGC	
PDI11	Vigun 07g123600	Protein disulfide isomerase 11; ER protein folding	F- AGGGATCTGGCTGAAAAGTACG	57 ºC
			R- ACCGGCTTTGTTGCTCTTTG	
GRP94	Vigun 08g005200	Glucose-regulated protein 94; ER protein folding	F- ACGCCGAGAAGTTTGAGTTC	57 ºC
			R- TTGTCCAAAGCGTCAGAAGC	

		chaperone		
SOS3	Vigun 10g174100	Salt overly sensitive 3; Ca^{2+} sensor in salt stress response	F - ATTTCAAGACGCCGATGCTG	55 ºC
			R - TGTGCTTCAAGAGTGTTGGG	
SOS2	Vigun 06g085300	Salt overly sensitive 2; protein kinase in salt stress response	F - AGCTAACGGTTGTTGAAGCC	55 ºC
			R – TCAACTTTTCCTCCCACACG	
SOS1	Vigun 03g157800	Salt overly sensitive 1; Na^+/H^+ antiporter in salt stress response	F - AAGTGCAACAACCCGTTTCG	55 ºC
			R – TTCCCAGAGCCAAACTGAGAC	
NHX1	Vigun 07g151400	Na^+/H^+ exchanger 1; vacuolar ion homeostasis	F- AACTCCAACGCACACTGTTC	57 ºC
			R- AAACCCCTTCCACCGAAAAC	

Source: Prepared by the author.

Supplementary Table S8 - R^2 (goodness of fit) and Q^2 (predictive ability) values of PLS-DA models for cowpea leaves and roots.

Leaves				
Measure	1 comps	2 comps	3 comps	4 comps
Accuracy	0,4	0,75	0,9	0,9
R2	0,86231	0,94277	0,98074	0,99067
Q2	0,38456	0,71582	0,77496	0,80304
Roots				
Measure	1 comps	2 comps	3 comps	4 comps
Accuracy	0,53333	0,95	1	1
R2	0,67861	0,8723	0,93723	0,96444
Q2	0,50879	0,75501	0,79486	0,80877

Source: Prepared by the author.

Supplementary Table S3 - Analysis of variance (ANOVA) of morphophysiological and biochemical data in cowpea plants.

Mean square		**Source variation**					
		Treatment	**Salinity**	**Treatment* salinity**	**Error**	**Corrected total**	**CV (%)**
Dry mass	**Leaf**	2.73*	2.85*	0.26^{NS}	12	15	16.02
	Stem	1.22*	1.26*	-2.13^{NS}	12	15	11.95
	Root	0.21*	0.10*	0.02^{NS}	12	15	20.93
Inorganic	**Na^+**	1844.70*	3852.68*	-3.73^{NS}	12	15	13,46

ions	**leaf**						
	K^+ leaf	0.0506*	8.1225*	2.92*	12	15	3,32
	Cl^- leaf	473123.86*	2034132.01*	31.59^{NS}	12	15	23,79
	Na^+ Stem	444.57*	1870.99*	-2.67^{NS}	12	15	10,33
	K^+ Stem	10.04*	29.8662*	59.48*	12	15	7,58
	Cl^- Stem	269703.64*	752625.65*	-1.57^{NS}	12	15	9,28
	Na^+ Root	7.9806*	391.2484*	80.30*	12	15	7,92
	K^+ Root	33.4373*	518.359*	76.07*	12	15	12,1
	Cl^- Root	269392.14*	7119664.79*	-1.34^{NS}	12	15	17,89
Gas exchange	***A***	29.55*	5.21^{NS}	13.25*	8	11	8,16
	gs	0.03*	0.11*	0.023*	8	11	15,18
	Ci/Ca	0.02*	0.06*	0.02*	8	11	5
	E	24.29*	19.51*	3.96^{NS}	8	11	11,65
Thermal regulation	**14 days**	0.14*	51.96*	4.95*	12	15	-53,52
	7 days	1.38^{NS}	22.80*	8.55*	12	15	-30,2
	24h	5.40^{NS}	22.80*	1.15^{NS}	12	15	-42,54
H_2O_2	**Leaf**	0.01*	0.22*	0.01*	12	15	18,36
	Root	0.05*	0.11*	0.34*	12	15	27,65

Source: Prepared by the author.

Supplementary Table S4 - Organic ion contente (Na^+, K^+ and Cl^-) in V4 stage cowpea.

Na^+ (µmol.g^{-1}DM)	**Leaf**		**Stem**		**Root**	
	- TM	**+ TM**	**- TM**	**+ TM**	**- TM**	**+ TM**
Control	4.93 ± 0.82^{Ba}	3.65 ± 0.85^{Ba}	25.51 ± 1.09^{Ba}	24.17 ± 4.06^{Ba}	45.51 ± 1.09^{Ba}	47.13 ± 4.41^{Ba}
75 mM NaCl	45.66 ± 4.37^{Aa}	17.68 ± 0.82^{Ab}	49.91 ± 3.67^{Aa}	40.29 ± 1.64^{Ab}	53.91 ± 4.08^{Ab}	60.58 ± 3.28^{Aa}
K^+ (µmol.g^{-1}DM)	**Leaf**		**Stem**		**Root**	
	- TM	**+ TM**	**- TM**	**+ TM**	**- TM**	**+ TM**
Control	17.73 ± 0.24^{Aa}	17.49 ± 0.59^{Ba}	22.67 ± 0.97^{Aa}	19.44 ± 1.25^{Ab}	20.12 ± 0.87^{Ab}	25.57 ± 4.11^{Aa}
75 mM NaCl	18.54 ± 0.67^{Ab}	19.78 ± 0.48^{Aa}	15.99 ± 1.59^{Bb}	21.14 ± 1.28^{Aa}	14.15 ± 0.87^{Ba}	8.79 ± 0.42^{Bb}
Cl^- (µmol.g^{-1}DM)	**Leaf**		**Stem**		**Root**	
	- TM	**+ TM**	**- TM**	**+ TM**	**- TM**	**+ TM**

Control	229.75 ± 0.01^{Ba}	281.93 ± 0.02^{Ba}	323.24 ± 0.01^{Ba}	224.39 ± 0.01^{Bb}	401.16 ± 0.01^{Ba}	307.82 ± 0.02^{Ba}
75 mM NaCl	1127.56 ± 0.05^{Aa}	722.01 ± 0.01^{Ab}	779.14 ± 0.03^{Aa}	555.39 ± 0.01^{Ab}	1582.74 ± 0.05^{Aa}	1883.98 ± 0.04^{Aa}

Source: Prepared by the author.

Supplementary Figure S1 - Leaf temperature (ΔT) in cowpea plants under salinity and TM priming. ΔT was measured at 24 h and 7 days after salinity onset. Values represent mean ± SE (n = 4). Different letters indicate significant differences by Tukey's test ($p < 0.05$); lowercase letters compare priming treatments, and uppercase letters compare salinity levels.

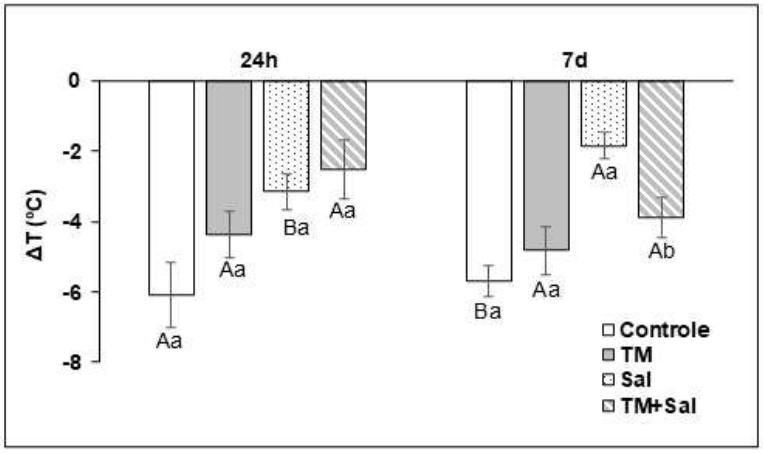

Source: Prepared by the author.

Supplementary Table S5 - List of detected compounds from the metabolomic profiling of shoots and roots of cowpea, including their classification in compound types, retention time, and corresponding Kyoto Encyclopedia of Genes and Genomes (KEGG) identifier or PubChem ID.

Metabolites	Compound type	Retention time (min)	Compound id
Pyruvic acid	Organic acids	7.11	C00022
Glycolic acid	Others	7.64	C00160
Lactic acid	Organic acids	8,05	C00186
Malonic acid	Organic acids	10.20	C00383
Valine	Amino Acids	10.38	C00183
Urea	Others	10,75	C00086
Alanine	Amino Acids	11.23	C00041
Leucine	Amino Acids	11.69	C00123
Isoleucine	Amino Acids	11.71	C00407
Glycine	Amino Acids	11.88	C00037
Succinic acid	Organic acids	11.96	C00042

Phosphoric acid	Others	12,07	C00009
Glyceric acid	Organic acids	12.3	C00258
Fumaric acid	Organic acids	12.43	C00122
Serine	Amino Acids	12.72	C00065
Threonine	Amino Acids	13	C00188
Beta-Alanine	Amino Acids	13,62	C00099
Malic acid	Organic acids	14.48	C00149
Aspartic acid	Amino Acids	14,88	C00049
Proline	Amino Acids	14.93	C00148
N-acetyl-Serine	Amino Acids	14,97	CID 65249
Putrescine	Polyamines	15.16	C00134
Threonic acid	Organic acids	15.24	C01620
Pyroglutamic acid	Amino acids	15.56	C01879
Glutamine	Amino Acids	16,06	C00064
Glutamic acid	Amino Acids	16.07	C00025
Fucose	Carbohydrates	16,26	C06471
Xylulose	Carbohydrates	16,54	C00312
Asparagine	Amino Acids	16,7	C00152
Ribose	Carbohydrates	16,87	C00121
Ribitol	Internal standard	17.41	C00474
Cinnamic acid	Others	17,99	C10438
Shikimic acid	Others	18.2	C00493
Citric acid	Organic acids	18.38	C00158
Dehydroascorbic acid	Organic acids	18.73	C05422
Fructose	Carbohydrates	19.01	C00095
Glucose	Carbohydrates	19,3	C00031
Galactose	Carbohydrates	19.48	C00124
Mannitol	Carbohydrates	19,6	C00392
Sorbitol	Carbohydrates	19.67	C00794
Myo-Inositol	Carbohydrates	21.15	C00137
Caffeic acid	Others	21.37	C01197
Spermidine	Polyamines	22	C00315
Cadaverine	Polyamines	22,53	C01672
Ribose-5-phosphate	Carbohydrates	23.62	C00117
Raffinose	Carbohydrates	24.99	C00492
Maltose	Carbohydrates	25.56	C00208
Sucrose	Carbohydrates	25.79	C00089
Trehalose	Others	27,35	C22876
Kestose	Carbohydrates	27.76	C03661
Maltotriose	Carbohydrates	33.37	C01835

Source: Prepared by the author.

Supplementary Table S6 - List of detected compounds from the lipidomic profiling of shoots and roots of cowpea, including their classification in compound types, retention time, and corresponding Kyoto Encyclopedia of Genes and Genomes (KEGG) identifier or PubChem ID.

Metabolites	Compound type	Retention time (min)	Compound id
Phosphoric acid	Others	15,48	C00009
Glycerol	Others	15,61	C00116
1-Hexadecanol	Fatty alcohols	15,82	C00823
Glycerol-3-phosphate	Others	30,74	C03189
Neophytadiene	Diterpene	31,92	CID 10446
Tetradecanoic acid	Fatty acids	32,25	C06424
Mevalonic acid	Fatty acids	36,01	C00418
Hexadecanoic acid	Fatty acids	37,03	C00249
Heptadecanoic acid	Fatty acids	39,27	CID 10465
Phytol	Diterpene	40,02	C01389
9,12-Octadecadienoic acid	Fatty acids	40,72	C01595
9,12,15-Octadecatrienoic acid	Fatty acids	40,87	C06426
9-Octadecenoic acid	Fatty acids	41	C00712
Alpha-Linolenic acid	Fatty acids	41,2	C06427
Octadecanoic acid	Fatty acids	41,41	C01530
Myo-Inositol 2-phosphate	Others	45,92	CID 25200860
Ethanolamine	Ohers	46,24	CID 700
All-trans-Squalene	Triterpene	52,54	CID 638072
Tetracosanoic acid	Fatty acids	52,73	C08320
Farnesol	Terpene	55,74	C01493
Alpha-tocopherol acetate	Vitamins	57,55	C13202
1-Octacosanol	Fatty alcohols	57,71	C08387
Alpha-Tocopherol	Vitamins	57,83	C02477
Cholesterol	Internal standard	57,94	C00187
Octacosanoic acid	Fatty acids	59,1	C21933
Campesterol	Steroids	59,59	C01789
Stigmasterol	Steroids	60,06	C05442
Beta-Sitosterol	Steroids	60,96	C01753

Source: Prepared by the author.

Supplementary Figure S2 - Variable importance in projection (VIP) scores of metabolites and lipids in cowpea plants. VIP models were generated from metabolic (A,B) and lipid (C,D) profiles of leaves and roots of V4-stage plants grown under control, 75 mM NaCl, TM, and TM + 75 mM NaCl treatments. Metabolites and lipids with VIP scores > 1.0 were considered major contributors to group discrimination.

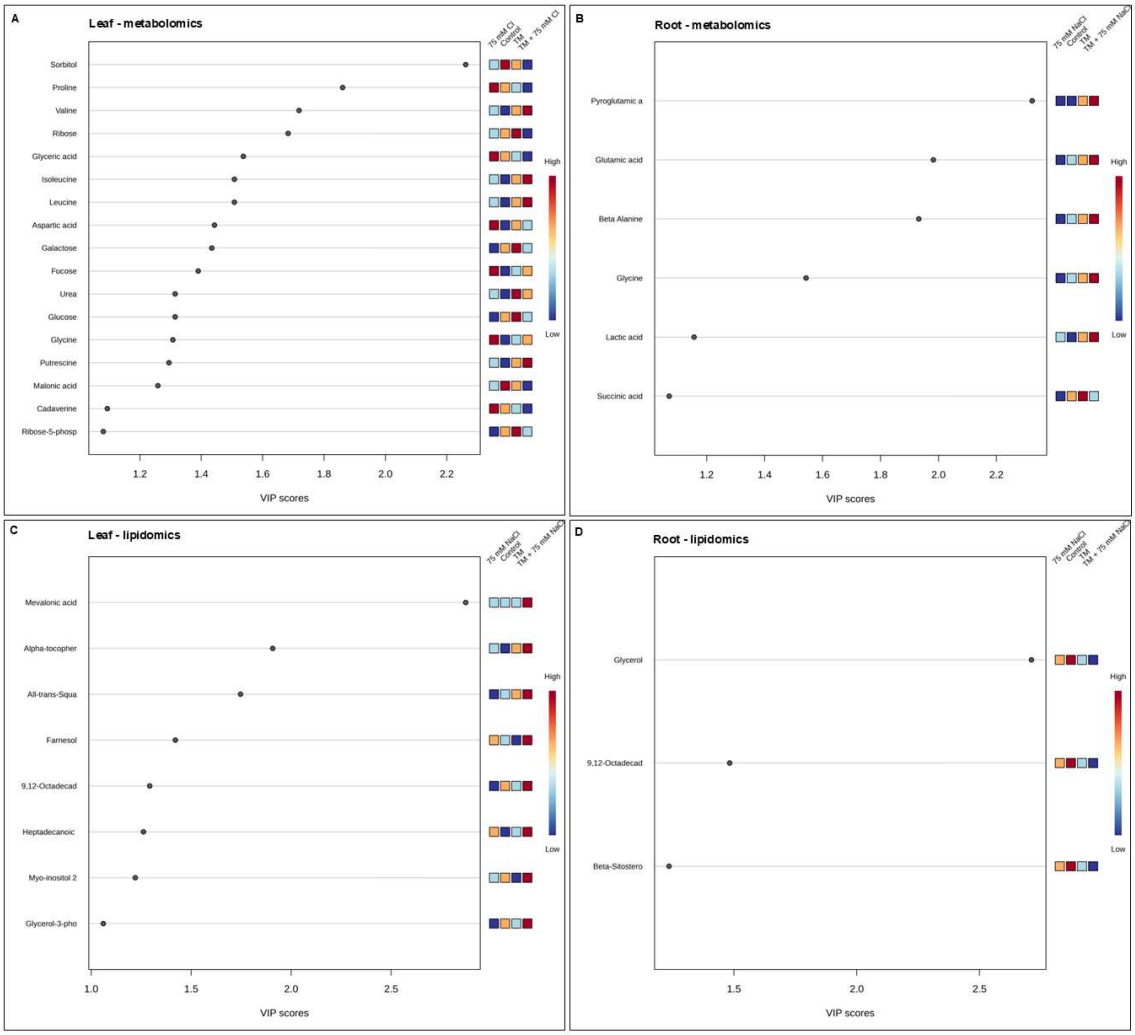

Source: Prepared by the author.

Supplementary Table S7 - Over-representation analysis (ORA) of differentially accumulated metabolites in TM + 75 mM NaCl vs. 75 mM NaCl.

Pathway	**Total**	**Expected**	**Hits**	**Raw p**	**Holm p**	**FDR**
Leaf metabolomics						
Galactose metabolism	27	0.175	3	0.000533	0.0426	0.0426
Fructose and mannose metabolism	20	0.13	2	0.00679	0.536	0.206
Pentose phosphate pathway	23	0.149	2	0.00894	0.698	0.206
Glutathione metabolism	28	0.182	2	0.0131	0.998	0.206

Glyoxylate and dicarboxylate metabolism	31	0.201	2	0.016	10.000	0.206
Glycine, serine and threonine metabolism	33	0.214	2	0.018	10.000	0.206
Arginine and proline metabolism	36	0.234	2	0.0213	10.000	0.213
Arginine biosynthesis	14	0.091	1	0.0876	10.000	0.663
Nicotinate and nicotinamide metabolism	15	0.0975	1	0.0936	10.000	0.663
Histidine metabolism	16	0.104	1	0.0995	10.000	0.663
Glycerolipid metabolism	16	0.104	1	0.0995	10.000	0.663
Starch and sucrose metabolism	18	0.117	1	0.111	10.000	0.685
Pantothenate and CoA biosynthesis	20	0.13	1	0.123	10.000	0.687
beta-Alanine metabolism	21	0.136	1	0.129	10.000	0.687
Alanine, aspartate and glutamate metabolism	28	0.182	1	0.168	10.000	0.792
Lipoic acid metabolism	28	0.182	1	0.168	10.000	0.792
Porphyrin metabolism	31	0.201	1	0.185	10.000	0.82
Amino sugar and nucleotide sugar metabolism	42	0.273	1	0.242	10.000	10.000
Root metabolomics						
Glutathione metabolism	28	0.091	3	0.000053	0.00422	0.00422
Butanoate metabolism	15	0.0487	2	0.000872	0.0689	0.0349
Propanoate metabolism	21	0.0682	2	0.00173	0.135	0.0462
Alanine, aspartate and glutamate metabolism	28	0.091	2	0.00309	0.238	0.0504
Glyoxylate and dicarboxylate metabolism	31	0.101	2	0.00378	0.287	0.0504
Porphyrin metabolism	31	0.101	2	0.00378	0.287	0.0504
Nitrogen metabolism	6	0.0195	1	0.0194	100.000	0.221
Arginine biosynthesis	14	0.0455	1	0.0447	100.000	0.443
Histidine metabolism	16	0.052	1	0.051	100.000	0.443
Citrate cycle (TCA cycle)	20	0.065	1	0.0634	100.000	0.443
Pantothenate and CoA biosynthesis	20	0.065	1	0.0634	100.000	0.443
beta-Alanine metabolism	21	0.0682	1	0.0665	100.000	0.443
Lipoic acid metabolism	28	0.091	1	0.0878	100.000	0.54
Glycine, serine and threonine metabolism	33	0.107	1	0.103	100.000	0.588
Arginine and proline metabolism	36	0.117	1	0.112	100.000	0.596
Pyrimidine metabolism	39	0.127	1	0.121	100.000	0.603
Leaf lipidomics						
Terpenoid backbone biosynthesis	18	0.0234	1	0.0233	1	1
Steroid biosynthesis	41	0.0533	1	0.0526	1	1
Root lipidomics						
Could not be performed						

Supplementary Table S8 - Over-representation analysis (ORA) of differentially accumulated metabolites in additional enrichment analyses.

Pathway	Total	Expected	Hits	Raw p	Holm p	FDR
Leaf metabolomics						
Control vs. 75 mM NaCl						
Galactose metabolism	27	0.105	2	0.00426	0.341	0.311
Arginine biosynthesis	14	0.0546	1	0.0534	1.000	0.611
Nicotinate and nicotinamide metabolism	15	0.0585	1	0.0572	1.000	0.611
Histidine metabolism	16	0.0624	1	0.0609	1.000	0.611
Starch and sucrose metabolism	18	0.0702	1	0.0683	1.000	0.611
Fructose and mannose metabolism	20	0.078	1	0.0756	1.000	0.611
Pantothenate and CoA biosynthesis	20	0.078	1	0.0756	1.000	0.611
beta-Alanine metabolism	21	0.0819	1	0.0793	1.000	0.611
Pentose phosphate pathway	23	0.0897	1	0.0865	1.000	0.611
Alanine, aspartate and glutamate metabolism	28	0.109	1	0.104	1.000	0.611
Glutathione metabolism	28	0.109	1	0.104	1.000	0.611
Lipoic acid metabolism	28	0.109	1	0.104	1.000	0.611
Glyoxylate and dicarboxylate metabolism	31	0.121	1	0.115	1.000	0.611
Porphyrin metabolism	31	0.121	1	0.115	1.000	0.611
Glycine, serine and threonine metabolism	33	0.129	1	0.122	1.000	0.611
Amino sugar and nucleotide sugar metabolism	42	0.164	1	0.153	1.000	0.721
Purine metabolism	70	0.273	1	0.244	1.000	1.000
Control vs. TM						
Valine, leucine and isoleucine biosynthesis	8	0.026	3	9.19E-07	0.000073	0.000073
Valine, leucine and isoleucine degradation	39	0.127	3	1.45E-04	0.0115	0.00582
Arginine biosynthesis	14	0.0455	1	0.0447	1.000.000	0.914
Pantothenate and CoA biosynthesis	20	0.065	1	0.0634	1.000.000	0.914
Glutathione metabolism	28	0.091	1	0.0878	1.000.000	0.914
Lipoic acid metabolism	28	0.091	1	0.0878	1.000.000	0.914
Glyoxylate and dicarboxylate metabolism	31	0.101	1	0.0969	1.000.000	0.914
Porphyrin metabolism	31	0.101	1	0.0969	1.000.000	0.914
Glycine, serine and threonine metabolism	33	0.107	1	0.103	1.000.000	0.914
Purine metabolism	70	0.227	1	0.208	1.000.000	1.000.000
Root metabolomics						

Control vs. 75 mM NaCl						
Valine, leucine and isoleucine biosynthesis	8	0.026	3	9.19E-07	0.000073	0.000073
Valine, leucine and isoleucine degradation	39	0.127	3	1.45E-04	0.0115	0.00582
Arginine biosynthesis	14	0.0455	1	0.0447	1.000.000	0.914
Pantothenate and CoA biosynthesis	20	0.065	1	0.0634	1.000.000	0.914
Glutathione metabolism	28	0.091	1	0.0878	1.000.000	0.914
Lipoic acid metabolism	28	0.091	1	0.0878	1.000.000	0.914
Glyoxylate and dicarboxylate metabolism	31	0.101	1	0.0969	1.000.000	0.914
Porphyrin metabolism	31	0.101	1	0.0969	1.000.000	0.914
Glycine, serine and threonine metabolism	33	0.107	1	0.103	1.000.000	0.914
Purine metabolism	70	0.227	1	0.208	1.000.000	1.000.000
Control vs. TM						
Could not be performed						
Leaf lipidomics						
Control vs. 75 mM NaCl						
Could not be performed						
Control vs. TM						
Could not be performed						
Root lipidomics						
Control vs. 75 mM NaCl						
Could not be performed						
Control vs. TM						
Linoleic acid metabolism	5	0.0065	1	0.00649	0.519	0.519
Biosynthesis of unsaturated fatty acids	36	0.0468	1	0.0463	1.000	1.000
Steroid biosynthesis	41	0.0533	1	0.0526	1.000	1.000

Source: Prepared by the author.

Supplementary Figure S3 - Additional pathway enrichment analyses. (A) Control vs. 75 mM NaCl (leaf metabolomics), (B) Control vs. TM (leaf metabolomics), (C) Control vs. 75 mM NaCl (root metabolomics), and (D) Control vs. TM (root lipidomics). In some comparisons, no significant enrichment was detected due to the limited number of differential metabolites.

Source: Prepared by the author.

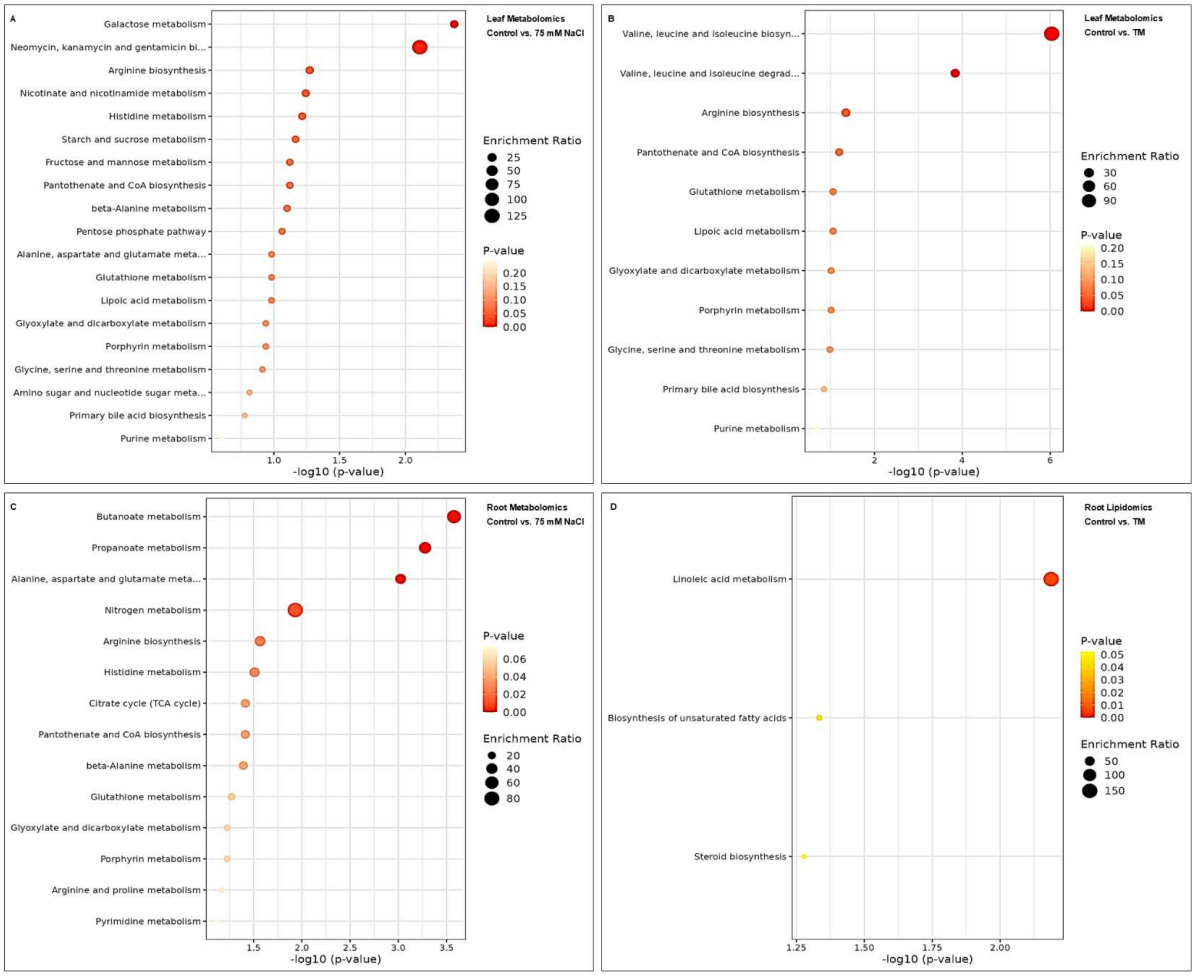

Source: Prepared by the author.

5 CAPÍTULO II: EARLY GENE EXPRESSION AND POST-TRANSLATIONAL MECHANISMS OF ER-INDUCED PRIMING TO PROMOTE SALT ACCLIMATION IN COWPEA (*Vigna unguiculata* [L.] Walp)

5.1 Abstract

Abiotic stress tolerance depends on rapid signal integration at the organelle level, where redox and proteostasis networks coordinate adaptive responses. Here, we investigated whether transient endoplasmic reticulum (ER) stress induced by foliar tunicamycin (TM) application could precondition cowpea (*Vigna unguiculata* [L.] Walp) plants for an early salinity acclimation. A time-resolved approach integrating H_2O_2 quantification, RT-qPCR of unfolded protein response (UPR) and salt transporter genes, and label-free proteomics was employed. TM spray induced a rapid but transient ER stress response, characterized by an early H_2O_2 burst, activation of *VuIRE1A–VubZIP60* signaling, and temporary gene expression upregulation of ER chaperones, all returning to near-basal levels within 24 h. Proteomic analysis confirmed moderate metabolic adjustment without global repression. In contrast, salinity alone triggered sustained ER stress, progressive induction of chaperones and Na^+ transporters, and broad downregulation of carbon metabolism and biosynthetic pathways. Importantly, TM priming attenuated the early oxidative burst under salinity, anticipated ER and salt overly sensitive (SOS) signaling, limited prolonged chaperone and ion transporter overactivation, and partially prevented salt-induced proteomic repression. Priming-specific differentially abundant proteins highlighted coordinated modulation of redox, translational, and stress-responsive pathways. Collectively, our findings support a model in which transient ER activation functions as a regulatory signal that enhances stress efficiency by optimizing redox balance, proteostasis capacity, and ionic homeostasis. This work positions ER-mediated priming as a promising strategy to improve salinity resilience in cowpea and identifies candidate molecular targets for future functional validation and breeding programs.

Keywords: Redox homeostasis. UPR. Proteome reprogramming.

5.2 Introduction

Plant survival under abiotic stress requires coordinated physiological adjustments at the whole-plant level (Suzuki et al., 2012; Mittler et al., 2022; Jiang et al., 2025; Zhao et al., 2025). These systemic responses are initiated by early stress perception mechanisms operating at cellular and subcellular interfaces, where membranes and organelles act as hubs for metabolic signal integration (Waszczak et al., 2018). This information is subsequently propagated systemically through reactive oxygen species (ROS) waves, calcium signaling, electrical signals, and phytohormone-mediated pathways, shaping adaptive plasticity and acclimation to complex and combined stress scenarios (Choi et al., 2014; Zandalinas et al., 2020; Jiang et al., 2025).

The signaling phase is critical, as rapid signal perception and integration determine downstream physiological trajectories, including ion homeostasis, metabolic reprogramming, and growth regulation under adverse conditions (Zhang et al., 2025; Zhao et al., 2025). At the whole-plant level, such signaling flexibility underpins phenotypic plasticity, contributing to yield stability and stress resilience under fluctuating environments, including heat and drought (Singh Sangha et al., 2025). In this context, stress priming refers to a phenomenon in which prior exposure to a mild stimulus enhances the speed or magnitude of subsequent stress responses (Bruce et al., 2007; Hilker et al., 2016). This enhanced responsiveness involves redox modulation, transcriptional reprogramming, and post-translational regulation, ultimately improving stress acclimation (Mauch-Mani et al., 2017).

Among chemical agents capable of eliciting controlled cellular stress responses, tunicamycin (TM) is a well-established inducer of endoplasmic reticulum (ER) stress in plants (Howell, 2013). TM inhibits N-linked glycosylation, leading to the accumulation of misfolded proteins in the ER lumen and activation of the unfolded protein response (UPR) (Liu and Howell, 2016). In plants, the UPR is a highly conserved stress signaling network that integrates multiple ER stress sensors to maintain proteostasis and coordinate downstream transcriptional reprogramming. The two canonical branches of plant UPR encompass the IRE1–bZIP60 pathway and the membrane-associated transcription factors bZIP17/bZIP28, which function in parallel to enhance ER protein-folding capacity through induction of molecular chaperones and ER quality control genes (Liu et al., 2022; Ayaz et al., 2024). Upon accumulation of unfolded proteins in the ER lumen, the ER chaperone BiP dissociates from these sensors, enabling IRE1 oligomerization and activation of its RNase domain, which catalyzes unconventional splicing of bZIP60 mRNA to generate a mobile transcription factor

that upregulates UPR targets including BiP, protein disulfide isomerases and other ER-associated folding catalysts. In parallel, stress conditions trigger the relocation of bZIP17 and bZIP28 from the ER to the Golgi, where they undergo regulated intramembrane proteolysis and the released N-terminal fragments translocate to the nucleus to activate overlapping UPR transcriptional programs and promote ER homeostasis (Liu et al., 2022; Ko, 2024). This dynamic signaling mechanisms enable flexible modulation of ER stress responses in the face of abiotic challenges, and their components have been linked to broader stress adaptation networks including salinity and heat stress (Guan et al., 2025). When ER stress is mild or transient, UPR activation promotes adaptive transcriptional and metabolic reprogramming aimed at restoring ER homeostasis and supporting cell survival (Ruberti et al., 2015; Angelos et al., 2017). In contrast, under severe or prolonged stress, UPR signaling may shift from protective adjustment to growth inhibition and programmed cell death (Williams et al., 2014).

A hallmark of early ER perturbation is the regulated production of reactive oxygen species (ROS), particularly hydrogen peroxide (H_2O_2), which acts as a signaling molecule coordinating transcriptional regulation, redox balance, and antioxidant responses (Černý et al., 2018). Redox-mediated adjustments modulate protein-folding capacity, antioxidant activity, and central metabolic pathways during ER stress, contributing to cellular homeostasis (Černý et al., 2018; Lima et al., 2022; Cavalcante et al., 2023). Accordingly, early quantification of H_2O_2 following TM application provides insight into the initial redox signaling events that preceded transcriptional, proteomic, and metabolomic reprogramming.

Experimental evidence indicates that tolerance to ER stress is species- and genotype-dependent. In sorghum, differential tolerance to tunicamycin-induced ER stress has been reported, with specific genotypes exhibiting enhanced metabolic capacity to cope with protein misfolding while sustaining cellular homeostasis and growth (Cavalcante et al., 2023). In parallel, ER stress signaling intersects with salinity responses by coordinating Na^+ exclusion, K^+ retention, and osmolyte accumulation to maintain cellular water balance, thereby reinforcing functional crosstalk among ER homeostasis and ionic and osmotic stress adjustments (Liu and Howell, 2016; Zhang et al., 2025). Recent findings demonstrate that rice seeds pre-treated with low TM concentrations exhibit enhanced germination and salt acclimation, highlighting the potential of ER-mediated signaling pathways to improve stress tolerance (Oliveira et al., 2025). Consistently, our previous work showed that leaf-applied TM priming enhanced salt tolerance in cowpea, supporting the broader relevance of this strategy across species and developmental stages (unpublished data; manuscript in preparation).

At the systems level, quantitative proteomics has emerged as a powerful approach

to map ER stress responses, revealing coordinated modulation of ER chaperones, redox regulators, intracellular components, and secretory proteins (Kosová et al., 2018). However, proteomic data alone cannot confirm the mechanistic involvement of ER signaling. To further substantiate the contribution of ER stress pathways to TM-mediated protection, targeted RT-qPCR analyses focusing on ER-resident UPR genes and salt-responsive ion transporters provide a complementary and mechanistically informative strategy. This approach links early ER–UPR activation to downstream ion-homeostasis mechanisms under salinity.

We further propose that foliar tunicamycin-induced transient ER activation prior to salt exposure establishes a preconditioned cellular state characterized by enhanced proteostasis capacity, redox modulation, and signaling readiness, thereby facilitating a faster and more coordinated response upon subsequent salinity challenge. Collectively, this study highlights the need for an integrative, time-resolved framework to understand how foliar TM application shapes early ER–UPR activation, H_2O_2-mediated redox signaling, and proteomic reprogramming in cowpea (*Vigna unguiculata* [L.] Walp.), a crop of high agronomic relevance in salt-affected regions. By integrating early H_2O_2 quantification, label-free proteomics, and targeted qPCR analyses of UPR- and salt homeostasis–related genes, this study examines the mechanistic relationship between ER stress signaling and salinity tolerance in cowpea leaves.

5.3 Material and methods

5.3.1 Plant material and experimental design

Cowpea (*Vigna unguiculata* [L.] Walp., genotype CE088) seeds obtained from the Active Germplasm Bank of the Federal University of Ceará (UFC) were germinated in vermiculite until the V2 stage. Seedlings were then transferred to a hydroponic system containing ¼-strength Hoagland nutrient solution and grown until the V4 stage (third fully expanded trifoliate leaf). At V4, plants received a foliar priming treatment consisting of 0.25 μg mL^{-1} tunicamycin (TM) supplemented with 0.05% (v/v) Tween 20, applied at 1.0 mL per leaflet (Oliveira et al., 2025). Control plants were sprayed with desalinated water containing 0.05% (v/v) Tween 20.

To monitor early TM-induced responses, leaf tissues were collected at 0, 1, 6, 12, and 24 h after TM application. Salinity stress was subsequently imposed by adding 75 mM NaCl to the nutrient solution, followed by a second series of collections at 0, 1, 6, 12, and 24

h after salt treatment. Samples from time points were used for H_2O_2 quantification and RT-qPCR analyses. For proteomic analysis, key endpoints were selected: Control (0 h), TM (24 h), NaCl (24 h), and TM + NaCl (24 h).

5.3.2 Hydrogen peroxide quantification

Hydrogen peroxide content was determined according to Velikova et al. (2000). Approximately 200 mg of fresh leaf tissue was homogenized in 1 mL of 5% (w/v) trichloroacetic acid (TCA) using chilled mortars and pestles. The homogenate was centrifuged at 12,000 × g for 15 min at 4 °C, and the supernatant was used immediately for analysis.

For the reaction mixture, 100 µL of TCA extract was mixed with 100 µL of 10 mM potassium phosphate buffer (pH 7.0) and 200 µL of 1 M potassium iodide. Samples were incubated in the dark before absorbance measurement of 390 nm. Hydrogen peroxide concentrations were calculated by interpolation from a standard curve prepared with known H_2O_2 concentrations.

5.3.3 Gene expression by RT-qPCR

Total RNA was extracted from cowpea leaves using TRIzol™ reagent according to the manufacturer's instructions. RNA quantity and purity were assessed spectrophotometrically, and integrity was verified by agarose gel electrophoresis. First-strand cDNA was synthesized from 1 µg of total RNA using M-MLV reverse transcriptase under standard conditions. Quantitative real-time PCR was performed using a CFX Opus 96 Dx system (Bio-Rad) with GoTaq® qPCR Master Mix in 10 µL reaction volumes.

The reference gene *VuUBQ3* was used for normalization. Primers targeting ER stress/UPR-related genes (e.g., *VuBiP*, *VubZIP60*, *VuPDI*, *VuIRE1*, *VubZIP17*) and salt-responsive ion transporters (*VuSOS* and *VuNHX*) were designed based on cowpea homologs identified in Phytozome and validated for specificity using BLAST (Supplementary Table S1). All reactions were performed in technical triplicates under the following cycling conditions: 95 °C for 2 min, followed by 40 cycles of 95 °C for 15 s, gene-specific annealing temperature for 15 s, and 60 °C for 20 s. Melting curve analysis confirmed single amplicon specificity. Primer efficiencies ranged from 90% to 110%. Relative transcript abundance was calculated using the $2^{-\Delta\Delta Ct}$ method (Livak & Schmittgen, 2001).

5.3.4 Proteomic analysis

5.3.4.1 Protein extraction and tryptic digestion

Approximately 150 mg of lyophilized material of each treatment was macerated in liquid nitrogen using a mortar and pestle, and then mixed with 1 mL of Urea/Thiourea extraction buffer composed of 7 M urea (GE Healthcare, Freiburg, Germany), 2M thiourea (GE Healthcare), 2% Triton X-100 (GE Healthcare), 1% dithiothreitol (DTT, GE Healthcare), and 1 mM phenylmethylsulfonyl fluoride (PMSF, Sigma-Aldrich). Samples were vortexed for 30 min at 8 °C in a refrigerator, followed by centrifugation at 16,000 × g for 20 min at 4 °C. The supernatants containing total proteins were collected, and the protein concentration was measured using Bradford reagent (Sigma-Aldrich).

The protein samples were precipitated using a methanol/chloroform method to remove any interfering compounds (Nanjo, et al. 2012). The samples were then resuspended in a solution containing 7 M urea and 2 M thiourea, followed by tryptic protein digestion (1:100 enzyme:protein, V5111, Promega, Madison, WI, USA) using the filter-aided sample preparation (FASP) method (Wisniewski, et al. 2009) with minor modifications (Botini et al., 2021). The peptides were vacuum-dried and solubilized in 50 µL of a solution containing 5% (v/v) acetonitrile (Thermo Fisher Scientific, Waltham, MA, USA) and 0.1% (v/v) formic acid (Sigma-Aldrich) in mass spectrometry (MS)-grade water (Sigma-Aldrich). The peptide concentration was estimated by measuring A205 nm using a NanoDrop 2000c spectrophotometer (Thermo Fisher Scientific). The peptides were stored at −80 °C until mass spectrometry analyses.

5.3.4.2 LC–MS/MS analysis, data processing and functional annotation

For LC-ESI-MS/MS analysis, 2 µg of peptides were injected into a nanoAcquity UPLC M-class system (Waters) coupled to a SYNAPT G2-Si mass spectrometer, following the parameters described by Xavier et al. (2023). Spectra were processed using ProteinLynx Global SERVER (PLGS) software v3.0.2 (Waters).

Proteins were identified against the *Vigna unguiculata* reference proteome (UniProtKB ID: UP000501690). Label-free quantification was performed using IsoQuant software v1.7 (Distler et al., 2014). Only proteins detected in all three biological replicates or uniquely present in a specific treatment were considered for comparative analyses.

Functional annotation was conducted using OmicsBox v3.0, integrating BLAST, InterProScan, and Gene Ontology (GO) enrichment tools to assign functional categories and pathways. Automated annotations were further manually curated using the UniProtKB database to validate and refine protein functional assignments.

5.3.5 Statistical analysis

Hydrogen peroxide (n = 4) and gene expression (n = 3) data were analyzed using one-way analysis of variance (ANOVA) followed by Tukey's test ($p \leq 0.05$) in SISVAR software (Ferreira, 2014) to compare mean differences among treatments.

Proteomic data (n=3) were analyzed separately due to the multivariate nature of protein abundance measurements. Label-free quantitative values were compared between treatments using Student's t-test ($p \leq 0.05$). Differentially accumulated proteins (DAPs) were defined based on statistical significance ($p \leq 0.05$) combined with $\log_2$ fold change thresholds of ≤ -0.6 (down-accumulated) or ≥ 0.6 (up-accumulated).

5.4 Results

5.4.1 Hydrogen peroxide dynamics following TM application and salinity

Hydrogen peroxide (H_2O_2) levels were quantified to evaluate early oxidative responses following tunicamycin (TM) application and salinity exposure. In TM-treated plants, H_2O_2 increased at 1 and 6 h, peaking at 6 h, and subsequently declined to control levels by 24 h, indicating a transient response (Figure 1A). Under salinity (Figure 1B), H_2O_2 accumulation was significantly influenced by the treatment x time interaction. Salt alone induced a sharp increase at 1 h, followed by a gradual decline, although levels remained higher than at 0 h. In contrast, TM+NaCl plants exhibited a markedly attenuated response, with consistently lower H_2O_2 levels at all time points. Notably, the early oxidative burst observed at 1 h under salt stress was significantly reduced in TM-primed plants, indicating that ER-induced priming mitigates salt-triggered oxidative stress and improves early redox homeostasis.

Figure 1 - Hydrogen peroxide (H_2O_2) contents in cowpea leaves during 24 h following tunicamycin (TM) application and subsequent salt exposure. (A) H_2O_2 levels at 1, 6, 12, and 24 h after TM treatment. Different lowercase letters indicate significant differences among time points (one-way ANOVA followed by Tukey's test, $p \leq 0.05$). (B) H_2O_2 content in plants subjected to 75 mM NaCl or TM priming followed by 75 mM NaCl (TM+NaCl) at 0, 1, 6, 12, and 24 h after salt exposure. Lowercase letters indicate differences among time points within each treatment, and uppercase letters indicate differences between treatments at the same time point (two-way ANOVA followed by Tukey's test, $p \leq 0.05$). Bars represent mean ± standard error (n = 4). ANOVA results are provided in Supplementary Table S2.

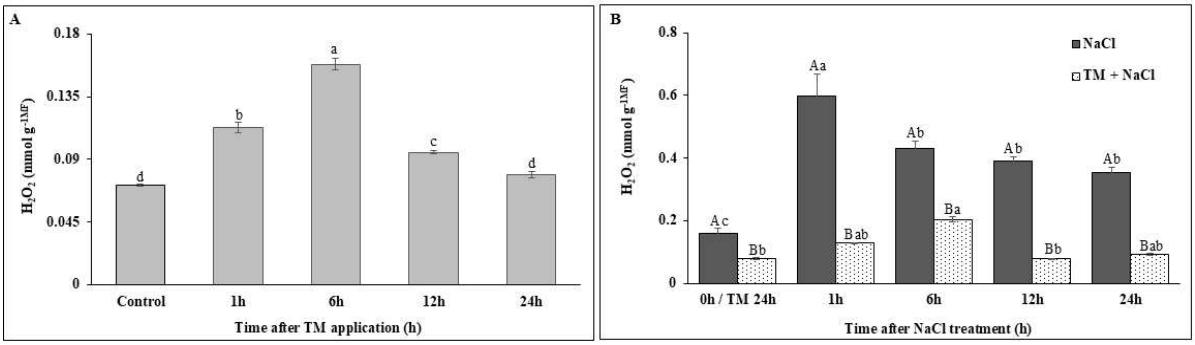

Source: Prepared by the author.

5.4.2 Gene expression of key genes related to ER and sodium transporters

Gene expression was quantified by RT-qPCR to characterize the temporal regulation of endoplasmic reticulum (ER) stress–related genes, including sensors, transcription factors, and downstream effectors, following tunicamycin (TM) spraying. Under TM treatment, all ER-associated genes analyzed, except *VubZIP17*, whose expression was not detected under these conditions, were significantly modulated over time. Overall, TM induced a clear time-dependent transcriptional activation of ER stress markers, with most genes reaching maximal expression at 12 h. *VuIRE1A* displayed an early induction pattern, peaking at 6 h and declining thereafter, although transcript levels remained higher than the control (Figure 2A). In contrast, *VubZIP60, VuBiP1, VuPDI11*, and *VuGRP94* exhibited a predominantly late response, with progressive transcript accumulation culminating at 12 h (Figure 2B–E). Intermediate expression levels were generally observed at 6 h and/or 24 h, whereas the control and 1 h time points showed the lowest transcript abundance.

.

Figure 2 - Relative gene expression of *VuIRE1A* (A), *VubZIP60* (B), *VuBiP1* (C), *VuPDI11* (D), and *VuGRP94* (E) in cowpea leaves during 24 h following tunicamycin (TM) treatment. Transcript levels were evaluated at 1, 6, 12, and 24 h after TM application by RT-qPCR and normalized to *VuUBQ3* as the reference gene. Different lowercase letters indicate significant differences among time points (one-way ANOVA followed by Tukey's test, $p \leq 0.05$). Bars represent mean ± standard error (n = 3)

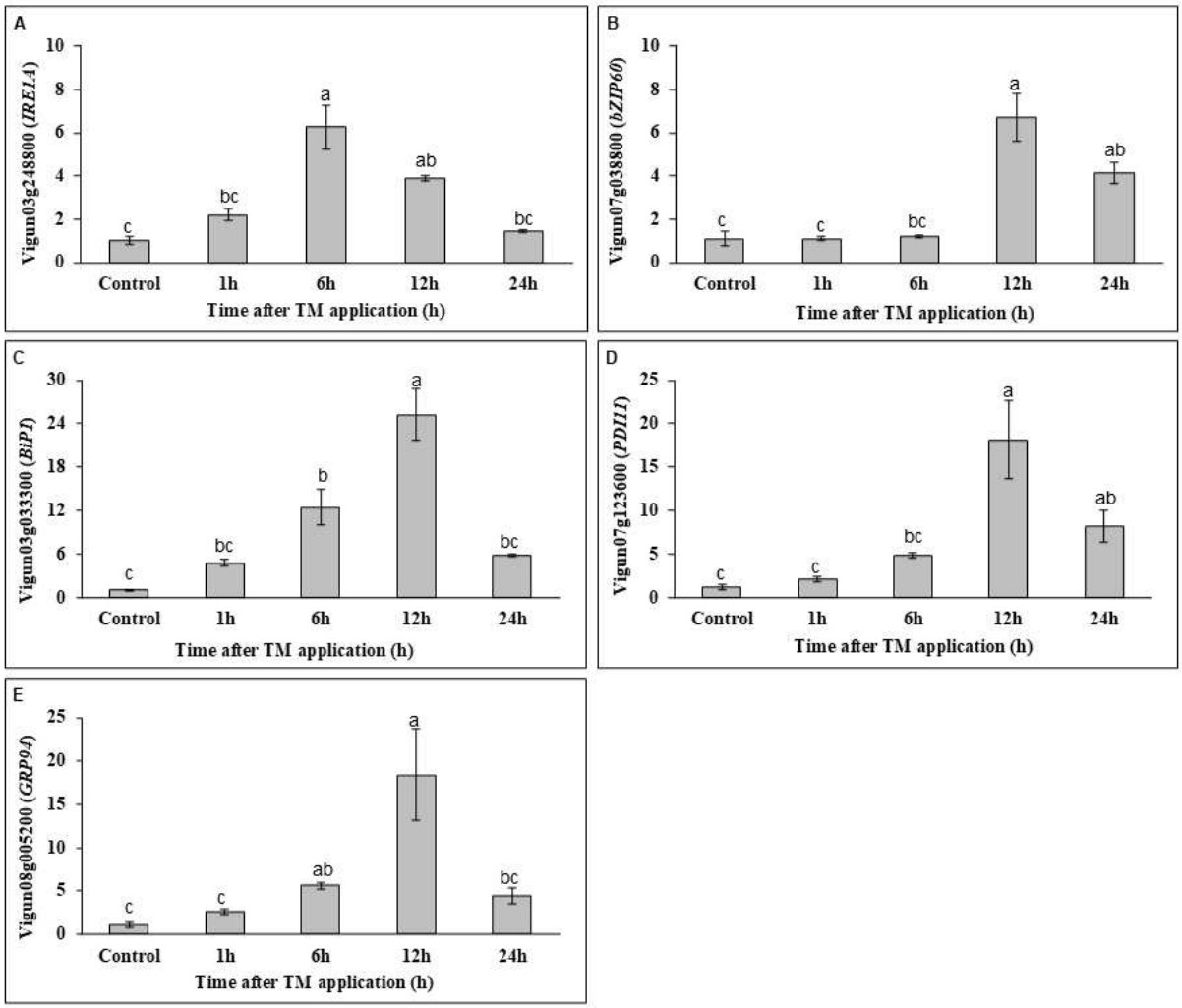

Source: Prepared by the author.

Gene expression analysis showed distinct transcriptional responses of ER stress–related genes to salinity and TM priming. For *VuIRE1A* (Figure 3A), treatment and time had significant effects, but their interaction was not significant. TM+NaCl plants exhibited higher transcript levels than salt-only plants throughout the evaluated period. Expression peaked at 1 h and gradually declined thereafter, indicating early activation of this ER stress sensor, enhanced by TM priming. In contrast, *VubZIP60* (Figure 3B) was significantly affected by the treatment x time interaction. Under salinity alone, transcript levels progressively increased,

reaching maximum values at 24 h. In TM+NaCl plants, expression peaked earlier at 12 h and declined at 24 h. Significant differences between treatments at 12 and 24 h indicate that TM priming anticipates and modulates UPR signaling. For *VuBiP1* (Figure 3C), treatment and time were significant, but their interaction was not. Salt-treated plants showed higher transcript levels than TM+NaCl plants, with expression increasing over time and peaking at 24 h. TM priming reduced overall expression without altering the temporal pattern. *VuPDI11* (Figure 3D) showed a significant treatment × time interaction. Under salinity, the expression increased at 12 and 24 h. In TM+NaCl plants, induction occurred at 12 h but was markedly reduced at 24 h, indicating modulation of late ER folding responses. Similarly, *VuGRP94* (Figure 3E) was significantly influenced by the interaction. Salinity induced a progressive increase up to 24 h, whereas TM+NaCl plants displayed attenuated expression, with significantly lower transcript levels at 6, 12, and 24 h. Overall, TM priming enhanced early ER stress signaling while limiting excessive late accumulation of ER chaperones and folding enzymes under salinity, suggesting a more regulated unfolded protein response in primed plants.

Figure 3 - Relative expression of ER stress–related genes in cowpea leaves subjected to salinity (75 mM NaCl) or tunicamycin priming followed by salinity (TM+NaCl). Transcript levels of *VuIRE1A* (A), *VubZIP60* (B), *VuBiP1* (C), *VuPDI11* (D), and *VuGRP94* (E) were quantified at 0, 1, 6, 12, and 24 h after salt exposure by RT-qPCR and normalized to *VuUBQ3* as the reference gene. For genes showing a significant treatment x time interaction (*VubZIP60*, *VuPDI11*, and *VuGRP94*), lowercase letters indicate differences among time points within each treatment, and uppercase letters indicate differences between treatments at the same time point (two-way ANOVA followed by Tukey's test, $p \leq 0.05$). For genes without significant interaction (*VuIRE1A* and *VuBiP1*), lowercase letters indicate differences among time points, and treatment effects were interpreted based on the main effects (two-way ANOVA, $p \leq 0.05$). Bars represent mean ± standard error (n = 3).

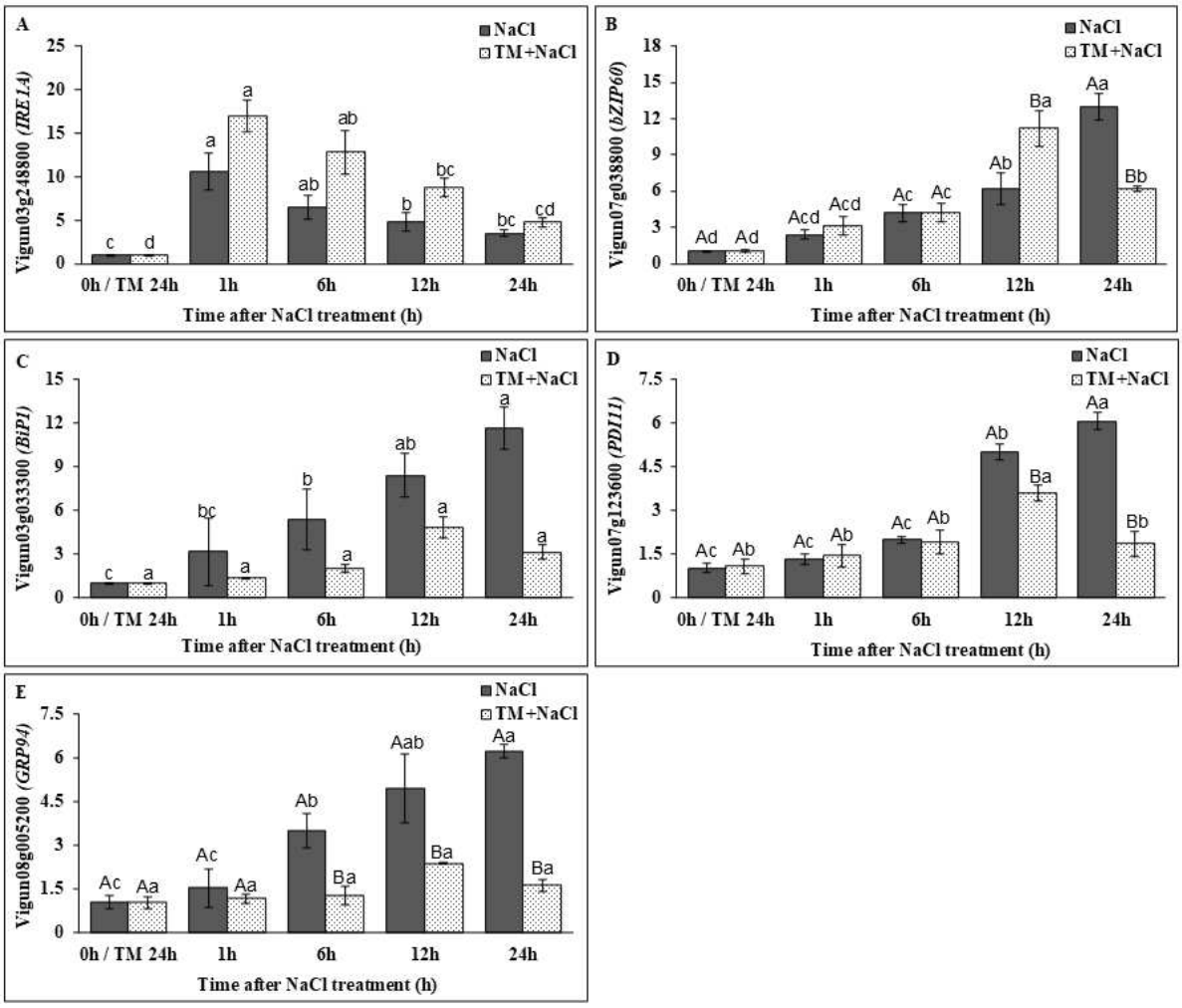

Source: Prepared by the author.

Gene expression analysis revealed distinct responses of salt transport–related genes to salinity and TM priming. For *VuSOS3* (Figure 4A), a significant treatment x time

interaction was observed. Under salinity, transcript levels progressively increased, with higher expression at 12 and 24 h. In TM+NaCl plants, expression was lower at 24 h, resulting in a significant difference between treatments, indicating attenuation of late SOS3 activation by TM priming. *VuSOS2* (Figure 4B) also showed significant interaction. Salt-treated plants displayed a gradual increase, peaking at 24 h. In contrast, TM+NaCl plants exhibited strong early induction at 1 h followed by reduced expression at later time points. Significant differences occurred at 1, 6, and 24 h, suggesting that TM priming anticipates SOS signaling. For *VuSOS1* (Figure 4C), a highly significant interaction was detected. Salinity induced a progressive increase, reaching maximum levels at 24 h. In TM+NaCl plants, expression remained more stable and significantly lower at 6, 12, and 24 h, indicating reduced late activation of Na^+ extrusion. Similarly, *VuNHX1* (Figure 4D) was significantly affected by the interaction. Salt treatment promoted progressive induction up to 24 h, whereas TM+NaCl plants showed lower expression at 24 h, reflecting moderated vacuolar Na^+ sequestration. Overall, TM priming altered the temporal regulation of salt transport genes, promoting earlier signaling activation (*VuSOS2*) while limiting excessive late induction of Na^+ transport components (*VuSOS1*, *VuNHX1*, and *VuSOS3*), suggesting improved ionic homeostasis under salinity.

Figure 4 - Relative expression of salt transport–related genes in cowpea leaves subjected to salinity (75 mM NaCl) or tunicamycin priming followed by salinity (TM+NaCl). Transcript levels of *VuSOS3* (A), *VuSOS2* (B), *VuSOS1* (C), and *VuNHX1* (D) were quantified at 0, 1, 6, 12, and 24 h after salt exposure by RT-qPCR and normalized to *VuUBQ3* as the reference gene. Lowercase letters indicate significant differences among time points within each treatment, and uppercase letters indicate significant differences between treatments at the same time point (two-way ANOVA followed by Tukey's test, $p \leq 0.05$). Bars represent mean ± standard error (n = 3).

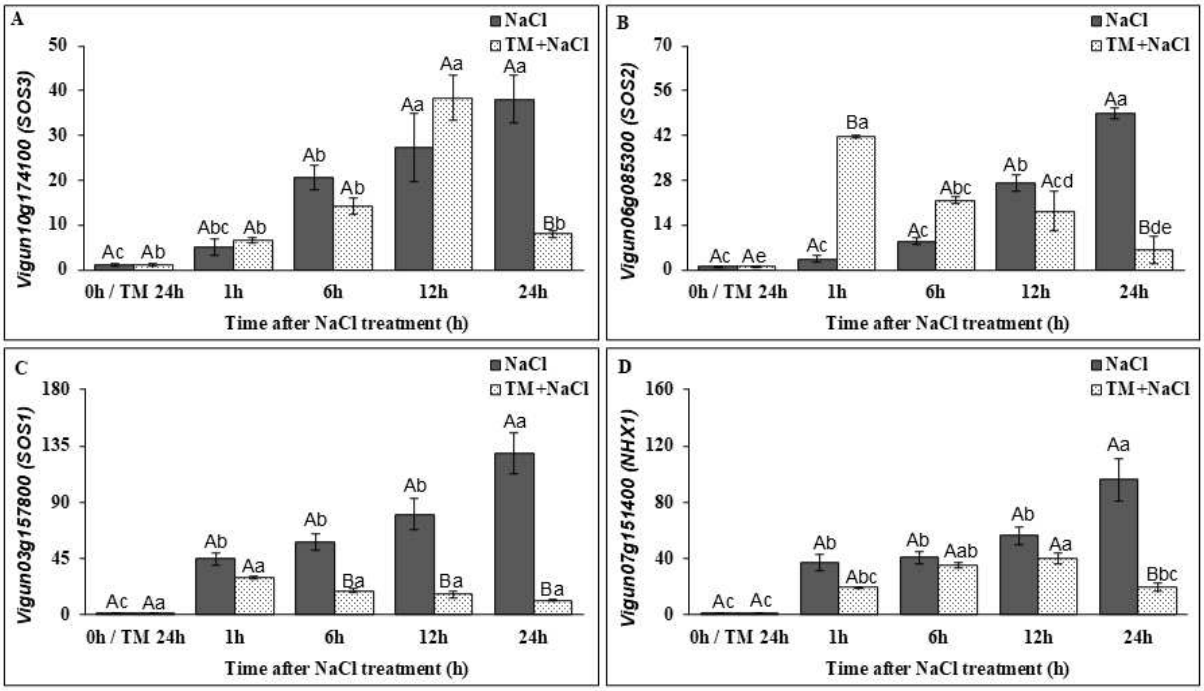

Source: Prepared by the author.

5.4.3 Proteomic profiling comparisons across experimental conditions

Plants subjected to TM (24 h), NaCl (24 h), and TM priming followed by NaCl (TM+NaCl, 24 h) were considered for proteomic analysis, since the 24 h time point reflects more stable and consolidated proteomic changes rather than early transient signaling events. The control consisted of plants harvested at 0 h and sprayed with distilled water containing 0.05% (v/v) Tween 20. A total of 747 proteins were identified across all treatments and differential abundance was defined using $\log_2$ fold change > 0.6 and $p < 0.05$. The quantification of differentially abundant proteins (DAPs) revealed that each treatment induced a distinct pattern of proteomic modulation, as detailed in Supplementary Table S3.

The volcano plots complement this quantitative assessment by illustrating the

distribution of proteins according to statistical significance and fold-change magnitude. In the TM vs Control comparison (Figure 5A), 23 proteins were significantly altered (8 upregulated and 15 downregulated), while 707 remained unchanged, indicating a modest proteomic effect of TM alone. NaCl vs Control (Figure 5B) resulted in 79 differentially abundant proteins (12 upregulated and 67 downregulated; 648 unchanged), showing a stronger proteomic impact of salinity, mainly characterized by downregulation. In TM+NaCl vs Control (Figure 5C), 43 proteins were significantly altered (16 upregulated and 27 downregulated; 691 unchanged). The lower number of downregulated proteins compared to NaCl alone indicated that TM priming partially attenuates salt-induced repression. Using NaCl as reference, TM vs NaCl (Figure 5D) exhibited 81 significant proteins (63 upregulated and 18 downregulated; 655 unchanged), with most changes occurring in the positive $\log_2$ fold-change direction, indicating a substantial TM effect relative to salinity. Additionally, TM+NaCl vs NaCl (Figure 5E) exhibited 18 significant proteins (16 upregulated and 2 downregulated; 718 unchanged).

Figure 5 - Volcano plots summarizing protein abundance changes across all experimental contrasts using significance thresholds of $|\log_2 FC| > 0.6$ and $p < 0.05$. (A) TM vs Control; (B) NaCl vs Control; (C) TM+NaCl vs Control; (D) TM vs NaCl; and (E) TM+NaCl vs NaCl. Each panel shows the distribution of upregulated, downregulated, and unchanged proteins for the respective comparison. Unchanged proteins correspond to those detected in both conditions that did not meet the significance criteria. Proteins uniquely detected in only one condition were not included in the unchanged category due to the absence of calculable fold change and statistical testing. (F) Venn diagram showing the distribution and overlap of differentially abundant proteins (DAPs) among TM vs Control, NaCl vs Control, and TM+NaCl vs NaCl. Overlaps were defined based on DAPs identified using $|\log_2 FC| > 0.6$ and $p < 0.05$.

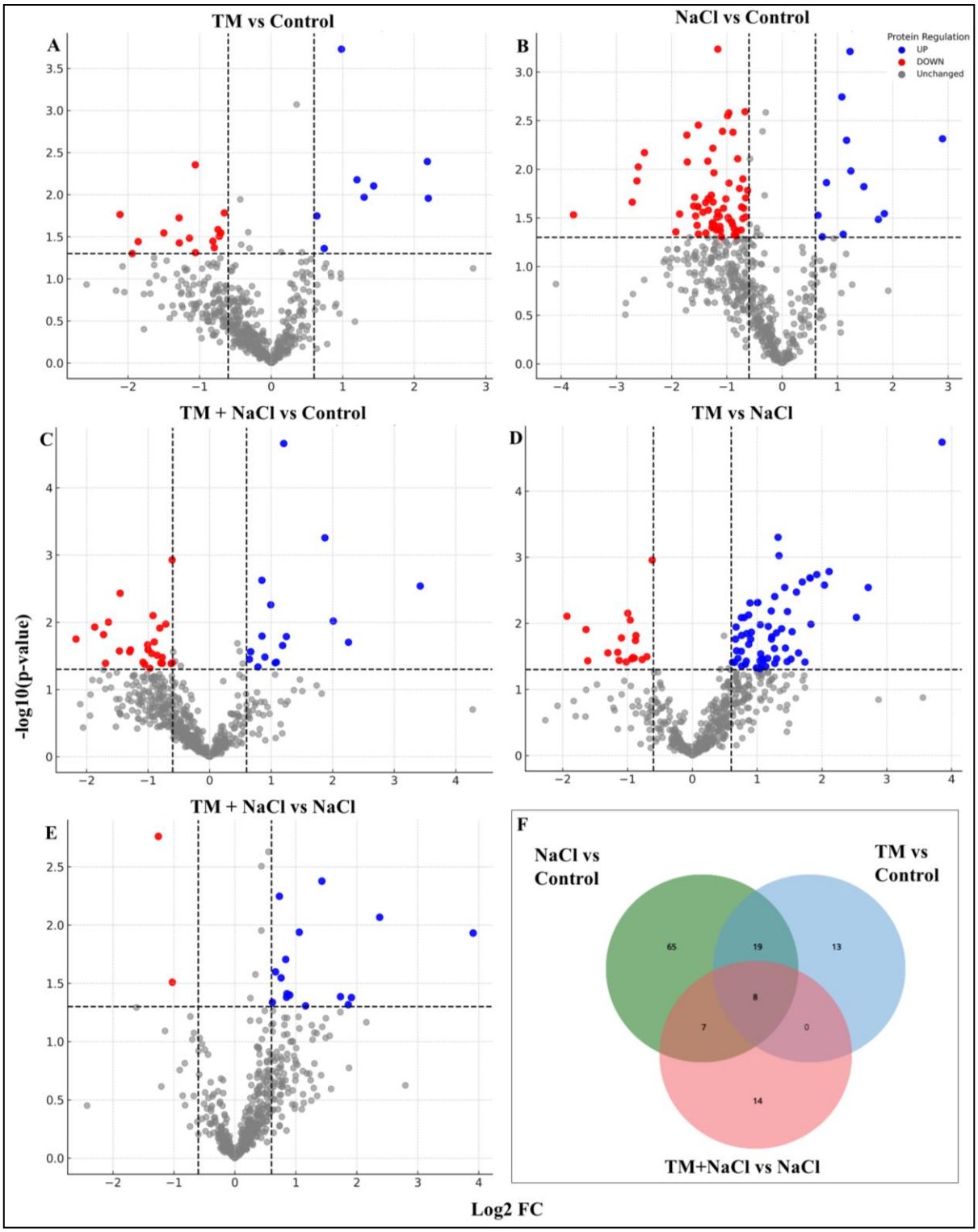

Source: Prepared by the author.

Intersection analysis of NaCl vs Control, TM vs Control, and TM+NaCl vs NaCl contrasts showed limited overlap among differentially abundant proteins (Figure 5F; Supplementary Table S4). A total of 13 proteins were exclusive to TM vs Control, 65 to NaCl vs Control, and 14 to TM+NaCl vs NaCl. Nineteen proteins were shared between TM vs Control and NaCl vs Control, and 7 were common to NaCl vs Control and TM+NaCl. No proteins were exclusively shared between TM vs Control and TM+NaCl, while 8 proteins were common to all three contrasts.

To obtain a comprehensive understanding of the biological processes modulated under salinity, ER stress, and their combined application, functional enrichment analysis was performed for the differentially abundant proteins identified in each contrast, FDR cutoff ≤ 0.05 (Supplementary Table S5). This approach enables the identification of pathways that are statistically overrepresented within each treatment condition, providing a system-level interpretation of proteomic reprogramming and allowing comparison of the dominant functional signatures associated with each stress scenario.

In the TM vs control contrast (Figure 6A), 40 differentially accumulated proteins (DAPs) were identified, with a predominance of downregulated proteins (65% among those with measurable fold change). KEGG pathway enrichment analysis revealed significant overrepresentation of pathways associated with carbon metabolism, general metabolic pathways, biosynthesis of secondary metabolites, amino acid biosynthesis, and carbon fixation in the Calvin cycle. Despite the statistical enrichment of these metabolic pathways, inspection of individual protein regulation revealed a non-uniform pattern within central carbon metabolism. The cytosolic-like glyceraldehyde-3-phosphate dehydrogenase (GAPDH; A0A4D6LYC5), a key glycolytic enzyme involved in carbon flux and NADH generation, was upregulated under TM treatment. Similarly, the mitochondrial glycine dehydrogenase (P protein; A0A4D6NRD4), a component of the glycine cleavage system linked to photorespiration and carbon metabolism, also showed increased accumulation. In contrast, the chloroplastic transketolase (A0A4D6LP55), an essential enzyme of the Calvin cycle and pentose phosphate pathway required for ribulose-1,5-bisphosphate regeneration, was downregulated. This mixed regulation pattern within Calvin cycle and carbon metabolism components suggests metabolic reorganization rather than uniform suppression. Additionally, proteins associated with ribosomal structure and one-carbon metabolism were predominantly downregulated, indicating selective modulation of translational processes. Collectively, these findings indicate that TM induces coordinated metabolic remodeling accompanied by targeted adjustment of the protein synthesis machinery, consistent with a controlled proteostatic

response rather than broad metabolic repression.

Figure 6 - KEGG pathway enrichment analysis of differentially accumulated proteins under ER stress and salinity treatments. Pathway enrichment analysis was performed using ShinyGO 0.85.1 based on KEGG database annotations of *Vigna unguiculata*. Differentially accumulated proteins (DAPs) identified in the contrasts (A) TM vs Control, (B) NaCl vs Control, and (C) TM + NaCl vs NaCl were used as input. Significantly enriched pathways were determined using a false discovery rate (FDR) cutoff ≤ 0.05 and ranked according to FDR values.

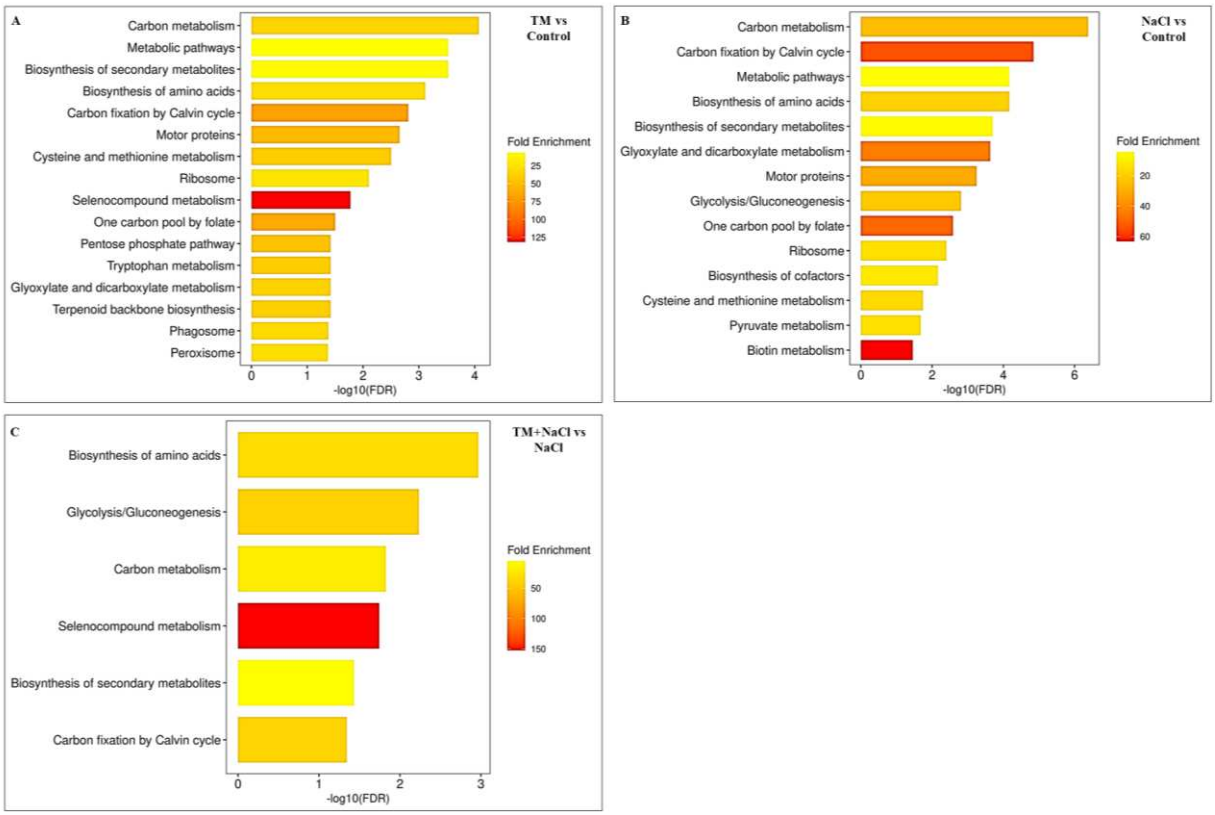

Source: Prepared by the author.

Complementary Gene Ontology (GO) enrichment analysis reinforced this interpretation. GO Biological Process (supplementary Figure S1A) terms were predominantly associated with metabolic process, cellular metabolic process, primary metabolic process, and cellular biosynthetic process, highlighting broad modulation of core metabolic functions. At the subcellular level, GO Cellular Component (supplementary Figure S1B) terms indicated enrichment of proteins associated with organelle, intracellular organelle, non-membrane-bounded organelle, and cytoskeleton, suggesting structural and compartmental adjustments

accompanying metabolic reprogramming.

In the NaCl vs control contrast (Figure 6B), 99 differentially accumulated proteins (DAPs) were identified, with a strong predominance of downregulated proteins (84.8% among those with measurable fold changes). KEGG pathway enrichment analysis revealed significant overrepresentation of pathways associated with carbon metabolism, carbon fixation in photosynthetic organisms, biosynthesis of amino acids, glycolysis/gluconeogenesis, TCA cycle, and general metabolic pathways. Protein-level inspection demonstrated that most components within these enriched pathways were down-accumulated, indicating coordinated suppression of central carbon metabolism and biosynthetic capacity under salinity. Among the downregulated proteins, the cytosolic-like glyceraldehyde-3-phosphate dehydrogenase (GAPDH; A0A4D6LYC5), a key enzyme in glycolysis involved in carbon flux and NADH generation, showed reduced accumulation. Similarly, chloroplastic triosephosphate isomerase (A0A4D6M9H9), a central enzyme in the Calvin cycle required for triose phosphate interconversion and regeneration, was downregulated. Salinity also affected amino acid and one-carbon metabolism, as evidenced by reduced levels of mitochondrial serine hydroxymethyltransferase (A0A4D6L005), a key enzyme linking glycine/serine interconversion and C1 metabolism. Additionally, proteins associated with translational machinery were markedly reduced, including plastid 50S ribosomal protein L1 (A0A4D6LKV0) and cytosolic 40S ribosomal protein S3a (A0A4D6LUZ2), reinforcing the suppression of protein synthesis under salt stress.

Complementary GO Biological Process enrichment (Supplementary Figure S1C) supported this pattern, highlighting primary metabolic process, cellular metabolic process, oxidation–reduction process, and biosynthetic processes among the significantly enriched categories. GO Cellular Component analysis (Supplementary Figure S1D) indicated enrichment of proteins localized to chloroplasts, plastids, ribosomes, and intracellular organelles, suggesting that salinity predominantly impacts photosynthetic and translational machinery. Collectively, these results indicate that salinity imposes systemic metabolic repression, characterized by coordinated downregulation of photosynthetic carbon assimilation, energy metabolism, and protein synthesis, reflecting a shift from growth-oriented metabolism toward a stress-survival mode.

In the TM + NaCl vs NaCl contrast (Figure 6C), 29 differentially accumulated proteins (DAPs) were identified, with a clear predominance of upregulated proteins (88.9% among those with measurable fold changes). KEGG pathway enrichment analysis revealed significant overrepresentation of pathways associated with carbon metabolism,

glycolysis/gluconeogenesis, biosynthesis of amino acids, and general metabolic pathways. Despite the overall predominance of up-accumulated proteins in this contrast, detailed inspection of individual protein regulation indicated that key components of central carbon metabolism remained down-accumulated. Notably, two cytosolic glyceraldehyde-3-phosphate dehydrogenase isoforms — GAPDH (A0A4D6LYC5) and GAPC1 (A0A4D6NH98) — were downregulated. These enzymes play central roles in glycolysis and carbon flux regulation and are also implicated in cellular redox balance and stress-related signaling. Additionally, 5-methyltetrahydropteroyltriglutamate–homocysteine S-methyltransferase (A0A4D6MZ10), a key enzyme associated with the sulfur cycle, methionine biosynthesis, and redox-related metabolic adjustments, was also down-accumulated under TM priming combined with salinity.

In contrast, proteins associated with ribosomal pathways and stress-responsive functions showed increased abundance. Complementary GO Biological Process enrichment (Supplementary Figure S1E) highlighted terms related to translation, cellular response to stress, and protein metabolic process. GO Cellular Component analysis (Supplementary Figure S1F) indicated enrichment of ribosome, cytosol, and intracellular organelle components. Collectively, these results indicate that TM priming under saline conditions promotes selective reinforcement of translational and stress-adaptive machinery while maintaining suppression of central carbon metabolism, suggesting a controlled metabolic adjustment rather than full restoration of growth-oriented pathways.

5.5 Discussion

5.5.1 TM leaf spray induces a transient endoplasmic reticulum stress response in cowpea

Our results demonstrated, for the first time, the temporal dynamics of tunicamycin (TM) action following foliar application in cowpea, revealing that TM induced a rapid but transient endoplasmic reticulum (ER) stress response rather than sustained cellular dysfunction. The early increase in H_2O_2 levels, peaking at 6 h and returning to basal values by 24 h, indicates that TM priming may triggers a controlled oxidative signal. The intimate relationship between ER protein folding and redox balance is well established, as oxidative protein folding within the ER lumen inherently generates reactive oxygen species (Černý et al., 2018). Thus, this transient ROS burst likely reflects activation of ER stress signaling rather than oxidative damage. The restoration of H_2O_2 to control levels at 24 h also suggests

effective engagement of antioxidant buffering systems, preventing prolonged redox imbalance.

The transcriptional dynamics of ER stress–related gene expressions reinforce this interpretation. *VuIRE1A* displayed early induction, consistent with rapid activation of ER stress sensing. In plants, the *IRE1–bZIP60* axis represents a central branch of the unfolded protein response (UPR), coordinating an adaptive transcriptional reprogramming (Deng et al., 2011; Liu & Howell, 2016). Downstream components, including *VubZIP60*, *VuBiP1*, *VuPDI11*, and *VuGRP94*, showed progressive transcript accumulation with peak expression at 12 h, followed by decline toward basal levels. Such kinetics are characteristic of mild and transient ER stress, in which UPR activation promotes restoration of ER protein-folding capacity and cellular protein homeostasis, thereby preventing the establishment of chronic ER dysfunction (Howell, 2013; Ruberti et al., 2015). Recent studies further highlight the role of ER-mediated signaling in coordinating metabolic and redox adjustments under abiotic stress (Mittler et al., 2022; Cavalcante et al., 2023).

The proteomic profile corroborated this moderate ER perturbation. The TM vs Control comparison revealed limited proteome remodeling without evidence of global metabolic collapse. Mixed regulation within central carbon metabolism suggests metabolic adjustment rather than uniform repression. Specifically, the upregulation of cytosolic glyceraldehyde-3-phosphate dehydrogenase (GAPDH; A0A4D6LYC5) indicates maintenance of glycolytic carbon flux and NADH generation, while increased accumulation of mitochondrial glycine dehydrogenase (A0A4D6NRD4), a component of the glycine cleavage system, suggests adjustment of photorespiratory and one-carbon metabolism under TM exposure. In contrast, downregulation of chloroplastic transketolase (A0A4D6LP55), a key enzyme of the Calvin cycle required for ribulose-1,5-bisphosphate regeneration, reflects selective modulation of carbon fixation rather than metabolic shutdown. Ribosomal components were predominantly downregulated, consistent with translational attenuation commonly associated with UPR activation and temporary resource reallocation toward protein quality control (Angelos et al., 2017). Importantly, the absence of widespread stress-protein overaccumulation indicates that ER stress had entered a resolution phase by 24 h.

Collectively, the transient ROS signal, temporally coordinated UPR activation, and limited proteomic remodeling indicate that TM spray induces a controlled and reversible ER stress response. Rather than causing sustained dysfunction, TM appears to trigger regulated proteostatic and redox reprogramming, potentially establishing a preconditioned physiological state, consistent with the concept of stress priming (Bruce et al., 2007; Hilker et

al., 2016).

5.5.2 Salinity promotes ER stress in cowpea leaves and negatively impacts the proteome

Salinity exposure promoted sustained ER stress in cowpea leaves, as evidenced by progressive induction of UPR-related genes. Under NaCl treatment, *VuIRE1A*, *VubZIP60*, *VuBiP1*, *VuPDI11*, and *VuGRP94* exhibited increasing transcript accumulation up to 24 h. Salt-induced ER stress has been reported in several plant species and is associated with osmotic imbalance, ionic toxicity, and secondary oxidative stress (Liu & Howell, 2016; Williams et al., 2014). Recent integrative analyses further emphasize that ER dysfunction under salinity is tightly linked to impaired energy metabolism and redox imbalance (Zandalinas et al., 2020; Zhao et al., 2025).

The persistent upregulation of ER chaperones suggests a continuous protein-folding burden. Under prolonged stress, UPR signaling may shift from adaptive restoration to growth inhibition (Simoni et al., 2022). Consistently, the NaCl vs Control contrast revealed strong predominance of downregulated proteins, indicating quick systemic proteomic repression. Central metabolic pathways, including carbon metabolism, carbon fixation, and amino acid biosynthesis, were broadly suppressed, reflecting reduced photosynthetic carbon assimilation and energy limitation (Mittler et al., 2022). At the protein level, downregulation of cytosolic GAPDH (A0A4D6LYC5) and chloroplastic triosephosphate isomerase (A0A4D6M9H9) indicates impaired glycolytic flux and Calvin cycle triose regeneration, respectively. Additionally, reduced accumulation of mitochondrial serine hydroxymethyltransferase (A0A4D6L005) suggests disruption of one-carbon metabolism and amino acid interconversion. The decline in plastidial 50S ribosomal protein L1 (A0A4D6LKV0) and cytosolic 40S ribosomal protein S3a (A0A4D6LUZ2) further supports translational repression under salinity. GO and KEGG enrichment further supported suppression of primary metabolic and biosynthetic processes, indicating a shift from growth-oriented metabolism toward stress survival mode. Ribosomal components were also reduced, suggesting translational inhibition, a common response under severe abiotic stress (Kosová et al., 2018).

The progressive induction of Na^+ transport genes (*VuSOS3, VuSOS2, VuSOS1, VuNHX1*) is consistent with activation of the canonical SOS pathway, which mediates Na^+ extrusion and vacuolar sequestration under salinity (Zhu, 2002; Zhang et al., 2025). Under salt stress, excess Na^+ triggers a rapid increase in cytosolic Ca^{2+} levels. This Ca^{2+} signal is

sensed by *SOS3*, a myristoylated Ca^{2+}-binding protein that functions as a cytosolic calcium sensor. Upon Ca^{2+} binding, *SOS3* interacts with and activates the protein kinase *SOS2*, forming a functional complex that phosphorylates and activates the plasma membrane Na^+/H^+ antiporter *SOS1*. Activated *SOS1* promotes Na^+ extrusion from the cytosol, while *NHX1* facilitates Na^+ sequestration into vacuoles using the proton gradient generated by vacuolar H^+ pumps, thereby contributing to cytosolic ion detoxification and maintenance of K^+/Na^+ balance. However, despite transcriptional activation of ion transporters, global metabolic repression suggests energetic constraints that may limit sustained adaptive capacity. Together, these data indicate that salinity imposes prolonged ER stress and systemic metabolic suppression, reshaping cellular homeostasis toward survival at the expense of growth and biosynthetic efficiency.

5.5.3 TM leaf spray mitigates early salt stress effects and promotes tolerance-oriented reprogramming: integration with physiological evidence

As previously demonstrated in Chapter 1, TM foliar application significantly alleviated the early physiological impacts of salinity, improving photosynthetic performance and growth parameters. Building upon this physiological evidence, the present analysis provides molecular and biochemical support showing that such protection is underpinned by tolerance-oriented reprogramming mechanisms.

TM priming attenuated both oxidative and transcriptional responses triggered by salt stress, indicating a more controlled and efficient stress perception. The reduced magnitude of the salt-induced oxidative burst suggests a recalibration of redox homeostasis, consistent with priming-induced modulation of ROS signaling (Mauch-Mani et al., 2017; Waszczak et al., 2018). At the ER signaling level, TM priming reshaped UPR kinetics. Enhanced early activation of *VuIRE1A* and *VubZIP60* followed by moderated late chaperone induction indicates improved temporal coordination. Such anticipatory activation is a hallmark of primed responses, enabling faster and more proportionate adaptation to subsequent stress (Hilker et al., 2016). Similarly, early induction of *VuSOS2* combined with reduced late overexpression of *VuSOS1* and *VuNHX1* suggests more efficient ionic homeostasis. The SOS pathway is energy-demanding (Zhu, 2002); therefore, earlier and controlled activation may reduce metabolic costs while maintaining Na^+ balance.

At proteomic level, TM priming attenuated salt-induced metabolic repression. Rather than reversing suppression of central metabolism entirely, priming redirected resources

toward stress-responsive and translational pathways. Notably, although central glycolytic enzymes such as GAPDH (A0A4D6LYC5) and GAPC1 (A0A4D6NH98) remained down-accumulated, the overall predominance of upregulated proteins suggests selective reinforcement rather than generalized recovery. Downregulation of 5-methyltetrahydropteroyltriglutamate–homocysteine S-methyltransferase (A0A4D6MZ10), associated with sulfur metabolism and methionine biosynthesis, may reflect redirection of methylation and redox-related pathways under primed conditions. In parallel, enrichment of ribosome-related proteins and translation-associated GO terms indicates reinforcement of protein synthesis capacity specifically linked to adaptive responses rather than growth restoration. This selective reinforcement aligns with systems-level reallocation of resources under primed states (Kosová et al., 2018). Importantly, these findings extend current knowledge of ER-mediated stress regulation to legumes, a crop group of high agronomic relevance in saline environments. While ER–salinity interactions have been explored in model species, evidence in grain legumes remains limited. Our results therefore provide new insights into ER-centered regulatory networks contributing to salt tolerance in cowpea. Overall, TM priming reprograms the temporal architecture of stress responses, promoting earlier signaling competence and reducing chronic metabolic damage. From an applied perspective, the identification of ER-associated signaling components and priming-responsive proteins offers promising molecular targets for breeding and biotechnological strategies aimed at improving salinity resilience in cowpea and other leguminous crops cultivated in salt-affected regions.

5.6 Conclusion

This study demonstrates that transient ER stress, induced by foliar tunicamycin application, functions as a regulatory signal rather than a damaging event in cowpea. TM triggers a controlled oxidative burst and short-lived UPR activation that reprograms proteostasis without causing global metabolic disruption. In contrast, salinity imposes sustained ER stress, late overactivation of ion transport systems, and broad repression of central metabolic pathways.

Importantly, TM priming reshapes the temporal architecture of salt responses, attenuating early oxidative imbalance, anticipating ER and SOS signaling, and limiting salt-induced proteomic repression. These findings support a model in which transient ER activation enhances stress efficiency by coordinating redox regulation, protein homeostasis, and ionic balance.Together, our results position the ER not merely as a stress-sensing

organelle, but as a central hub for adaptive preconditioning under salinity. The priming-specific molecular signatures identified here, particularly components of the *IRE1A–bZIP60* axis, ER chaperones with refined temporal regulation, and key ion transporters such as *SOS* pathway members and *NHX1* represent promising targets for functional validation and future breeding strategies aimed at improving abiotic stress resilience.

5.7 References

Angelos, E.; Ruberti, C.; Kim, S.J.; Brandizzi, F. Maintaining the factory: The roles of the unfolded protein response in cellular homeostasis in plants. *Plant J.* **2017**, *90*, 671–682.

Aliya, A.; Abdul J.; Xiaoli, Z.; Khalid, A.K.; Chunmei, H.; Ying, L.; Xilin H. In-depth characterization of bZIP genes in the context of unfolded protein response in plants. *Plants* **2024**, 13, 1160.

Botini, N.; Almeida, F.A.; Cruz, K.Z.C.M.; Reis, R.S.; Vale, E.M.; Garcia, A.B.; Santa-Catarina, C.; Silveira, V. Stage-specific protein regulation during somatic embryo development of *Carica papaya* L. 'Golden'. *Biochim. Biophys. Acta Proteins Proteom.* **2021**, *1869*, 140561.

Bruce, T.J.A.; Matthes, M.C.; Napier, J.A.; Pickett, J.A. Stressful "memories" of plants: Evidence and possible mechanisms. *Plant Sci.* **2007**, *173*, 603–608.

Cavalcante, F.L.P.; da Silva, S.J.; de Sousa Lopes, L.; de Oliveira Paula-Marinho, S.; Guedes, M.I.F.; Gomes-Filho, E.; de Carvalho, H.H. Unveiling a differential metabolite modulation of sorghum varieties under increasing tunicamycin-induced endoplasmic reticulum stress. *Cell Stress Chaperones* **2023**, *28*, 889–907.

Černý, M.; Habánová, H.; Berka, M.; Luklová, M.; Brzobohatý, B. Hydrogen peroxide: Its role in plant biology and crosstalk with signalling networks. *Int. J. Mol. Sci.* **2018**, *19*, 2812.

Choi, W.G.; Toyota, M.; Kim, S.H.; Hilleary, R.; Gilroy, S. Salt stress-induced Ca^{2+} waves are associated with rapid, long-distance root-to-shoot signaling in plants. *Proc. Natl. Acad. Sci. U.S.A.* **2014**, *111*, 6497–6502.

Deng, Y.; Humbert, S.; Liu, J.X.; Srivastava, R.; Rothstein, S.J.; Howell, S.H. Heat induces the splicing by IRE1 of a mRNA encoding a transcription factor involved in the unfolded protein response in *Arabidopsis*. *Proc. Natl. Acad. Sci. U.S.A.* **2011**, *108*, 7247–7252.

Distler, U.; Kuharev, J.; Navarro, P.; Levin, Y.; Schild, H.; Tenzer, S. Drift time-specific collision energies enable deep-coverage data-independent acquisition proteomics. *Nat. Methods* **2014**, *11*, 167–170.

Ferreira, D.F. Sisvar: A guide for its bootstrap procedures in multiple comparisons. *Cienc. Agrotec.* **2014**, *38*, 109–112.

Guan, P.; Zhao, D.; Zhang, C.; Qiu, Z.; Chen, Q.; Solyanikova, I.P.; Sun, P.; Cui, P.; Yu, R.; Zhang, X.; Li, Y.; Hu, L. Identification and Analysis of Endoplasmic-Reticulum-Stress- and Salt-Stress-Related Genes in *Solanum tuberosum* Genome: StbZIP60 Undergoes Splicing in Response to Salt Stress and ER Stress. *Agronomy* **2025**, 15, 1224.

Hilker, M.; Schwachtje, J.; Baier, M.; Balazadeh, S.; Bäurle, I.; Geiselhardt, S.; Hincha, D.K.; Kunze, R.; Mueller-Roeber, B.; Rillig, M.C.; Rolff, J.; Romeis, T.; Schmülling, T.; Steppuhn, A.; van Dongen, J.; Whitcomb, S.J.; Wurst, S.; Zuther, E.; Kopka, J. Priming and memory of stress responses in organisms lacking a nervous system. *Biol. Rev.* **2016**, *91*, 1118–1133.

Howell, S.H. Endoplasmic reticulum stress responses in plants. *Annu. Rev. Plant Biol.* **2013**, *64*, 477–499.

Jiang, Z.; van Zanten, M.; Sasidharan, R. Mechanisms of plant acclimation to multiple abiotic stresses. *Commun. Biol.* **2025**, *8*, 655.

Ko, D.K.; Brandizzi, F. Dynamics of ER stress-induced gene regulation in plants. *Nature Reviews Genetics* **2024**, 25, 513–525.

Kosová, K.; Vítámvás, P.; Urban, M.O.; Prášil, I.T.; Renaut, J. Plant abiotic stress proteomics: The major factors determining alterations in cellular proteome. *Front. Plant Sci.* **2018**, *9*, 122.

Lima, K.R.P.; Cavalcante, F.L.P.; Paula-Marinho, S.O.; Pereira, I.M.C.; Lopes, L.S.; Nunes, J.V.S.; Coutinho, Í.A.C.; Gomes-Filho, E.; Carvalho, H.H. Metabolomic profiles exhibit the influence of endoplasmic reticulum stress on sorghum seedling growth over time. *Plant Physiol. Biochem.* **2022**, *170*, 192–205.

Liu, J.-X.; Howell, S.H. Managing the protein folding demands in the endoplasmic reticulum of plants. *New Phytol.* **2016**, *211*, 418–428.

Liu, Y.; Lv, Y.; Wei, A.; Guo, M.; Li, Y.; Wang, J.; Wang, X.; Bao, Y. Unfolded protein response in balancing plant growth and stress tolerance. *Frontiers in Plant Science* **2022**, 13, 1019414.

Livak, K.J.; Schmittgen, T.D. Analysis of relative gene expression data using real-time quantitative PCR and the 2^(-ΔΔCT) method. *Methods* **2001**, *25*, 402–408.

Mauch-Mani, B.; Baccelli, I.; Luna, E.; Flors, V. Defense priming: An adaptive part of induced resistance. *Annu. Rev. Plant Biol.* **2017**, *68*, 485–512.

Mittler, R.; Zandalinas, S.I.; Fichman, Y.; Van Breusegem, F. Reactive oxygen species signalling in plant stress responses. *Nat. Rev. Mol. Cell Biol.* **2022**, *23*, 663–679.

Nagashima, Y.; Mishiba, K.; Suzuki, E.; Shimada, Y.; Iwata, Y.; Koizumi, N. Arabidopsis

IRE1 catalyses unconventional splicing of bZIP60 mRNA to produce the active transcription factor. *Sci. Rep.* **2011**, *1*, 29.

Nanjo, Y.; Skultety, L.; Uváčková, L.; Klubicová, K.; Hajduch, M.; Komatsu, S. Mass spectrometry-based analysis of proteomic changes in the root tips of flooded soybean seedlings. *J. Proteome Res.* **2012**, *11*, 372–385.

Oliveira, F.D.B.; Pereira, I.M.C.; Costa, I.R.S.; Cavalcante, F.L.P.; Coutinho, Í.A.C.; Alves, M.S.; de Oliveira Paula-Marinho, S.; Gomes-Filho, E.; Carvalho, H.H. Endoplasmic reticulum activation via tunicamycin seed priming enhances salt acclimation in rice seedlings. *Plant Sci.* **2025**, *358*, 112567.

Ruberti, C.; Kim, S.J.; Stefano, G.; Brandizzi, F. Unfolded protein response in plants: One master, many questions. *Curr. Opin. Plant Biol.* **2015**, *27*, 59–66.

Simoni, E.B.; Oliveira, C.C.; Fraga, O.T.; Reis, P.A.B.; Fontes, E.P.B. Cell death signaling from endoplasmic reticulum stress: Plant-specific and conserved features. *Front. Plant Sci.* **2022**, *13*, 835738.

Singh Sangha, J.; Wang, W.; Knox, R.; Ruan, Y.; Cuthbert, R.D.; Isidro-Sánchez, J.; Li, L.; He, Y.; DePauw, R.; Singh, A.; Cutler, A.; Wang, H.; Selvaraj, G. Phenotypic plasticity of bread wheat contributes to yield reliability under heat and drought stress. *PLoS ONE* **2025**, *20*, e0312122.

Suzuki, N.; Koussevitzky, S.; Mittler, R.; Miller, G. ROS and redox signalling in the response of plants to abiotic stress. *Plant Cell Environ.* **2012**, *35*, 259–270.

Velikova, V.; Yordanov, I.; Edreva, A. Oxidative stress and some antioxidant systems in acid rain-treated bean plants: Protective role of exogenous polyamines. *Plant Sci.* **2000**, *151*, 59–66.

Waszczak, C.; Carmody, M.; Kangasjärvi, J. Reactive oxygen species in plant signaling. *Annu. Rev. Plant Biol.* **2018**, *69*, 209–236.

Williams, B.; Verchot, J.; Dickman, M.B. When supply does not meet demand—ER stress and plant programmed cell death. *Front. Plant Sci.* **2014**, *5*, 211.

Wiśniewski, J.R.; Zougman, A.; Nagaraj, N.; Mann, M. Universal sample preparation method for proteome analysis. *Nat. Methods* **2009**, *6*, 359–362.

Xavier, L.R.; Corrêa, C.C.G.; da Paschoa, R.P.; Vieira, K.d.S.; Pacheco, D.D.R.; Gomes, L.d.E.S.; Duncan, B.C.; da Conceição, L.d.S.; Pinto, V.B.; Santa-Catarina, C.; Silveira, V. Time-dependent proteomic signatures associated with embryogenic callus induction in *Carica papaya* L. *Plants* **2023**, *12*, 3891.

Zanda Linas, S.I.; Fichman, Y.; Devireddy, A.R.; Sengupta, S.; Azad, R.K.; Mittler, R.

Systemic signaling during abiotic stress combination in plants. *Proc. Natl. Acad. Sci. U.S.A.* **2020**, *117*, 13810–13820.

Zhang, H.; Yu, C.; Zhang, Q.; Qiu, Z.; Zhang, X.; Hou, Y.; Zang, J. Salinity survival: Molecular mechanisms and adaptive strategies in plants. *Front. Plant Sci.* **2025**, *16*, 1527952.

Zhao, W.; Chen, X.; Wang, J.; Cheng, Z.; Ma, X.; Zheng, Q.; Xu, Z.; Zhang, F. Emerging mechanisms of plant responses to abiotic stress. *Plants* **2025**, *14*, 3445.

Zhu, J.K. Salt and drought stress signal transduction in plants. *Annu. Rev. Plant Biol.* **2002**, *53*, 247–273.

5.8 Supplementary data

Supplementary Table S1 - Reference and target gene primer sequences.

Gene symbol	Gene Identifier	Functional Annotation	Primer sequence (5'-3')	Annealing temperature
UBQ3	Vigun 03g105700	Protein ubiquitination; constitutive expression	F- TCTTGTCTTGCGACTCCGTG	55 ºC
			R- TCGTGTCTGAACTCTCGACC	
IRE1A	Vigun 03g248800	Inositol-requiring enzyme 1A; ER stress response	F- TTTTGCGTGACACCAGTGAC	55 ºC
			R- TTTTCCACCCAAGGCATCTG	
bZIP60	Vigun 07g038800	Basic leucine zipper 60; UPR-related transcription factor	F - TTGAGGAATAGGGATGCTGCTG	62 ºC
			R - AGCAGCACTGAAGCAAATGC	
BiP1	Vigun 03g033300	Binding immunoglobulin protein 1; ER protein folding chaperone	F- AACGACAAGGACAAGCTTGC	57 ºC
			R- TCATCGAGCCATTCCAATGC	
PDI11	Vigun 07g123600	Protein disulfide isomerase 11; ER protein folding	F- AGGGATCTGGCTGAAAAGTACG	57 ºC
			R- ACCGGCTTTGTTGCTCTTTG	
GRP94	Vigun 08g005200	Glucose-regulated protein 94; ER protein folding chaperone	F- ACGCCGAGAAGTTTGAGTTC	57 ºC
			R- TTGTCCAAAGCGTCAGAAGC	
SOS3	Vigun 10g174100	Salt overly sensitive 3; Ca^{2+} sensor in salt stress response	F - ATTTCAAGACGCCGATGCTG	55 ºC
			R - TGTGCTTCAAGAGTGTTGGG	
SOS2	Vigun 06g085300	Salt overly sensitive 2; protein kinase in salt stress response	F - AGCTAACGGTTGTTGAAGCC	55 ºC
			R – TCAACTTTTCCTCCCACACG	
SOS1	Vigun 03g157800	Salt overly sensitive 1; Na^+/H^+ antiporter in salt stress response	F - AAGTGCAACAACCCGTTTCG	55 ºC
			R – TTCCCAGAGCCAAACTGAGAC	
NHX1	Vigun	Na^+/H^+	F- AACTCCAACGCACACTGTTC	57 ºC

	07g151400	exchanger 1; vacuolar ion homeostasis	R- AAACCCCTTCCACCGAAAAC	

Source: Prepared by the author.

Supplementary Table S2 - Analysis of variance (ANOVA) of hydrogen peroxide (H_2O_2) in cowpea plants.

Mean square	Source variation					
	Treatment	Time	Treatment* Time	Error	Corrected total	CV (%)
Time after TM application	0.004874*	-	-	15	19	6,32
Time after NaCl treatment	0.716365*	0.064072*	0.038629*	30	39	23,56

Source: Prepared by the author.

Supplementary Table S3 - Summary of differentially abundant proteins (DAPs), including up-regulated, down-regulated, and condition-specific proteins for all contrasts.

COMPARISON	UP	DOWN	UNIQUE (TREATMENT)	UNIQUE (CONTROL)	TOTAL DAPS
TM vs Control	8	15	8	9	40
NaCl vs Control	12	67	5	15	99
TM+NaCl vs Control	16	27	3	10	56
TM vs NaCl	63	18	10	1	92
TM+NaCl vsNaCl	16	2	7	4	29

Source: Prepared by the author.

Supplementary Table S4 - Comprehensive list of differentially abundant proteins (DAPs) used for the Venn diagram analysis across the three key contrasts: TM vs Control, NaCl vs Control, and TM + NaCl vs NaCl. The table indicates the regulation status of each protein in its respective contrast, including upregulated (UP), downregulated (DOWN), and uniquely detected proteins (Unique in treatment or Unique in control), according to the thresholds $|\log_2 FC| > 0.6$ and $p < 0.05$. Color code: blue, upregulated; red, downregulated; yellow, exclusively detected in the treatment; green, exclusively detected in the control.

TM vs Control		NaCl vs Control		TM+NaCl vs NaCl	
A0A4D6LYC5	UP	A0A4D6LYC5	UP	A0A4D6LYC5	DOWN
A0A4D6LU22	UP	A0A4D6LU22	UP	A0A4D6M4T1	Unique NaCl
A0A4D6N381	UP	A0A4D6N381	UP	A0A4D6N8K0	Unique NaCl
A0A4D6LEZ3	UP	A0A4D6LEZ3	UP	A0A4D6L0Y5	Unique NaCl
A0A4D6LSV6	UP	A0A4D6LSV6	Unique Control	A0A4D6KLW4	Unique TM+NaCl
A0A4D6NRD4	UP	A0A4D6KN14	Unique NaCl	A0A4D6L7H8	Unique TM+NaCl
A0A4D6M041	UP	A0A4D6M4T1	Unique NaCl	A0A4D6N1W1	Unique TM+NaCl
A0A4D6MLY0	UP	A0A4D6N8K0	Unique NaCl	A0A4D6NH98	DOWN
A0A4D6KN14	Unique TM	A0A4D6L0Y5	Unique NaCl	A0A4D6MQP3	Unique TM+NaCl
A0A4D6M4T1	Unique TM	A0A4D6M3D1	Unique Control	A0A4D6LNE0	Unique TM+NaCl
A0A4D6N8K0	Unique TM	A0A4D6M6D4	Unique Control	A0A4D6NTD9	UP
A0A4D6L0Y5	Unique TM	A0A4D6MEK7	Unique Control	A0A4D6LC99	UP
A0A4D6LWF7	Unique TM	A0A4D6MGN3	Unique Control	A0A4D6NJF2	UP
A0A4D6M2E3	Unique TM	A0A4D6MK54	Unique Control	A0A4D6LJS4	Unique NaCl
A0A4D6MBJ3	Unique TM	A0A4D6NGA8	Unique Control	A0A4D6M8T5	UP
A0A4D6N8H9	Unique TM	A0A4D6KLW4	Unique Control	A0A4D6LLY3	UP
A0A4D6M3D1	Unique Control	A0A4D6L7H8	Unique Control	A0A4D6NCK1	UP
A0A4D6M6D4	Unique Control	A0A4D6N1W1	Unique Control	A0A4D6L976	UP
A0A4D6MEK7	Unique Control	A0A4D6KY82	UP	A0A4D6NW51	UP
A0A4D6MGN3	Unique	A0A4D6MES7	UP	A0A4D6LJQ2	UP

	Control				
A0A4D6MK54	Unique Control	A0A4D6L864	UP	A0A4D6LX28	UP
A0A4D6NGA8	Unique Control	A0A4D6M238	UP	A0A4D6KW71	UP
A0A4D6KLW4	Unique Control	A0A4D6NH98	UP	A0A4D6L058	UP
A0A4D6L7H8	Unique Control	I2E2N5	UP	A0A4D6MR83	UP
A0A4D6N1W1	Unique Control	A0A4D6MLV0	UP	A0A4D6NLX6	UP
A0A4D6LPD8	DOWN	A0A4D6NA31	UP	A0A4D6LZ50	UP
A0A4D6LXV8	DOWN	A0A4D6M982	Unique Control	I2E2Q5	UP
A0A4D6L988	DOWN	A0A4D6LH23	Unique Control	A0A4D6LPD8	Unique TM+NaCl
A0A4D6MDV6	DOWN	A0A4D6MQP3	Unique Control	A0A4D6MZ10	Unique TM+NaCl
A0A4D6LP55	DOWN	A0A4D6LNE0	Unique Control		
A0A4D6KY95	DOWN	A0A4D6KJX4	DOWN		
A0A4D6MDF0	DOWN	A0A4D6KH54	DOWN		
A0A4D6MC81	DOWN	A0A4D6KTW9	DOWN		
A0A4D6MYA9	DOWN	A0A4D6M2T0	DOWN		
A0A4D6KJC3	DOWN	A0A4D6M9D1	DOWN		
A0A4D6LYW3	DOWN	A0A4D6NSZ2	DOWN		
A0A4D6LJA4	DOWN	A0A4D6N3Y3	DOWN		
A0A4D6M6P0	DOWN	A0A4D6NNY3	DOWN		
A0A4D6LKV0	DOWN	A0A4D6MDB9	DOWN		
A0A4D6L572	DOWN	A0A4D6LID6	DOWN		
		A0A4D6M9H9	DOWN		
		A0A4D6M9M0	DOWN		
		A0A4D6LHT9	DOWN		
		A0A4D6NSG9	DOWN		
		A0A4D6MNZ1	DOWN		
		A0A4D6NP90	DOWN		
		A0A4D6NE09	DOWN		
		A0A4D6KL64	DOWN		
		A0A4D6MBV7	DOWN		
		A0A4D6MCL4	DOWN		
		A0A4D6L005	DOWN		
		A0A4D6NWJ4	DOWN		
		A0A4D6L3E6	DOWN		
		A0A4D6N7W8	DOWN		
		A0A4D6L5Q4	DOWN		

		A0A4D6LJS6	DOWN		
		A0A4D6LBJ4	DOWN		
		A0A4D6KTE5	DOWN		
		A0A4D6MFZ9	DOWN		
		A0A4D6NIS2	DOWN		
		A0A4D6M9W5	DOWN		
		A0A4D6ML62	DOWN		
		A0A4D6MN02	DOWN		
		A0A4D6NLN4	DOWN		
		A0A4D6NCS7	DOWN		
		A0A4D6MF88	DOWN		
		A0A4D6MXT5	DOWN		
		A0A4D6MYB2	DOWN		
		A0A4D6ME55	DOWN		
		A0A4D6M5W6	DOWN		
		A0A4D6MMA2	DOWN		
		A0A4D6N0A5	DOWN		
		A0A4D6MR83	DOWN		
		A0A4D6NLX6	DOWN		
		A0A4D6LZ50	DOWN		
		I2E2Q5	DOWN		
		A0A4D6LA38	DOWN		
		A0A4D6NIV3	DOWN		
		A0A4D6LHL3	DOWN		
		A0A4D6ML48	DOWN		
		A0A4D6KKH4	DOWN		
		A0A4D6KIK7	DOWN		
		A0A4D6LEK9	DOWN		
		A0A4D6KUP9	DOWN		
		A0A4D6N2P5	DOWN		
		A0A4D6N545	DOWN		
		A0A4D6MAK1	DOWN		
		A0A4D6LJ91	DOWN		
		A0A4D6M9Q1	DOWN		
		A0A4D6LPD8	Unique Control		
		A0A4D6MC81	DOWN		
		A0A4D6MYA9	DOWN		
		A0A4D6KJC3	DOWN		
		A0A4D6LYW3	DOWN		
		A0A4D6LJA4	DOWN		
		A0A4D6M6P0	DOWN		
		A0A4D6LKV0	DOWN		

		A0A4D6L572	DOWN		
		A0A4D6LUZ2	Unique NaCl		

Source: Prepared by the author.

Supplementary Table S5 - Enrichment analysis was performed using ShinyGO 0.85.1 based on KEGG database annotation. Only significantly enriched pathways (FDR-adjusted $p < 0.05$) are shown. The table includes the Enrichment FDR, nGenes, Fold Enrichment, pathway name, and the list of proteins identified in each enriched pathway.

Enrichment FDR	nGenes	Fold Enrichment	Pathways	Proteins
TM vs Control				
8.4E-05	4	36.2	Carbon metabolism	A0A4D6NRD4 A0A4D6LP55 A0A4D6LYC5 A0A4D6MEK7
3.0E-04	7	6.8	Metabolic pathways	A0A4D6NRD4 A0A4D6LP55 A0A4D6MDV6 A0A4D6L572 A0A4D6LYC5 A0A4D6LWF7 A0A4D6MEK7
3.0E-04	6	9.4	Biosynthesis of secondary metabolites	A0A4D6NRD4 A0A4D6LP55 A0A4D6L572 A0A4D6LYC5 A0A4D6LWF7 A0A4D6MEK7
7.7E-04	3	28.5	Biosynthesis of amino acids	A0A4D6LP55 A0A4D6LYC5 A0A4D6LWF7
1.5E-03	2	68.9	Carbon fixation by Calvin cycle	A0A4D6LP55 A0A4D6LYC5
2.2E-03	2	52.6	Motor proteins	A0A4D6N8K0 A0A4D6MBJ3
3.1E-03	2	40.7	Cysteine and methionine metabolism	A0A4D6MDV6 A0A4D6LWF7
7.9E-03	2	23.9	Ribosome	A0A4D6LKV0 A0A4D6M6D4
1.7E-02	1	131.5	Selenocompound	A0A4D6LWF7

			metabolism	
3.2E-02	1	62.9	One carbon pool by folate	A0A4D6MDV6
3.8E-02	1	46.6	Pentose phosphate pathway	A0A4D6LP55
3.8E-02	1	40.2	Tryptophan metabolism	A0A4D6MEK7
3.8E-02	1	37.1	Glyoxylate and dicarboxylate metabolism	A0A4D6MEK7
3.8E-02	1	39.1	Terpenoid backbone biosynthesis	A0A4D6L572
4.2E-02	1	31.4	Phagosome	A0A4D6MBJ3
4.3E-02	1	28.9	Peroxisome	A0A4D6MEK7
NaCl vs Control				
4.2E-07	7	24.9	Carbon metabolism	A0A4D6MXT5 A0A4D6MCL4 A0A4D6L005 A0A4D6M9H9 A0A4D6LYC5 A0A4D6MEK7 A0A4D6NH98
1.4E-05	4	54.1	Carbon fixation by Calvin cycle	A0A4D6MXT5 A0A4D6MCL4 A0A4D6M9H9 A0A4D6LYC5
6.8E-05	12	4.6	Metabolic pathways	A0A4D6MXT5 A0A4D6LHT9 A0A4D6MCL4 A0A4D6L005 A0A4D6M9H9 A0A4D6L572 A0A4D6L5Q4 A0A4D6LYC5 A0A4D6KJX4 A0A4D6N2P5 A0A4D6MEK7 A0A4D6NH98
6.8E-05	5	18.7	Biosynthesis of amino acids	A0A4D6L005 A0A4D6M9H9 A0A4D6LYC5 A0A4D6N2P5 A0A4D6NH98
2.0E-04	9	5.5	Biosynthesis of secondary metabolites	A0A4D6MXT5 A0A4D6L005 A0A4D6M9H9

				A0A4D6L572 A0A4D6LYC5 A0A4D6KJX4 A0A4D6N2P5 A0A4D6MEK7 A0A4D6NH98
2.3E-04	3	43.7	Glyoxylate and dicarboxylate metabolism	A0A4D6MXT5 A0A4D6L005 A0A4D6MEK7
5.6E-04	3	31	Motor proteins	A0A4D6NIS2 A0A4D6N8K0 A0A4D6KH54
1.5E-03	3	21	Glycolysis/Gluconeogenesis	A0A4D6M9H9 A0A4D6LYC5 A0A4D6NH98
2.6E-03	2	49.4	One carbon pool by folate	A0A4D6L005 A0A4D6N2P5
4.0E-03	3	14.1	Ribosome	A0A4D6LKV0 A0A4D6M6D4 A0A4D6LUZ2
6.9E-03	3	11.2	Biosynthesis of cofactors	A0A4D6L005 A0A4D6L5Q4 A0A4D6N2P5
1.8E-02	2	16	Cysteine and methionine metabolism	A0A4D6MXT5 A0A4D6N2P5
2.1E-02	2	14.2	Pyruvate metabolism	A0A4D6MXT5 A0A4D6LHT9
3.5E-02	1	63.1	Biotin metabolism	A0A4D6L5Q4
TM+NaCl vs NaCl				
1.1E-03	3	33	Biosynthesis of amino acids	A0A4D6LYC5 A0A4D6MZ10 A0A4D6NH98
5.9E-03	2	41.3	Glycolysis/Gluconeogenesis	A0A4D6LYC5 A0A4D6NH98
1.5E-02	2	20.9	Carbon metabolism	A0A4D6LYC5 A0A4D6NH98
1.8E-02	1	152.2	Selenocompound metabolism	A0A4D6MZ10
3.7E-02	3	5.4.	Biosynthesis of secondary metabolites	A0A4D6LYC5 A0A4D6MZ10 A0A4D6NH98

4.5E-02	1	39.9	Carbon fixation by Calvin cycle	A0A4D6LYC5

Source: Prepared by the author.

Supplementary Figure S1 - Gene Ontology (GO) enrichment analysis of differentially abundant proteins (DAPs) identified in the three main contrasts. Biological Process (BP) and Cellular Component (CC) categories are shown for (A,B) TM vs Control, (C,D) NaCl vs Control, and (E,F) TM + NaCl vs NaCl. Only significantly enriched GO terms (FDR-adjusted $p < 0.05$) are presented.

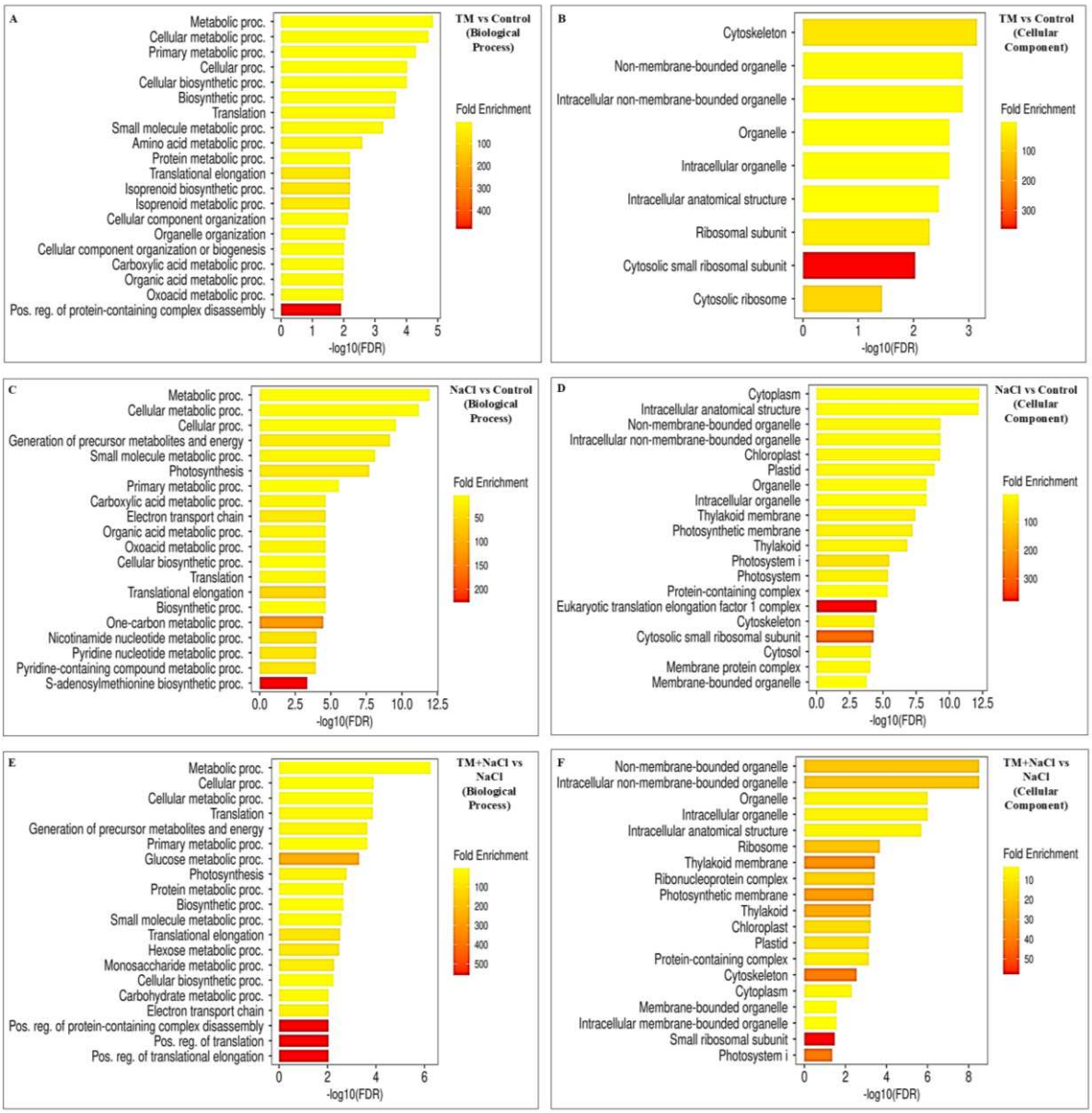

Source: Prepared by the author.

6 CONSIDERAÇÕES FINAIS

Os resultados desta tese demonstram que a ativação transitória e controlada da via de resposta ao estresse do retículo endoplasmático (UPR) atua como mecanismo integrador na aclimatação ao estresse salino em feijão-caupi. A indução moderada dessa via, por meio da aplicação foliar de tunicamicina, não provocou disfunção persistente, mas desencadeou um estado fisiológico preparatório caracterizado por melhor coordenação redox, ajuste da homeostase iônica e reorganização metabólica seletiva.

Os dados integrados indicam que a tolerância ao sal não depende exclusivamente da intensificação das respostas de defesa, mas da reorganização temporal eficiente das redes celulares. Enquanto a salinidade isolada promoveu ampla repressão metabólica e translacional, o priming associado à ativação da UPR favoreceu a manutenção seletiva de funções adaptativas, reduzindo o custo energético do estresse e atenuando a progressão para um estado de colapso metabólico.

Esses achados posicionam o retículo endoplasmático como um centro regulador estratégico na integração entre sinalização redox, proteostase e homeostase iônica. Contudo, embora a tunicamicina tenha sido utilizada como ferramenta experimental para induzir a UPR, sua aplicação direta em campo não é viável devido à sua natureza antibiótica e aos potenciais impactos ambientais. Assim, o valor desta tese reside na demonstração de que a ativação controlada da sinalização do RE pode funcionar como mecanismo de priming, abrindo caminho para a identificação de indutores sintéticos seguros ou estratégias genéticas capazes de modular essa via sem comprometer a sustentabilidade agrícola.

Como perspectivas futuras, torna-se essencial validar funcionalmente outros componentes-chave da UPR identificados neste estudo, investigar a interação dessa via com outros sistemas de sinalização de estresse e explorar moléculas ou reguladores endógenos que possam estimular respostas semelhantes às observadas com TM. Tais avanços poderão contribuir para o desenvolvimento de cultivares mais resilientes à salinidade, baseados na modulação estratégica de redes adaptativas celulares.

REFERÊNCIAS

ALIYA, A. *et al*. In-depth characterization of bZIP genes in the context of unfolded protein response in plants. **Plants**, v. 13, p. 1160, 2024. DOI 10.3390/plants13081160.

ATTA, K. *et al*. Impacts of salinity stress on crop plants: improving salt tolerance through genetic and molecular dissection. **Frontiers in Plant Science**, Lausanne, v. 14, p. 1241736, 2023. DOI 10.3389/fpls.2023.1241736.

BALASUBRAMANIAM, T. *et al*. Plants' response mechanisms to salinity stress. **Plants**, v. 12, n. 12, p. 2253, 2023. DOI 10.3390/plants12122253.

BRUCE, T. J. A. *et al*. Stressful "memories" of plants: Evidence and possible mechanisms. **Plant Science**, Shannon, v. 173, n. 6, p. 603-608, 2007. DOI 10.1016/j.plantsci.2007.09.002.

CAVALCANTE, F. L. P. *et al*. Unveiling a differential metabolite modulation of sorghum varieties under increasing tunicamycin-induced endoplasmic reticulum stress. **Cell Stress and Chaperones**, New York, v. 28, n. 6, p. 889-907, 2023. DOI 10.1007/s12192-023-01382-5.

ČERNÝ, M. *et al*. Hydrogen peroxide: Its role in plant biology and crosstalk with signalling networks. **International Journal of Molecular Sciences**, v. 19, n. 9, p. 2812, 2018. DOI 10.3390/ijms19092812.

DENNING, G. Sustainable intensification of agriculture: the foundation for universal food security. **NPJ Sustainable Agriculture**, v. 3, p. 7, 2025. DOI 10.1038/s44264-025-00047-3.

ELBEIN, A. D. Inhibitors of the biosynthesis and processing of N-linked oligosaccharide chains. **Annual Review of Biochemistry**, Palo Alto, v. 56, p. 497-534, 1987. DOI 10.1146/annurev.bi.56.070187.002433.

EMBRAPA. Agrobalsas 2025: Cultivares de feijão-caupi marcam presença em debate e vitrine tecnológica. **Embrapa**, Brasília, DF, 2025. Disponível em: https://www.embrapa.br/busca-de-noticias/-/noticia/100401580/agrobalsas-2025-cultivares-de-feijao-caupi-marcam-presenca-em-debate-e-vitrine-tecnologica

EVELIN, H. *et al*. Mitigation of salinity stress in plants by arbuscular mycorrhizal symbiosis: Current understanding and new challenges. **Frontiers in Plant Science**, Lausanne, v. 10, p. 470, 2019. DOI 10.3389/fpls.2019.00470.

FU, H.; YANG, Y. How plants tolerate salt stress. **Current Issues in Molecular Biology**, v. 45, n. 7, p. 5914-5934, 2023. DOI 10.3390/cimb45070374.

HOWELL, S. H. Endoplasmic reticulum stress responses in plants. **Annual Review of Plant Biology**, Palo Alto, v. 64, p. 477-499, 2013. DOI 10.1146/annurev-arplant-050312-120053.

IWATA, Y.; KOIZUMI, N. Unfolded protein response followed by induction of cell death in cultured tobacco cells treated with tunicamycin. **Planta**, Berlin, v. 220, n. 5, p. 804-807, 2005. DOI 10.1007/s00425-004-1479-z.

KOSOVÁ, K. *et al*. Plant abiotic stress proteomics: The major factors determining alterations in cellular proteome. **Frontiers in Plant Science**, Lausanne, v. 9, p. 122, 2018. DOI 10.3389/fpls.2018.00122.

LIU, J. X.; HOWELL, S. H. Managing the protein folding demands in the endoplasmic reticulum of plants. **New Phytologist**, London, v. 211, n. 2, p. 418-428, 2016. DOI 10.1111/nph.13915.

MARZEC, M. *et al*. GRP94: An HSP90-like protein specialized for protein folding and quality control in the endoplasmic reticulum**. Biochimica et Biophysica Acta – Molecular Cell Research,** v. 1823, n. 3, p. 774-787, 2012. DOI 10.1016/j.bbamcr.2011.10.013.

MAUCH-MANI, B. *et al*. Defense priming: An adaptive part of induced resistance. **Annual Review of Plant Biology**, Palo Alto, v. 68, p. 485-512, abr. 2017. DOI 10.1146/annurev-arplant-042916-041132.

MITTLER, R. *et al*. Reactive oxygen species signalling in plant stress responses. **Nature Reviews Molecular Cell Biology**, London, v. 23, p. 663-679, 2022. DOI: 10.1038/s41580-022-00499-2.

OBATA, T.; FERNIE, A. R. The use of metabolomics to dissect plant responses to abiotic stresses. **Cellular and Molecular Life Sciences**, Basel, v. 69, n. 19, p. 3225-3243, 2012. DOI 10.1007/s00018-012-1091-5.

OLIVEIRA, F. D. B. *et al*. Endoplasmic reticulum activation via tunicamycin seed priming enhances salt acclimation in rice seedlings. **Plant Science**, Shannon, v. 358, p. 112567, 2025. DOI 10.1016/j.plantsci.2025.112567.

PRAXEDES, S. C. *et al*. Salt stress tolerance in cowpea is poorly related to the ability to cope with oxidative stress. **Acta Botanica Croatica**, Zagreb, v. 73, n. 1, 2014.

ROSEGRANT, M. W. *et al*. Food and nutrition security under changing climate and socioeconomic conditions. **Global Food Security**, Amsterdam, v. 41, p. 100755, 2024. DOI 10.1016/j.gfs.2024.100755.

RUBERTI, C. *et al*. Unfolded protein response in plants: one master, many questions. **Current Opinion in Plant Biology**, London, v. 27, p. 59-66, 2015. DOI 10.1016/j.pbi.2015.05.016.

SANGA, D. L. *et al*. Soil salinization under irrigated farming: A threat to sustainable food security and environment in semi-arid tropics. **Journal of Agricultural Science and Practice**, v. 9, n. 3, p. 32-47, 2024.

SOUZA, C. L. C. de *et al*. Adaptability and yield stability of cowpea genotypes in the Mid-North region of Brazil. **Revista Brasileira de Ciências Agrárias**, v. 17, n. 3, e1614, 2022.

SUZUKI, N. *et al*. ROS and redox signalling in the response of plants to abiotic stress. **Plant, Cell & Environment**, Oxford, v. 35, n. 2, p. 259-270, 2012. DOI 10.1111/j.1365-3040.2011.02336.x.

WILLIAMS, B.; VERCHOT, J.; DICKMAN, M. B. When supply does not meet demand-ER stress and plant programmed cell death. **Frontiers in Plant Science**, Lausanne, v. 5, p. 211, 2014. DOI 10.3389/fpls.2014.00211.

YU, C. Y. *et al*. What's unique? The unfolded protein response in plants. **Journal of Experimental Botany,** Oxford, v. 73, n. 5, p. 1268-1276, 2022. DOI https://doi.org/10.1093/jxb/erab513.

ZHOU, H. *et al*. Insights into plant salt stress signaling and tolerance. **Journal of Genetics and Genomics**, v. 51, n. 1, p. 16-34, 2024. DOI 10.1016/j.jgg.2023.08.007.

ZULFIQAR, F. *et al*. Chemical priming enhances plant tolerance to salt stress. **Frontiers in Plant Science**, Lausanne, v. 13, p. 946922, 2022. DOI 10.3389/fpls.2022.946922.